Analytical Solution for SAGD with Consideration of Temperature Variation along the Edge of a Steam Chamber

by

Xiaoxing Shi

A thesis submitted in partial fulfillment of the requirements for the degree of

Master of Science

in

Petroleum Engineering

Department of Civil and Environmental Engineering
University of Alberta

ABSTRACT

Steam-assisted gravity drainage (SAGD) is a widely-used method for heavy-oil and bitumen recovery. Analytical models were presented in the literature for bitumen-production rate and steam-to-oil ratio (SOR) for SAGD. They often overestimate bitumen-production rate substantially. Various attempts were made to correct for simplifying assumptions made in their derivations. However, no research has been conducted to solve for temperature at the edge of a steam chamber. Although bitumen-production rate and SOR depend significantly on temperature near the chamber edge in SAGD, previous analytical models assumed the injected-steam temperature to uniformly distribute along the edge of a steam chamber. The main objective of this research is to investigate temperature variation along the edge of a steam chamber.

Local material balance and Darcy's law are applied to each cross section perpendicular to the edge of a steam chamber. Then, they are coupled with the global material balance for the chamber geometry that is an inverted triangle. New analytical equations are presented for bitumen-production rate and SOR, in addition to variables as functions of elevation from the production well, such as oil flow rate, temperature, and composition along the linear-chamber edge. Bitumen-production rate and SOR can be calculated for a given temperature at a certain elevation from the production well. The new analytical model is validated on the basis of numerical flow simulations.

Comparison of the analytical model with numerical simulations shows that bitumen-production rate and SOR can be accurately estimated when the new model is used with the temperature taken from the midpoint of the edge of a steam chamber. The temperature that gives accurate results is 60%-90% of the injected-steam temperature in the cases tested. Hence, the analytical model presented in this research requires a representative temperature (i.e., temperature at the midpoint of the chamber edge) for a given time for a given SAGD operation, unlike

previously-proposed models. This is plausible because the assumption of one-dimensional heat conduction on a moving chamber edge is expected to be less accurate near the top and bottom of a steam chamber, in which multi-dimensional heat transfer is significant owing to heat losses to the over and underlying formation rocks. Numerical simulations show that such heat losses are necessary for a steam chamber to have a linear edge. In addition, multidimensional flow near the bottom of the reservoir causes substantial heat convection, and makes the one-dimensional conduction equation inaccurate. Hence, the previous assumption of the injected-steam temperature at the chamber edge is simplistic, and gives inaccurate results for oil-production rate in SAGD.

Among widely-used assumptions for analytical SAGD models, most simplistic assumptions are identified, such as single-oleic phase flow, one-dimensional flow along the edge of a steam chamber, and one-dimensional heat conduction ahead of the chamber edge. The new analytical model is also applied to estimate bitumen-production rate and SOR for three SAGD projects, although there are various uncertainties in actual field data, such as reservoir heterogeneity.

ACKNOWLEDGEMENTS

I would like to express my deepest gratitude to my supervisor, Dr. Ryosuke Okuno, for his endless patience and insightful guidance during my program. I greatly appreciate the opportunity to pursue my research under Dr. Okuno's supervision. I've learnt a lot from him in terms of logical thinking and rigorous attitude towards research, which will definitely benefit me throughout my life.

I am thankful to my committee members, Dr. Juliana Leung and Dr. Huazhou (Andy) Li, for their invaluable feedback on my research. Many thanks to Dr. Tae J. Kwon for attending my defense as the chair. I also want to thank my colleagues, Ashutosh Kumar and Arun Venkat Venkatramani, for providing data and help for this research.

I gratefully acknowledge the financial support received from Japan Petroleum Exploration Co., Ltd., Japan Canada Oil Sands Ltd., and the Natural Sciences and Engineering Research Council of Canada (RGPIN 418266).

I am grateful to my best friends, Jingwen Cui and Yanmin Xu. Thank you for being by my side. I also want to thank all my friends. I will never forget the precious time spent with you. Last, but not the least, I want to thank my parents and my family for their unconditional love and believing in me as always.

TABLE OF CONTENTS

LIST OF TABLES

LIST OF FIGURES

NOMENCLATURE

Roman Symbols:

a	: A constant which equals to 0.4 and is used in Reis' model
a'	: A history matching correction factor used in Kesharvarz et al. (2016)
a_c	: The coefficient in Corey's equation
C	: Constant of integration
C_s	: Solvent concentration
D	: Solvent diffusion coefficient
F	: Degree of freedom
g	: Gravitational acceleration
H	: Vertical distance from reservoir top to the production well
I_o	: Integration of kinematic viscosity of oleic phase in the cross-section perpendicular to steam chamber edge
k	: Permeability
k_{ro}	: Relative permeability of oleic phase
k_{rw}	: Relative permeability of water phase
k_{rocw}	: Relative permeability of oleic phase at connate water saturation
k_{rwio}	: Relative permeability of water phase at irreducible oil saturation
k_{rave}	: Average value of relative permeability in each cross-section ahead of steam chamber
K	: Thermal conductivity
l	: Distance starting from production well in the direction along steam chamber edge
L	: Lateral distance between observation well and production well
m	: Term used in Equation (2.6) to describe how bitumen viscosity changes with temperature
M	: Heat capacity
N_C	: Number of components
N_P	: Number of phases
q_o	: Oil flow rate
q_s	: Steam injection rate
Q'_{inj}	: The injection rate of latent heat carried by the injected steam

Q'_{SC} : The rate of heat required for chamber expansion

Q'_{AC} : The rate of heat used for the reservoir ahead of the edge of a steam chamber

Q'_{OB} : The rate of heat loss to the overburden formation

Q'_{PO} : The rate of heat carried by produced bitumen

S_w : Water saturation

S_{wc} : Connate water saturation

S_{or} : Residual oil saturation

ΔS_o : Reducible oil saturation of reservoir

t_o : Time when steam chamber reaches a certain height

T : Temperature

T_e : Chamber edge temperature

T_S : Steam saturation temperature under injection pressure

U : Chamber edge advancing velocity which is normal to the edge

U_f : Front velocity of steam chamber edge proposed in Zargar and Farouq Ali's model

U_o : Flow velocity of oleic phase along steam chamber edge

v : Chamber edge advancing velocity in horizontal direction

W_S : Width of steam chamber at ceiling

Δy : Unit length in the direction along the production well

z : Elevation

Greek Symbols:

α : Thermal diffusivity of reservoir

β_θ : Parameter used to describe the extent to which flow direction deviates from steam chamber edge

β_ξ : Parameter used to evaluate the inaccuracy of temperature profile ahead of steam chamber

γ : Heat penetration depth

ξ : Distance normal to the steam chamber edge

θ : Angle between steam chamber edge and horizontal

θ_{ave} : Average angle of oil flow along the chamber edge

μ : Dynamic viscosity

ν	: Kinematic viscosity
ν_{os}	: Kinematic viscosity of bitumen at steam temperature
ρ	: Density
σ	: Time since steam zone reached a specific width
τ	: Term defined by Equation (2.13)
φ	: Porosity of reservoir
ω	: Acentric factor

Subscript:

D	: Dimensionless
e	: Steam chamber edge
g	: Gas phase
L	: The point where the perpendicular of steam chamber edge, ξ, intersects with production layer
o	: Oleic phase
R	: Reservoir
S	: Steam
ceiling	: At the bottom of overburden formation

Abbreviations

ES-SAGD	: Expanding solvent steam-assisted gravity drainage
OOIP	: Original oil in place
SAGD	: Steam-assisted gravity drainage
SOR	: Steam-oil ratio (refers to instantaneous steam-oil ration in this thesis)

CHAPTER 1 INTRODUCTION

1.1 Background

There is more than 315 billion barrels of recoverable oil in oil sands in Alberta, Canada. Oil sands are mixture of sand, clay, water and bitumen. Oil sands that deposit within 65 meters deep are mined, but more than 80% of total reserves in Alberta are buried deep underground, requiring an efficient recovery method to produce (Butler, 1997). Bitumen has high viscosity under reservoir conditions, making it hard to flow. However, bitumen viscosity is highly sensitive to temperature and drops substantially from several million centipoises to less than 10 centipoises when it is heated to 500 K from reservoir temperature (Mehrotra and Svrcek, 1986).

There are many thermal recovery methods proposed regarding to bitumen production. Steam-assisted gravity drainage (SAGD) is a widely used method (Farouq Ali, 2003). SAGD is a matured in situ thermal recovery technology in bitumen production (Butler et al., 1981; Butler and Stephens, 1981; Butler, 1994; Butler, 1997; Reis, 1992; Akin, 2005; Sharma and Gate, 2010; Li and Chen, 2015). It takes advantage of the high sensitivity of bitumen viscosity to temperature. In SAGD, there are two parallel horizontal wells with a vertical interval of 5-10 meters locating at the bottom of a reservoir. Steam at saturation temperature (i.e., wet steam) is injected through the upper well, creating a steam chamber in the reservoir above the wells. The latent heat carried by injected steam increases reservoir temperature. High temperature decreases bitumen viscosity, making bitumen mobile and flow downwards to the lower production well under gravity. Then, bitumen is produced to the surface.

To improve energy efficiency and decrease the amount of steam injected, co-injection of steam and solvent is proposed later (Nasr et al., 2003; Gupta et al., 2005; Gupta and Gittins, 2006), such as expanding-solvent steam-assisted gravity drainage (ES-SAGD). Dilution of solvent in oil phase further decreases oil phase viscosity and enhance bitumen production. Operation strategies and optimization methods focusing on the choice of solvent and solvent injection concentration have been proposed (Keshavarz et al., 2015a; Keshavarz et al., 2015b; Ardali et al., 2010; Gates and Gutek, 2008). ES-SAGD and other solvent-assisted SAGD are more complicated than SAGD in terms of oil recovery mechanisms. However, they have been pilot tested and implemented by several companies in Alberta, such as Cold Lake SA-SAGD Experimental Pilot project by Imperial Oil Resources and Conoco Surmont ES-SAGD project by ConocoPhillips Canada Resources Corporation.

Exploitation of bitumen by SAGD has many environmental concerns, such as high consumption of energy and water, greenhouse gas emission, and tailing management. various aspects. Because high temperature wet steam is continuously injected into reservoir, a large amount of energy and water is consumed to produce steam. As a result of combustion during steam generation, massive greenhouse gas is produced. Tailing management is one of the most severe environmental challenges facing the oil sands industry. Tailings which are composed of solids and chemical compounds are a by-product of bitumen extraction. It will pollute water and harm habitats of wild animals if it is not treated properly. Additionally, there are also possibilities of accidents in SAGD. In 2006, a catastrophic release of steam occurred in a Total project, which made a large hole of 125m×75m on the surface (ERCB, 2010).

SAGD is often divided into three stages: chamber-rising stage, sideway-expanding stage and depletion stage (Butler et al., 1981; Chung and Butler, 1988; Edmunds et al., 1994). Before the start of operation, in order to achieve heat communication between injection well and production well, there is a preheat period when continuous steam circulates in the horizontal well pairs. After preheating, steam is injected into reservoir and steam chamber starts to expand upward during the chamber-rising stage. After a steam chamber reaches the top of the reservoir, it is the sideway expanding stage of SAGD. During this stage, steam chamber begins to expand in sideway. Most analytical models are developed to describe bitumen production during the sideway-expansion stage, which is also the focus of this research.

Analytical studies have been conducted to gain a general understanding of bitumen production and evaluate production performance in SAGD. Many different analytical models have been developed to analyze various aspects of SAGD. Butler's model is the first systematic model that analytically reflects SAGD production.

Butler's first model (Butler et al., 1981) uses the combination of material balance and Darcy's law to calculate production rate. Chamber-edge temperature is assumed to be a constant value along the chamber edge, which can be viewed as the implicit assumption regarding energy balance in Butler et al. (1981). Butler et al. (1981) showed a concave interface of a SAGD chamber. Also, its bottom moves away from the production well, and its top expands to infinity. The chamber geometry of Butler et al. (1981) is not reasonable according to observations and simulation results (Butler and Stephens, 1981; Butler, 1997). There is a constant of 2.0 in the final expression of his model. This constant 2.0 comes from derivation. It is because oil flow rate is linear with the square root of elevation in the derivation of Butler et al. (1981).

To fix the bottom of interface to the production well, Butler and Stephens (1981) proposed a modified model named "Tandrain". They tried to solve the problem of chamber edge bottom moving away from production well by simply changing chamber shape with a new constant 1.5 instead of 2.0 in the previous derivation, without making fundamental changes in the derivation. Later, Butler (1994) assumed the interface remained straight from the bottom to the top and modified the previous model. He assumed there is a point on the edge of a steam chamber where heat transfer ahead of the interface is under steady-state. The location of this point is chosen where production rate is maximum. With these assumptions, the constant is changed to 1.3. Although calculated production rate is reduced by decreasing the constant 2.0 to 1.5 to 1.3, this "Lindrain" model still overestimates production rate. As will be discussed in this research, Butler's unreasonable chamber shape comes from the assumption that steam chamber edge temperature (T_e) is constant along the chamber edge. Butler's equations do not consider energy balance explicitly, and the constant T_e dictates the concave edge with the bottom being detached from the production well. Hence, the implicit assumption regarding energy balance made by a constant T_e determines the chamber shape of Butler.

Another widely-used model was developed by Reis (1992). He assumed an inverted-triangle steam chamber, which has been widely accepted in the literature (Chung and Butler, 1988; Butler, 1994; Akin, 2005; Bharatha et al., 2005; Edmunds and Peterson, 2007; Miura and Wang, 2012; Zargar and Farouq Ali, 2016). Use of an inverted-triangle steam chamber is not only reasonable based on the literature (Chung and Butler, 1988; Rabiei Faradonbeh et al., 2016a), but also a pragmatic way to reflect complicated energy balance in SAGD operations. Global material balance based on the assumed linear edge of a steam chamber is coupled with Darcy's law to calculate bitumen-production rate. Reis' model increased the accuracy for prediction of bitumen-production rate in comparison with Butler's models (Butler et al., 1981; Butler and Stephens, 1981; Butler,1994), but it still overestimates bitumen-production rate (Sharma and Gates, 2010; Mojarad and Dehghanpour, 2016).

Although Reis' assumption of a linear edge of a steam chamber improved the accuracy of calculation of bitumen-production rate, he assumed a constant temperature along the steam chamber from the bottom to the top. As will be shown in this research, this is a mathematical inconsistency; that is, a linear edge of a steam chamber requires temperature to vary along the edge. Furthermore, Reis' assumption that the chamber edge is at injected-steam temperature is shown to be higher than what is analytically required. The derivation of Reis' model requires inconsistent use of local and global material balance, as will be shown in this research.

Various prior models added different considerations by making various modifications, such as a modified fluid model, consideration of multiphase flow and temperature dependence of reservoir properties, to the aforementioned two models: Butler et al. (1981) and Reis (1992). These models are discussed below.

Previous studies are based on dead bitumen. Bharatha et al. (2005) studied the issue of dissolved gas and explained the increased production rate. Based on Butler's model (1994), Bharatha (2005) modified fluid model with consideration of dissolved gas in reservoir in the calculation of dead bitumen saturation and oil phase flow rate. Dissolved gas in oil phase is dependent on temperature. The ignorance of temperature variation along the edge and varying temperature distribution ahead of steam chamber at different elevation will cause inaccurate calculation of oil flow rate.

Multiphase flow is ignored in Butler's (Butler et al., 1981; Butler and Stephens, 1981; Butler, 1994) and Reis' (1992) models. Sharma and Gates (2010) considered multiphase flow by adding a relative permeability distribution ahead of chamber edge to Butler (Butler et al., 1981). This modification improves the accuracy of calculation of oil flow rate, resulting in better prediction of oil production rate. However, except for more accurate Darcy's law, they only considered local material balance in the differential element on the chamber edge, without accounting for global material balance and varying temperature along the chamber edge. Thus, there is still deviation in calculation results.

In order to further revise Sharma and Gates' (2010) model, Li and Chen (2015) also considered the multiphase flow effect on oil flow rate. They used a different oil saturation distribution ahead of chamber edge in their model and improved the accuracy of prediction. However, they did not consider the variable fluid properties along the steam chamber edge caused by varying temperature distribution along the chamber edge. Different temperature will lead to different oleic phase properties, thus resulting in different saturation distribution in different elevation.

Emulsion of water and oil is not considered in Butler's (Butler et al., 1981). Emulsion will increase oil phase viscosity and ignorance of this effect will overestimate oil production rate.

Mojarad and Dehghanpour (2016) considered the effect of emulsion on oil flow during drainage and proposed a new fluid model with the consideration of the effect of emulsion on oil phase viscosity. They incorporated this fluid model into Butler's (Butler et al., 1981) model and obtained a new equation for oil production rate. However, the variation in oil phase properties, especially viscosity, caused by varying temperature distributions ahead of chamber edge is not considered in their models, causing deviation in the calculation results.

Reservoir properties are changing with temperature. However, this variation is ignored in all previous models. The following two analytical models investigate in the change of porosity and thermal conductivity in the SAGD respectively.

Cokar et al. (2013) discussed thermal expansion in SAGD production. In SAGD, steam carrying a large amount of heat is injected into reservoir. Reservoir temperature rises. Due to thermal expansion of reservoir rock, porosity will decrease, leading to a change in absolute permeability. This will make prior models inaccurate. Cokar et al. (2013) improved the analytical model by taking this thermal expansion of reservoir rock into consideration. They defined a changing porosity that is dependent on temperature and a changing absolute permeability that is dependent on porosity. They incorporated this changing permeability into Butler's model (Butler et al., 1981). Since the change in absolute permeability is caused by thermal expansion of rock, temperature is important in this model. Moreover, they also did not consider varying chamber edge temperature and different temperature distribution ahead of chamber edge. This ignorance will impair their model's accuracy.

Irani and Cokar (2016) discussed thermal properties used in analytical model in SAGD and their dependence of temperature. They stated that thermal conductivity changes with temperature and proposed a model with thermal conductivity expressed as a function of temperature. Although their study did not consider the chamber edge temperature changing with elevation, their study emphasized the importance of accurate temperature description in SAGD analytical model. The varying chamber edge temperature proposed in this thesis will give a more accurate temperature distribution at different elevation inside reservoir.

There are also some analytical models that are modification of Reis' model (1992).

In the previous analytical models, the effects steam distillation and asphaltene deposition on bitumen viscosity are not considered. Akin (2005) corrected the calculation of bitumen viscosity under different temperature and pressure by providing a new fluid model with the consideration of the existence of asphaltene content in the oil. As the concentration of asphaltene in oil increases, viscosity increases. With the corrected viscosity table of bitumen, Akin (2005) followed the derivation of Reis. Darcy's law and global material balance are combined in order to solve for production rate. Unlike Reis used a maximum chamber edge moving velocity in the heat conduction equation, Akin (2005) used the same heat conduction equation as Butler's (Butler et al., 1981). Compared to Butler's (Butler and Stephens, 1981) and Reis' (1992) model, Akin's model (2005) improved the calculation results of production rate. However, as bitumen viscosity and asphaltene concentration in oil change with temperature, failure of considering temperature variation along the edge can not reflect oil flow viscosity ahead of steam chamber, resulting in inaccurate production rate.

In previous analytical models, heterogeneity of reservoir is ignored, but real reservoirs are heterogeneous. Azad and Chalaturnyk (2010) discussed permeability heterogeneity inside reservoir by using geomechanical modelling. Permeabilities of flow at different angles are different due to the unequal vertical and horizontal permeability. Azad and Chalaturnyk (2010) calculated permeability of oil phase flow when it flows at different directions and incorporated this new permeability into Reis' model (1992). They improved the accuracy of Reis' model (1992). However, the variable chamber edge temperature along the edge is still not considered, making this model flawed.

Zargar and Farouq Ali (2016) discussed two different ways to model SAGD process: constant volume displacement and constant heat injection. Their constant volume displacement approach proposed a new parameter named front velocity which is used to describe the temperature profile front movement. Instead of using the chamber advancing velocity in heat conduction equations in Butler's and Reis' models, they used this front velocity in their model to obtain temperature profile ahead of chamber edge. They incorporated this temperature distribution ahead of steam chamber into Reis's model (1992) and gained better calculation results. However, the use of this constant front velocity at different elevation can not describe the varying temperature distribution ahead of steam chamber which is caused by different chamber moving velocity and chamber edge temperature. Thus, the model can not describe the oil properties and flow rate ahead of the chamber edge accurately.

Unlike all aforementioned models concerning about flow and material balance, Zargar and Farouq Ali's (2016) tried to calculation production rate from energy aspect and they presented their second approach of constant heat injection based on energy balance in SAGD. They controlled the energy injection rate and calculated the amount of oil that can be produced under this rate from energy balance. However, this approach depends on the calculation of heat, which is determined by temperature. Failure to consider temperature variation along the chamber edge leads to inaccurate calculation of heat inside reservoir, thus inaccurate production rate calculation.

Moreover, there are studies into solvent-assisted-SAGD (SA-SAGD). In SA-SAGD, solvent is co-injected with steam to further decrease bitumen viscosity and enhance production. Bitumen viscosity will decrease due to the comprehensive effect of temperature increase and solvent dilution in oleic phase, resulting in higher production rate. Thus, solvent distribution is another important topic in the analysis of SA-SAGD. The existence of solvent will decrease chamber edge temperature and cause more varying chamber edge temperature along the interface. Because temperature and solvent dilution in oleic phase are interdependent, the ignorance of varying chamber edge temperature is more significant in SA-SAGD.

When solvent is co-injected to the reservoir, its concentration in the oil phase determines oil phase viscosity. Gupta and Gittins (2012) proposed an equation to include solvent concentration in oleic phase. They proposed an exponential distribution of solvent concentration ahead of steam chamber as a result of solvent-dilution process. They modified fluid model with consideration of solvent and incorporated it into Butler's model (Butler and Stephens, 1981). Their model can better mimic the drainage of oil and solvent in SAGD. However, as solvent concentration in oil phase is affected by temperature. Because temperature varies along the edge of a steam chamber, solvent concentration varies along the edge. Failure of this consideration of variation makes the calculation of production rate and solvent distribution ahead of steam chamber inaccurate.

Rabiei Faradonbeh et al. (2016a; 2016b) discussed two models to describe ES-SAGD production, i.e., steady state model and unsteady state model. In their steady state model, they extended Reis' model (1992) by assuming steady state temperature and solvent distribution ahead of steam chamber edge. Their results also supported the assumption of linear steam chamber edge under steady state. However, they failed to consider the variable chamber edge temperature in the analytical model and this leaded to inaccurate description of oil flow ahead of steam chamber.

In their unsteady state model, they found that the interface between steam chamber and reservoir became concave under unsteady temperature and solvent distribution in both SAGD and SA-SAGD. However, he did not consider the lower chamber edge temperature in the top reservoir.

This resulted in a more concave calculated chamber edge shape in SAGD in this model. Without consideration of lower chamber edge temperature in the top of reservoir, the advancing velocity of chamber edge in the top is overestimated, resulting in the curved shape. That is similar to Butler's first analytical model (Butler et al., 1981) with concave steam chamber edge.

In summary, temperature variation along the edge of a steam chamber is ignored in all previous analytical models, which does not match field observation and simulation results (Sheng, 2013).

Heat transfer in the reservoir is assumed one-dimensional heat conduction under quasi-steady state. This assumption is not always accurate in the SAGD process. Butler (1985) analyzed solution for the quasi-steady state temperature distribution for two limiting cases: when steam chamber edge is advancing at a constant velocity and when steam chamber edge is stationary. He stated that the actual temperature distribution was between these two limiting situations and proposed a simple approximation between them. Kesharvarz et al. (2016) also discussed this problem and applied it to analyze the rise of steam chamber during ramp-up stage. Their work indicates that the inaccurate temperature distribution ahead of steam chamber will cause calculation deviation in production rate.

Sharma and Gates (2010) analyzed the heat transfer process at the chamber edge and stated that heat transfer is not only by heat conduction but also by heat convection. They proposed a temperature distribution expression based on heat conduction and convection. Validation shows that their equation gives better results compared with simulation results.

However, for the simplicity of the developed model in this thesis, quasi-steady state heat conduction is applied to the analytical model. Deviation caused by this assumption will be further addressed in sensitivity analysis in section 3.3.3.

Steam-oil ratio (SOR) is an important parameter used in efficiency and economic evaluation of SAGD production. It describes the amount of steam in cold water equivalent (CWE) needed to produce a certain amount of bitumen. Low SOR means high energy efficiency and vice versa. Different enhancement and optimization methods have been proposed to decrease SOR in SAGD production.

Butler (1987) calculated cumulative steam-oil ratio (CSOR) for the first time. In Butler's calculation, heat required for SAGD production is segregated into following parts: heat to raise steam chamber temperature, heat to raise produced oil temperature, heat lost to overburden and heat stored in the reservoir ahead of steam chamber. An average chamber advancing velocity is used to calculate heat needed for the reservoir ahead of the edge of a steam chamber.

Edmunds and Peterson (2007) also calculated CSOR for SAGD production. In their calculation, they used cumulative heat loss to a semi-infinite plane by Carslaw and Jaeger (1959) to calculate the heat loss to overburden. They also asserted that the summation of heat needed for the reservoir ahead of the edge of a steam chamber and heat loss below production well equals to one-third of heat loss to overburden. Unlike Butler's way of calculating cumulative oil production, they used Reis' inverted triangle-shape steam chamber assumption to calculate. Miura and Wang (2012) modified Edmunds and Peterson (2007) by proposing an improvement for residual oil saturation calculation.

Keshavarz et al. (2016) calculated CSOR in the similar way for ramp-up stage of SAGD as Butler. Vertical rising velocity of steam chamber in this stage is assumed constant which equals to the average vertical growth velocity before it reaches overburden rock.

Reis (1992) calculated SOR by considering heat loss to overburden rock, heat required for chamber expansion and heat for the reservoir ahead of the edge of a steam chamber. Heat produced by oil production is not considered in his calculation. To calculate the steam injection rate based on energy balance instead of calculating the cumulative heat injection, every part of calculation needs to take derivative of time. Because steam chamber edge temperature in Reis' model is constant, temperature distributions ahead of steam chamber are the same at different elevations, which is not the real case according to field observations and simulations (Sheng, 2013). Reis' calculation of production and heat is not accurate. Thus, the calculation results of SOR in Reis' are inaccurate.

Irani and Cokar (2016) also investigated into SOR calculation. They asserted that heating caused by sub-cool, which is the temperature difference between injection temperature and producer temperature, equals to the heat loss to underlying formation. Thus, heat loss to the underlying formation is not considered in this section.

1.2 Problem Statement

The previous section described various analytical studies of SAGD. Most of them are based on either the derivation of Butler (Butler et al., 1981) or Reis (1992). Butler's original model (Butler et al., 1981) is mathematically correct under the assumptions made. One of the assumptions is that temperature along the edge of a steam chamber is uniformly set to the temperature of the injected steam at the operating pressure. However, the unrealistic chamber geometry of Butler (Butler et al., 1981) indicates that significant overestimation of bitumen-production rate by his model may be related to the implicit assumption regarding energy balance provoked by the constant chamber-edge temperature. Based on simulation results and field observation (ConocoPhillips, 2008; JACOS, 2012; Shell, 2008; Sheng, 2013), chamber-edge temperature is unlikely constant when the chamber shape is an inverted triangle. Considering the primary importance of temperature for bitumen production in SAGD, Butler's model is not expected to be a solid foundation for any additional physics (e.g., multiphase flow) for reliable estimation of bitumen production in SAGD.

The other group of analytical studies of SAGD is based on Reis (1992). Although the assumption of an inverted-triangle chamber has been well accepted in the literature, the derivation has inconsistency between the assumed chamber geometry and chamber-edge temperature; that is, a steam chamber cannot be an inverted triangle if temperature along the chamber edge is uniform at the injected-steam temperature. In the literature, however, no research has presented how temperature should vary along the edge of an inverted-triangle chamber. No previous analytical model considered variable chamber-edge temperature. Hence, fluid properties along the chamber edge was treated as they were under the same condition along the edge.

There are a few obvious reasons for temperature to vary along the chamber edge. One is that non-condensable gas accumulates in the upper part of a seam chamber due to the effect of gravity. This non-condensable gas can be methane in the original bitumen, and also light components of the injected solvent in the ES-SAGD. Accumulation of non-condensable gas in the upper part of a chamber tends to reduce temperature (Keshavarz et al., 2015a). Sheng (2013) mentioned that there would be non-condensable gas accumulation in the top of a SAGD chamber.

Another reason is heat loss to overburden rocks (i.e., a heat sink). A steam chamber usually has a large contact area with overburden rocks. A substantial amount of heat is transferred to the overburden, which lowers the temperature near the top of a SAGD chamber.

Temperature, in turn, affects how fluid properties vary along the chamber edge through thermodynamic equilibrium, especially oleic-phase composition along the chamber edge. Dissolution of water and non-condensable gas in the oleic phase helps decrease bitumen viscosity and enhance bitumen production (Venkatramani and Okuno, 2016). Coupled effects of temperature and solvent dilution on oleic-phase viscosity enhance bitumen recovery in ES-SAGD. Not considering compositional variation causes inaccurate calculation of fluid properties.

Therefore, there is a critical need to understand how temperature varies along the edge of a steam chamber, and its impact on bitumen-production rate and SOR. Even for the simple chamber geometry of an inverted-triangle, no paper has been published on temperature variation along the linear chamber edge. Analytical solution of SAGD requires many other simplifying assumptions commonly regarding phase distribution, heat conduction, and flow dimensionality. As discussed in the previous section, various researchers attempted to correct for them. However, such efforts should be made on the basis of mathematically correct solution for temperature under the assumed chamber geometry.

1.3 Research Objectives

The first main objective of this research is to analytically investigate temperature variation along the edge of an inverted-triangle steam chamber for SAGD. Analytical solutions are presented for oil-flow rate, temperature, and composition along the edge of a steam chamber as functions of elevation for a given bitumen production rate at a given operating pressure. Since this research is based on commonly-used assumptions after Butler (Butler et al., 1981; Butler and Stephens, 1981; Butler, 1994) and Reis (1992), a unified way to derive different models is presented.

The second main objective is to investigate under what conditions the analytical solution is more accurate. To this end, simulation studies are conducted to determine under what conditions the assumptions made for the analytical solution are more accurate. This will clarify which assumptions are simplistic or reasonable among the traditional set of assumptions for SAGD after Reis (1992) and Butler (Butler et al., 1981; Butler and Stephens, 1981; Butler, 1994). The research will also provide a method to use the analytical solutions to estimate bitumen-production rate and SOR accurately for a representative temperature for a given time for a given SAGD operation. Objectives are summarized below.

1. Present analytical solutions for oil-flow rate, temperature, and composition along the edge of an inverted-triangle SAGD chamber for a given bitumen production rate and pressure.
2. Present analytical models for bitumen-production rate and SOR for SAGD with an inverted-triangle chamber.

3. Present a unified way to derive different models proposed for SAGD in the literature. Prior models can be shown as special cases of the general model presented.
4. Compare the new analytical models with prior models in terms of bitumen-production rate and SOR on the basis of simulation cases, including the following field cases: ConocoPhillips Surmont project, JACOS Hangingstone project, and Shell Hilda Lake project.
5. Clarify under what conditions traditional assumptions made for SAGD are reasonable or simplistic.
6. Clarify which assumptions are simplistic or reasonable among those assumptions commonly used for analytical solutions for SAGD. There are mainly four factors analyzed: two-phase flow, oil-phase flow direction, temperature distribution ahead of chamber edge, and maximum chamber-edge advancing velocity.

1.4 Structure of Thesis

This thesis is composed of five chapters. The first chapter gives an overview of this thesis. Review of related publications, description of the problems discussed in this thesis and statement of major research objectives are presented.

Chapter 2 describes the analytical model developed. All assumptions and equations used in the analytical model are explained in detail in this section. A step-wised procedure of application of developed model is provided for the convenience of later calculations. Then, the developed model is applied for SOR calculation. The SOR-calculation method of Reis (1992) is improved in this research, in which assumptions made by Reis (1992) are replaced with the corresponding ones made in this research. Since there are a smaller number of assumptions made in the developed model, prior models can be reproduced from the developed model with additional assumptions made in other models. Reproduction and discussion of prior models are included Chapter 2.

In Chapter 3, the developed model is applied to twelve different fine scale simulation cases under various conditions. Simulation cases in this chapter have different permeabilities, different amounts of methane in live bitumen, different water dissolution and water compressibility. Calculations are performed to validate the developed model, including production rate, chamber-edge temperature distribution, and SOR. Based on flash calculation, the oleic-phase composition can be obtained from the chamber-edge temperature calculated. Calculation results are compared with simulation results.

In addition, four factors affecting the accuracy of the developed model in production rate and chamber-edge temperature are discussed: two-phase flow, flow direction, temperature distribution ahead of the chamber edge, and maximum chamber-edge advancing velocity. Different criteria are proposed to evaluate the effect of each parameter on the accuracy of developed model. Analyses conducted in different simulation cases at different time are compared. SOR-calculation results in different simulation cases are discussed.

Chapter 4 is for validation of the developed model by use of SAGD field data. Three field cases, Surmont project, Hangingstone project and Hilda Lake project, are used in this chapter. Reservoir properties and related parameters are from filed data. Calculations show that the developed model gives more accurate production rate than all previous models.

Chapter 5 summarizes the contents of all previous chapters and gives conclusions of this research. Future research is also suggested in this chapter.

CHAPTER 2 THEORY

This chapter presents a general derivation of bitumen-production rate and steam-oil ratio for SAGD on the basis of the class notes for “Thermal Methods in Heavy Oil Recovery” (Okuno, 2015). Previous equations, such as Butler’s and Reis’ equations, are shown as special cases of the general derivation.

This research focuses on the second stage of SAGD; i.e., side-way expansion. At this stage, a steam chamber has reached the ceiling of the reservoir, and expands sideway. Production rate in this stage is relatively stable in comparison with the other two stages, which are chamber-rising stage and depletion stage. Since the majority of oil production takes place during this sideway-expansion stage, this is the most important stage in terms of oil production in SAGD.

2.1 Analytical model for SAGD production

The model presented in this section consists of the following:

- Local material balance applied to a cross section perpendicular to the edge of a steam chamber
- Darcy’s law applied to the oil phase flowing along the chamber edge
- Global material balance applied to the entire reservoir.

Figure 2.1 shows a schematic for the chamber geometry assumed, which is identical to Reis (1992). Only half of a steam chamber is analyzed. The assumptions used in this section are commonly used in the literature (Butler, 1994; Reis, 1992; Akin, 2005; Bharatha et al., 2005; Edmunds and Peterson, 2007; Miura and Wang, 2012; Zargar and Farouq Ali, 2016), and are summarized below:

1) A steam chamber is an inverted triangle with its vertex fixed at the production well
2) One-dimensional flow parallel to the edge of a steam chamber
3) Homogeneous, isotropic reservoir
4) No chemical reaction
5) No interaction between fluid and rock
6) Incompressible oil
7) Laminar flow
8) Negligible capillary pressure
9) Vapor-phase flow parallel to the edge of a steam chamber is negligible
10) Density of vapor phase is negligible in comparison with that of oil phase

11) Constant permeability to the oil phase ahead of the edge of a steam chamber

12) 1-D quasi-steady state heat conduction through the moving interface of a steam chamber

13) Heat losses to under and overlaying formation rocks.

Local material balance for the oil phase flow for a cross-section perpendicular to the edge is

$$\frac{d}{dt}\int_0^{\infty}\int_0^{\Delta y} \varphi S_o \, dy d\xi + \int_0^{\infty}\int_0^{\Delta y} \frac{\partial}{\partial l} U_o dy d\xi = 0, \quad (2.1)$$

where φ is porosity, ΔS_o represents the mobile oil saturation, which equals to the difference between oil saturation initially inside the reservoir and residual oil saturation. Δy is the unit length along the horizontal production well, $d\xi$ is the unit length in the ξ direction, which is perpendicular to the edge of a steam chamber. U_o is the Darcy velocity for the oil phase flowing along the chamber edge.

Equation (2.1) can be written as follows after integration:

$$-\varphi \Delta S_o U \Delta y + \partial q_o / \partial l = 0, \quad (2.2)$$

where U is the advancing velocity of the chamber edge, q_o is the oil-flow rate, and the l coordinate points upward parallel to the edge of a steam chamber. That is, in the notation of this thesis, q_o is negative when the oil phase flows downward parallel to the edge.

The angle between the steam-chamber edge and the horizontal line is defined as θ ($\neq 0$), which decreases as bitumen is produced. Dividing Equation (2.2) by $\sin\theta$,

$$-\varphi \Delta S_o v \Delta y + \partial q_o / \partial z = 0, \quad (2.3)$$

where v is the advancing velocity of the interface measured in the horizontal direction at elevation z, which is the vertical distance from the production well.

1-D Darcy's law for the oil and vapor phase along the chamber edge is

$$U_o = -(k k_{ro}/\mu_o)(\partial P_o/\partial l + \rho_o g \sin\theta), \quad (2.4)$$

$$U_g = -(k k_{rg}/\mu_g)(\partial P_g/\partial l + \rho_g g \sin\theta), \quad (2.5)$$

where μ_o and μ_g are dynamic viscosity of the oil and vapor phase respectively, k is the absolute permeability of reservoir, k_{ro} and k_{rg} are relative permeability for the oil and vapor phase respectively, P_o and P_g are pressure of oil and vapor phase respectively, ρ_o and ρ_g are density of oil and vapor phase respectively. k_{ro} is assumed to be constant, according to assumption 11 (unity in this research).

Rearranging Equation (2.4) by defining $\Delta\rho = \rho_o - \rho_g$.

$$U_o = -(k k_{ro}/\mu_o)(\partial P_o/\partial l + \rho_g g \sin\theta + \Delta\rho g \sin\theta). \quad (2.6)$$

According to assumptions 8 and 9, from Equation (2.5) and Equation (2.6), oil-flow rate can be written as

$$U_o = -(kk_{ro}/\mu_o)\Delta\rho g \sin\theta. \tag{2.7}$$

According to assumption 10, $\Delta\rho = \rho_o$. According to assumption 11, k_{ro}=1. Thus, the above equation is rearranged as

$$U_o = -k\rho_o g \sin\theta/\mu_o = -kg\sin\theta/\nu_o, \tag{2.8}$$

where ν_o is the kinematic viscosity of oil.

Integrating oil flow rate in Equation (2.8) over the cross-section considered in the direction normal to steam chamber edge, the production rate at a particular elevation is

$$q_o = \int_0^{\xi_L} U_o \Delta y d\xi = -\int_0^{\xi_L}(kg\sin\theta/\nu_o)\Delta y d\xi = -kg\sin\theta\,\Delta y \int_0^{\xi_L}(1/\nu_o)d\xi. \tag{2.9}$$

"I_o" is defined as

$$I_o = \int_0^{\xi_L}\frac{1}{\nu_o}d\xi, \tag{2.10}$$

where ξ_L is the distance from steam chamber edge to the intersection point of its perpendicular and production layer. Unlike Butler's model, the integration of the right-hand side of I_o is not from zero to infinite. According to Figure 2.1, it is integrated in the normal direction from the chamber edge to the elevation of the production well.

In addition, calculation of "I_o" requires distribution of oil phase kinematic viscosity ahead of chamber edge. Because kinematic viscosity changes with temperature, temperature profile ahead of steam chamber edge is required. Assumptions of conduction-only heat transfer inside reservoir and quasi-steady state of steam chamber expansion give the following temperature distribution (Carslaw and Jaeger, 1959),

$$(T - T_R)/(T_e - T_R) = \exp(-U\xi/\alpha) = \exp(-\xi v \sin\theta/\alpha), \tag{2.11}$$

where T_e is the local chamber-edge temperature, U is the local chamber-edge advancing velocity in the normal direction, α is the thermal diffusivity of reservoir. Thermal diffusivity is determined by the composition of heat transfer media, i.e., the reservoir. As operation goes on, fluid composition ahead of chamber edge is changing with time and position. However, it is assumed constant in the analytical model. The value of thermal diffusivity used here is the thermal diffusivity of the reservoir fully saturated with the original reservoir fluid.

Using Equation (2.11) in the developed analytical model gives

$$T_{(\xi,z)} = T_R + \left[T_{e(z)} - T_R\right]\exp\left[-\xi v_{(z)}\sin\theta/\alpha\right], \tag{2.12}$$

where v is the horizontal advancing velocity of the edge of a steam chamber at a given elevation z.

Using Equation (2.12), I_o can be written in terms of temperature, instead of the spatial variable of ξ. Based on Equation (2.12), Equation (2.10) is rewritten as:

$$I_o = (1/U)\int_{T_{L(z)}}^{T_{e(z)}} \alpha/[\nu_o(T - T_R)]\,dT, \quad (2.13)$$

where T_L is the temperature at ξ_L where ξ intersects with the elevation of the production well. According to Figure 2.1, $\xi_L = z/\cos\theta$. Substitution of this into Equation (2.12) gives T_L at various elevations as follows:

$$T_{L(z)} = T_R + \left[T_{e(z)} - T_R\right]\exp\left[-v_{(z)} z\tan\theta/\alpha\right]. \quad (2.14)$$

Let us define a dimensionless variable, τ, as follows:

$$\tau_{(z)} = UI_o = \int_{T_{L(z)}}^{T_{e(z)}} \alpha/[\nu_o(T - T_R)]\,dT. \quad (2.15)$$

Darcy's law is written as

$$vq_o + kg\tau\Delta y = 0. \quad (2.16)$$

The final step of the derivation is to combine the material balance, Equation (2.3), and Darcy's law, Equation (2.16), and to satisfy the global material balance specific to the assumed chamber geometry (i.e., assumption 1). Using Equations (2.3) and (2.16),

$$\frac{\partial {q_o}^2}{\partial z} = -2\varphi\Delta S_o kg\tau(\Delta y)^2. \quad (2.17)$$

The chamber-edge advancing velocity in the horizontal direction is linear with respect to elevation z as follows:

$$v = zv_{max}/H = v_{max}z_D, \quad (2.18)$$

where v_{max} is the maximum chamber advancing velocity in the horizontal direction and it equals to the horizontal advancing velocity at the top of steam chamber; H is the vertical distance between the reservoir top and the production well; and dimensionless elevation z_D is defined as $z_D = z/H$.

Using Equations (2.16) and (2.18), the following expression of τ can be obtained:

$$\tau = -v_{max}z_D q_o/(kg\Delta y). \quad (2.19)$$

Substituting Equation (2.19) into Equation (2.17),

$$\frac{\partial q_o}{\partial z} = \varphi\Delta S_o v_{max} z_D \Delta y. \quad (2.20)$$

Integration of Equation (2.20) gives,

$$q_{o(z)} = \varphi\Delta S_o v_{max}\Delta y z^2/(2H) + C, \quad (2.21)$$

where C is the constant of integration.

Expansion of a steam chamber results in a decrease in the amount of oil left in the reservoir. Hence, a bitumen production rate ($q_{oil\text{-}prod}$) equals to the rate at which the volume of a steam chamber increases (the global material balance). This is shown for a half of the reservoir as follows:

$$q_{o(z=0)} = C = -\varphi \Delta S_o H v_{max} \Delta y/2 = -q_{oil-prod}. \tag{2.22}$$

The negative sign for $q_{oil\text{-}prod}$ arises due to the notation used for Darcy's law that q_o is positive in the upward direction along the edge of a steam chamber. Substituting Equation (2.22) into Equation (2.20),

$$q_{o(z)} = -\varphi \Delta S_o H \Delta y v_{max}(1 - z_D^2)/2 = (1 - z_D^2) q_{o(z=0)}. \tag{2.23}$$

Substituting Equation (2.22) into Equation (2.19),

$$\tau = \varphi \Delta S_o H {v_{max}}^2 z_D (1 - {z_D}^2)/(2kg). \tag{2.24}$$

Let us define τ_D as follows:

$$\tau_D = \tau/\left[\varphi \Delta S_o H {v_{max}}^2/(2kg)\right] = z_D(1 - {z_D}^2). \tag{2.25}$$

How τ_D changes with z_D is shown in Figure 2.2.

Eliminating v_{max} in Equation (2.24) by using Equation (2.22),

$$\tau = 2 z_D (1 - {z_D}^2) {q_{oil-prod}}^2/(kg\varphi \Delta S_o H \Delta y^2). \tag{2.26}$$

Rearranging Equation (2.26),

$$q_{oil-prod} = \sqrt{\tau k g H \varphi \Delta S_o \Delta y^2/\left[2(1 - {z_D}^2) z_D\right]}, \tag{2.27}$$

where $\tau_{(z)} = UI_o = \int_{T_{L(z)}}^{T_{e(z)}} \alpha/[\nu_o(T - T_R)]\, dT$. The negative solution for $q_{oil\text{-}prod}$ was discarded. Equation (2.27) is obviously independent of z_D because of the global material balance, Equation (2.22), within the current derivation based on the assumptions listed previously. That is, Equation (2.27) describes the consistency to be satisfied among the variables and assumptions used; in particular, the relationship between the vertical profile of temperature, $T(z_D)$, and production rate, $q_{oil\text{-}prod}$.

A steam chamber is assumed to be an inverted triangle in this analytical model. Chung and Butler (1988) showed that this was reasonable based on the Hele-Shaw and sandpack laboratory models. An inverted-triangle chamber was also used in many prior analytical models (Butler, 1994; Reis, 1992; Akin, 2005; Bharatha et al., 2005; Edmunds and Peterson, 2007; Miura and

Wang, 2012; Zargar and Farouq Ali, 2016). In real SAGD operations, however, it is unlikely that the vertical cross section of a steam chamber is an inverted triangle. Later in this thesis, calculation results indicate that this assumption can be a reasonable approximation in relatively-homogeneous bitumen reservoirs.

Other steam chamber shapes can also be implemented into this analytical model by substituting Equation (2.18) which expresses chamber-advancing velocity at different elevations. Solution for the three major equations with other steam-chamber shapes can also give production rate and temperature along the edge of a steam chamber accordingly.

Moreover, the linear chamber edge requires variable temperature along the edge of a steam chamber. If temperature is constant as in Butler's model (Butler et al., 1981), steam-chamber edge becomes S-shaped, which unreasonably expands to infinity at the top and moves away from the production well in the bottom.

One application of the results above is to obtain $\tau(z_D)$ for a given $q_{oil\text{-}prod}$ by use of Equation (2.26), and then obtain $T_e(z_D)$ by use of Equation (2.15). It is also possible to uniquely determine the composition of the oil phase at the edge of a steam chamber as a function of z_D if the fluid system consists of bitumen, water, and one non-condensable gas (i.e., methane). This is because the phase transition at the chamber edge (between two and three phases) is uniquely determined for a fixed temperature and pressure for a ternary fluid system. In other words, oil phase composition and temperature are interdependent for a given operating pressure for such a ternary system. As will be shown in next chapters in detail, however, the resulting $T_e(z_D)$, and therefore oleic phase composition, does not satisfactorily follow results observed in numerical simulations due to a few simplistic assumptions required in the derivation. These assumptions are briefly discussed below.

There are heat losses to the overburden and underlying formation rocks in reality. Heat loss to the overburden is large in SAGD, due to the large contact area between a high-temperature steam chamber and overburden rock. Therefore, the one-dimensional quasi-steady state temperature distribution ahead of the chamber edge is inaccurate near the top of the reservoir.

Although the heat loss to underlying formation is relatively small, the quasi-steady state heat conduction assumption is not accurate in the bottom of reservoir. This is because steam chamber advancing velocities in the bottom of reservoir are low. The quasi-steady state temperature distribution ahead of chamber edge will become inaccurate with a nearly stationary interface (Butler, 1985; Keshavarz et al., 2016).

The main motivation for the derivation of Equation (2.27) is to address the question as to at what elevation the analytical solution is most accurate. Application of the analytical solution to numerical simulation results is expected to clarify at which elevation the representative chamber-edge temperature should be obtained that is most consistent with the classical set of assumptions for SAGD. Note that previous researchers used the injected-steam temperature as the representative chamber-edge temperature applied to global material balance.

As will be shown later, the analytical solution is expected to be most accurate when T_e is taken near the middle elevation, z_D=0.5. This is conceivable because the one-dimensional quasi-steady state assumption used to obtain temperature distribution ahead of the steam-chamber edge is expected to be more accurate in the middle of the reservoir, in comparison with near the top and bottom. Validation cases will show that this method can provide much improved predictions of oil production rate compared to previous models, such as Butler's and Reis', if τ in the middle of the reservoir is used.

A step-wise description of the algorithm that calculates the oil production rate based on the new theory is given below.

1. Obtain the properties of the reservoir and bitumen, such as reservoir thickness (H), reservoir width (Δy), reservoir temperature (T_R), operation pressure (P), permeability (k), mobile oil saturation (ΔS_o), porosity (φ), thermal diffusivity (α), a relationship between temperature and bitumen kinematic viscosity, and steam chamber edge temperature in the middle of the steam-chamber edge (T_e).
2. Set T_L to T_R at the midpoint.
3. With the T_e taken from the middle elevation, use Equation (2.15) to calculate the value of τ for z_D = 0.5.
4. Substitute the result of τ at the midpoint into Equation (2.27), and calculate the oil production rate, $q_{oil\text{-}prod}$.
5. Use the calculated $q_{oil\text{-}prod}$ to calculate a new T_L according to Equation (2.14), Equation (2.18) and Equation (2.22). Use the new T_L to calculate $q_{oil\text{-}prod}$ by repeating aforementioned steps. If the new $q_{oil\text{-}prod}$ equals to previous value (e.g., deviation less than 1.0 m^3/day),

continue to the next step; if $q_{oil\text{-}prod}$ is different from previous value, use the new $q_{oil\text{-}prod}$ and repeat this step.

6. Substitute the oil production rate into Equation (2.26) and solve for $\tau(z_D)$. Then, solve Equation (2.15) for the chamber edge temperature, T_e, at various elevations. This gives $T_e(z_D)$.
7. Perform flash calculations to calculate the amount of methane in the L phase of three-phase equilibrium at the operation pressure and T_e. This gives the amount of methane in the oleic phase along the chamber edge.

In step 7, the system is assumed to contain three components: water, bitumen and methane. On the steam-chamber edge, the system is under three-phase equilibrium. According to the phase rule, degree of freedom in this system is two since there are three components and three phases. Based on the assumption that pressure is constant in the steam chamber, temperature will uniquely determine the composition in the three phases.

2.2 Application of developed model for SOR calculation

The heat injected mainly goes to four parts: heat carried by produced oil (Q_{PO}), heat loss to the overburden formation rocks (Q_{OB}), heat inside a steam chamber (Q_{SC}), and heat ahead of a steam chamber (Q_{AC}). Derivation of SOR shown here is based on a half of a steam chamber, which is the same as the derivation of production rate in Chapter 2.1. Because a steam chamber is assumed to be an inverted triangle, it has a large contact area with the overburden rocks at a high temperature of the steam chamber. This causes a large amount of heat loss to the overburden rock. However, temperature on the interface between the reservoir and underlying formation is relatively low; hence, there is a limited heat loss to the underlying formation. In addition, the cooling in the liquid pool at the bottom of a steam chamber due to sub-cool equals to the amount of heat loss to underlying formation (Irani and Cokar, 2016). Thus, heat loss to underlying formation rocks is omitted in the calculation (Reis, 1992; Irani and Cokar, 2016; Keshavarz et al., 2016; Zargar and Farouq Ali, 2016).

Instantaneous SOR can be calculated by the following energy balance equation:

$$Q'_{inj} = Q'_{SC} + Q'_{AC} + Q'_{OB} + Q'_{PO}, \tag{2.28}$$

where Q'_{inj} is the injection rate of latent heat carried by the injected steam in J/s; Q'_{SC} is the rate of heat required for chamber expansion in J/s; Q'_{AC} is the rate of heat used for the reservoir ahead of the edge of a steam chamber in J/s; Q'_{OB} is the rate of heat loss to the overburden formation in J/s; and Q'_{PO} is the rate of heat carried by produced bitumen in J/s. The sensible heat of hot water is not considered under the assumption that the heat carried by the produced hot water is equal to the sensible heat of the injected steam.

Q'_{SC} can be calculated by the increasing rate of heat inside the steam chamber. Heat inside the half steam chamber used here is

$$Q_{SC} = 0.5M_R(T_S - T_R)W_S H\Delta y, \quad (2.29)$$

where W_S is the width of the top (ceiling) of the half steam chamber, M_R is the volumetric heat capacity of reservoir. Thus, the rate Q'_{SC} can be expressed as

$$Q'_{SC} = dQ_{SC}/dt = 0.5M_R(T_S - T_R)(dW_S/dt)Hdy = 0.5M_R(T_S - T_R)v_{max}H\Delta y. \quad (2.30)$$

To obtain Q'_{AC}, the heat stored in the reservoir ahead of the edge of a steam chamber is calculated.

$$d^2Q_{AC} = M_R(T - T_R)d\xi dl\Delta y, \quad (2.31)$$

where dl is the unit length in the upward direction along the edge of a steam chamber. Then, a temperature distribution ahead of a steam chamber is obtained by the one-dimensional quasi-steady state conduction. According to Carslaw and Jaeger (1959), it is expressed as

$$(T - T_R)/[T_{e(z)} - T_R] = \exp[-U_{(z)}\xi/\alpha] = \exp(-\xi v_{max} z_D \sin\theta/\alpha). \quad (2.32)$$

Substitution of Equation (2.32) into Equation (2.31) yields

$$d^2Q_{AC(z)} = M_R[T_{e(z)} - T_R]\exp(-\xi v_{max} z_D \sin\theta/\alpha)d\xi dl\Delta y. \quad (2.33)$$

Equation (2.33) can be integrated from $\xi = 0$ to the level of the production well in the perpendicular direction, as follows:

$$dQ_{AC(z)} = M_R[T_{e(z)} - T_{L(z)}]\alpha dl\Delta y/(v_{max} z_D \sin\theta). \quad (2.34)$$

The unit length of the steam-chamber edge, dl, can be expressed as $dl = dz/\sin\theta$. Hence, Equation (2.34) becomes

$$dQ_{AC(z)} = M_R[T_{e(z)} - T_{L(z)}]\alpha dz\Delta y/(v_{max} z_D \sin^2\theta)\,. \quad (2.35)$$

To obtain Q_{AC}, Equation (2.35) is integrated in terms of elevation, z, as shown in Figure 2.1. The temperature at the edge of a steam chamber (T_e) varies with z. To simplify the calculation in this research, T_e is considered constant for a layer of one-meter thickness when Equation (2.35) is integrated over the reservoir thickness, H. Thus, Q_{AC} is expressed as a summation of the heat residing ahead of a steam chamber for each one-meter layer with the corresponding T_e. Thus, integration of Equation (2.35) yields

$$Q_{AC}=\sum_{i=1}^{N_L} M_R\left[T_{e(z)}-T_{L(z)}\right]\alpha h_i\Delta y/(v_{max}z_D\sin^2\theta), \tag{2.36}$$

where N_L is the number of one-meter layers, and h_i is set to one meter in this thesis.

Then, Q'_{AC} is

$$Q'_{AC}=dQ_{AC}/dt=-\sum_{i=1}^{N_L} 2M_R\left[T_{e(z)}-T_{L(z)}\right]\alpha h_i\sin^{-3}\theta\cos\theta\Delta y/(v_{max}z_D)\,(d\theta/dt). \tag{2.37}$$

According to the linear geometry assumed for a steam chamber, the angle between the steam chamber edge and horizontal line can be expressed as

$$\theta=\arctan(H/W_S). \tag{2.38}$$

Therefore,

$$d\theta/dt=-Hv_{max}/\left(H^2+W_S{}^2\right). \tag{2.39}$$

Substitution of Equation (2.39) into Equation (2.37) gives

$$Q'_{AC}=\sum_{i=1}^{N_L} 2M_R\left[T_{e(z)}-T_{L(z)}\right]\alpha h_i\Delta y/(z\tan\theta). \tag{2.40}$$

The heat loss to the overburden (Q_{OB}) is given by

$$Q_{OB}=-\alpha M_{over}\int_0^{W_S}\left.\frac{dT}{dz}\right|_{z=H}(t-\sigma)dW\Delta y, \tag{2.41}$$

where M_{over} is volumetric heat capacity of the overburden formation, σ is the time since the steam zone reached a specific width, t is the time since the commencement of operation, α is the thermal diffusivity of the reservoir, and $\left.\frac{dT}{dz}\right|_{z=H}$ can be obtained according to the one-dimensional unsteady state heat transfer equation of Carslaw and Jaeger (1959). The temperature at the bottom of the overburden formation ($T_{ceiling}$) is equal to the temperature at the contact area between the steam chamber and overburden formation. It is assumed that $T_{ceiling}$ is constant all over the contact area in the deviation. Then,

$$\begin{aligned}Q_{OB}&=2M_{over}\left(T_{ceiling}-T_R\right)\sqrt{\alpha/\pi}\int_0^{W_S}\sqrt{(t-\sigma)}\,dW\Delta y\\&=(4/3)M_{over}\left(T_{ceiling}-T_R\right)\sqrt{\alpha/(\pi v_{max})}\,W_S^{\frac{3}{2}}\Delta y.\end{aligned} \tag{2.42}$$

The heat-loss rate to overburden (Q'_{OB}) is

$$Q'_{OB}=dQ_{OB}/dt=2M_{over}\left(T_{ceiling}-T_R\right)\Delta y\sqrt{\alpha v_{max}W_S/\pi}. \tag{2.43}$$

When it is reasonable to assume $T_{ceiling}$ to be the steam-chamber temperature (T_S), Equation (2.43) becomes

$$Q'_{OB}=2M_{over}(T_S-T_R)\Delta y\sqrt{\alpha v_{max}W_S/\pi}. \tag{2.44}$$

The amount of heat carried by the produced oil is:

$$Q'_{PO} = q_o(T_S - T_R)M_o, \quad (2.45)$$

where q_o is the oil production rate and can be obtained by the analytical model presented in this thesis. M_o is the volumetric heat capacity of the produced oil. The temperature of the produced oil is assumed to be T_S.

The relationship between the rate of the injected steam (CWE, cold water equivalent in m^3/s), q_S, and the rate of the heat provided can be expressed as

$$q_s = Q_{inj}'/(\rho_w L_s x), \quad (2.46)$$

where ρ_w is the volumetric density of water, L_S is the latent heat carried by the injected steam in J/kg and x is steam quality.

In summary, steam injection rate can be calculated by combining the above equations as:

$$\begin{aligned} q_s = [1/(\rho_w L_s x)]\{&0.5M_R(T_S - T_R)v_{max}H\Delta y \\ &+ \sum 2M_R\left[T_{e(z)} - T_{L(z)}\right]\alpha h\Delta y/(z\tan\theta) \\ &+ 2M_{over}\left(T_{ceiling} - T_R\right)\Delta y\sqrt{\alpha v_{max}W_S/\pi} \\ &+ q_{prod}(T_S - T_R)M_o\}. \end{aligned} \quad (2.47)$$

$$SOR = q_s/q_{oil-prod}. \quad (2.48)$$

2.3 Reproduction and discussion on prior models

In the developed model, UI_o, which is defined as τ in the derivation, is varying with elevation for the following reasons. First, based on the linear chamber edge assumption, local chamber edge advancing velocity changes in linear relationship with elevation. Second, chamber edge temperature is variable along the edge. These two variables result in varying temperature distribution ahead of the edge. Additionally, the length of cross-section elements ahead of steam chamber edge for integration for τ (Equation 2.15) is changing with elevation. Thus, the accuracy of local material balance is improved, and the developed model gives more-accurate results.

However, in all prior models, τ is implicitly assumed to be constant. Prior models, including Butler's and Reis', are reproduced based on the developed model with additional assumptions made in their analytical models. Then, this section illustrates the reasons why they often give inaccurate results.

2.3.1 Butler's models

Butler substantially contributed to systematic understanding of bitumen production in SAGD. Butler's theory of SAGD covered many aspects of SAGD, including production rate and steam-oil ratio.

In Butler et al. (1981), the temperature at the edge of a steam chamber was assumed to be the injected steam temperature (T_S). Darcy's law was integrated from the edge of a steam chamber to infinity. Consequently, τ_B was implicitly assumed to be constant with elevation.

τ_B in Butler et al. (1981) is defined in Equation (2.49), similarly to Equation (2.15), except for different integration ranges.

$$\tau_B = UI_o = U\int_0^\infty \frac{1}{\nu_o} d\xi = \int_{T_R}^{T_S} \alpha/[\nu_o(T - T_R)]\, dT. \tag{2.49}$$

In addition, for bitumen, kinematic viscosity changes with temperature (Mehrotra and Svrcek, 1986) and Equation (2.50) shows the expression of how kinematic viscosity changes with temperature.

$$\nu_s/\nu_o = [(T - T_R)/(T_S - T_R)]^m, \tag{2.50}$$

where ν_s is the kinematic viscosity of bitumen at injected steam temperature, T_R is the original reservoir temperature, T_S is injected steam temperature, m is a constant describing how bitumen viscosity changes with temperature. The value of m is specific to fluid sample and it is around 3-4 for heavy oil. In this thesis, the following method is applied to calculate the constant "m."

Temperature and oleic phase viscosity in the grid blocks outside of steam chamber are output from simulation results. All the data are used to fit the above equation and the value of "m" can be obtained.

With the help of Equation (2.50) and Equation (2.11), calculation of τ_B can be simplified as

$$\tau_B = UI_o = \alpha/m\nu_S. \quad (2.51)$$

Substituting τ_B into Equation (2.17) and integrating Equation (2.17) in terms of elevation, z.

$$q_o{}^2 = -2\varphi\Delta S_o kg\tau_B(\Delta y)^2 z + C, \quad (2.52)$$

where C is the constant of integration; i.e., $q_{o(z=0)}{}^2 = C$.

Production rate $q_{oil\text{-}prod}$ is

$$q_{oil-prod}{}^2 = q_o{}^2{}_{(z=0)} - q_o{}^2{}_{(z=H)} = 2\varphi\Delta S_o Hkg\tau_B(\Delta y)^2.$$

$$q_{oil-prod} = \sqrt{2\varphi\Delta S_o Hkg\tau_B}\Delta y = \sqrt{2\varphi\Delta S_o Hkg\alpha/(m\nu_S)}\,\Delta y. \quad (2.53)$$

From Equation (2.52),

$$q_{o(z=0)}{}^2 = 2\varphi\Delta S_o Hkg\tau_B(\Delta y)^2 = C. \quad (2.54)$$

Substituting Equation (2.54) into Equation (2.52),

$$q_o{}^2 = 2\varphi\Delta S_o kg\tau_B(\Delta y)^2(H - z) \quad (2.55)$$

Thus,

$$q_{o(z=0)} = -\sqrt{2\varphi\Delta S_o kg\tau_B(H - z)}\Delta y = -\sqrt{2\varphi\Delta S_o kg\tau_B H(1 - z_D)}\Delta y \quad (2.56)$$

Dimensionless oil flow rate is

$$q_D = \sqrt{1 - z_D}, \quad (2.57)$$

where $q_D = q_o/q_{o(z=0)}$. Figure 2.3 shows how dimensionless flow rate changes with elevation. Using Equation (2.16) and Equation (2.56) to calculate steam chamber shape as

$$v = -\,kg\tau_B\Delta y/q_o = \sqrt{kg\tau_B/[2\varphi\Delta S_o H(1 - z_D)]}. \quad (2.58)$$

Dimensionless chamber edge advancing velocity is

$$v_D = 1/\sqrt{1 - z_D} \quad (2.59)$$

where $v_D = v/v_{(z=0)}$. Figure 2.4 shows how dimensionless chamber advancing velocity changes with elevation which also reflects the steam chamber shape.

Equation (2.59) and Figure 2.4 show that steam chamber advancing velocity is not in linear relationship with elevation, which will result in a non-linear chamber edge as shown in Figure 2.4. This is the reason for the curved interface obtained in Butler et al. (1981). In other words, use of

τ_B that is constant with z results in Butler's concave interface (Figure 2.4). The bottom of this concave interface moves away from production well and its top reaches to infinity, which is unlikely in reality.

To make a correction for the unreasonable interface of a steam chamber, Butler and Stephens (1981) modified the bottom of the steam chamber edge to a tangential line to the production well. This modification was named as the "Tandrain" model. With this modification, the constant "2.0" in Equation (2.56) was replaced by 1.5. Furthermore, Butler (1994) proposed the "Lindrain" model, and replaced "1.5" with "1.3." This was to convert the concave top of the steam chamber edge to a linear line. These modifications increased accuracy of his models, but fundamental problems in the derivation were not clarified.

Butler's models usually overestimate production rate, as demonstrated in the next chapter and in the literature (Sharma and Gates, 2010; Li and Chen, 2015). The temperature at the edge of a steam chamber was assumed to be constant at the injected steam temperature, which resulted in higher temperature in the top of the reservoir and higher oil flow rate. Moreover, the integration of oil flow in Butler's models is from the chamber edge to infinity, i.e., Equation (2.49). The overestimation in oil production also comes from this range of integration. In the top of the reservoir, there is a large space ahead of a steam chamber; hence, the integration can be performed from the chamber edge to infinity. However, there is a limited heated zone, where bitumen is heated and flows under gravity, ahead of a steam chamber in the middle and bottom of the reservoir. Then, the integration should be conducted within the heated zone, the range of which varies with elevation.

In addition, energy balance in his model is not accurate, which can be seen from the concave chamber shape. The constant steam temperature as chamber edge temperature is a result of energy balance. He ignored heat loss to overburden that causes lower chamber edge temperature in the top of the reservoir. This ignorance leads to the fast advancing chamber at the top, making the steam chamber expends to infinity in the concave shape of Butler's model.

2.3.2 Reis' model

In Reis' model (1992), steam chamber is assumed an inverted triangle. Applying global material balance to reservoir:

$$q_{o(z=0)} = -\varphi \Delta S_o H v_{max} \Delta y/2, \tag{2.60}$$

where v_{max} is the maximum chamber edge advancing velocity in the horizontal direction and $v_{max} = dW_S/dt$.

In Chapter 2.1, it is known that Darcy's law applied globally gives Equation (2.16) as follows:

$$vq_o + kg\tau\Delta y = 0. \tag{2.16}$$

This equation is assumed to be

$$v_{max}q_o + kg\tau_R\Delta y = 0, \tag{2.61}$$

where τ_R is the τ used in the reproduction of Reis' model (1992).

Combining Equation (2.60) and Equation (2.61) gives:

$$q_{o(z=0)}{}^2 = \varphi\Delta S_o Hkg\tau_R(\Delta y)^2/2. \tag{2.62}$$

Thus,

$$q_o = -\sqrt{\varphi\Delta S_o Hkg\tau_R/2}\Delta y. \tag{2.63}$$

However, Equation (2.60) is somewhat inconsistent because the value of v and q_o in the equation are taken from two different elevations:

$$q_{o(z=0)} = -\,\varphi\Delta S_o Hv_{(z=H)}\Delta y/2. \tag{2.60}$$

So is Equation (2.61) as:

$$v_{(z=H)}q_{o(z=0)} + kg\tau_R\Delta y = 0. \tag{2.61}$$

The inconsistency in these equations requires that τ_R

$$\tau_R = \alpha/(am\nu_S) = \tau_B/a, \tag{2.64}$$

where a =0.4. Equation (2.64) shows that τ_R is constant.

Putting Equation (2.64) into Equation (2.63) and rearranging the equation gives

$$q_o = -\sqrt{\varphi\Delta S_o Hkg\,\alpha/(2am\nu_S)}\,\Delta y. \tag{2.65}$$

Reis' model overestimates oil production rate (Sharma and Gates, 2010; Li and Chen, 2011). The overestimation mainly comes from the following reasons.

1) Chamber edge temperature, T_e, is assumed equal to steam temperature, T_S, along the interface.
2) Integrations of Darcy's law ahead of steam chamber are all from chamber edge to infinity.

Besides, Reis' model contains the mathematical inconsistency as described above.

2.3.3 Zargar and Farouq Ali's model

Zargar and Farouq Ali (2016) presented two approaches to calculation of production rate during the depletion stage of SAGD. In their first method called "Constant Volumetric

Displacement," they introduced a new parameter named "front velocity" to describe the movement of the steam-chamber edge.

They considered that the temperature front of T_S is moving at a constant velocity in the normal direction with respect to the steam-chamber edge at each time step. In Figure 2.5, the temperature front is initially at the steam-chamber interface (AP). It advances in the horizontal direction without rotation. That is, it moves from AP, to CD, and finally to BE at the front velocity U_f. The movement of the temperature front and that of the steam chamber edge should be equivalent to each other. Based on their assumption of an inverted triangle-shape steam chamber, the chamber expansion is achieved by the rotation of a chamber edge with its bottom being fixed at the production well. The area covered by this movement of the steam-chamber edge, the triangle ABP as shown in Figure 2.5, should be the same as the area covered by the movement of the temperature front, the parallelogram ACDP in Figure 2.5. Thus, the front velocity can be expressed as

$$U_f = v_{max} \sin\theta/2. \quad (2.66)$$

Thus, the quasi-steady state temperature distribution in the reservoir ahead of a steam chamber at all elevation is given as

$$(T - T_R)/(T_S - T_R) = \exp(-U_f \xi/\alpha) = \exp(-\xi v \sin\theta/2\alpha), \quad (2.67)$$

which is different from Equation (2.11) used in this research.

Applying the above equation to Darcy's law,

$$q_o = kg \sin\theta\, \Delta y \int_0^\infty (1/\nu_o) d\xi = kg \sin\theta\, \tau/U_f, \quad (2.68)$$

where τ_Z is defined as

$$\tau_Z = U_f \int_0^\infty 1/\nu_o\, d\xi. \quad (2.69)$$

Solution for oil flow rate by combing the above Darcy's Law with global material balance yields

$$q_o = \Delta y \sqrt{kg\varphi \Delta S_o H \tau_Z}. \quad (2.70)$$

In addition, using Equation (2.50) which expresses the relationship between bitumen kinematic viscosity and temperature to solve for τ_Z gives:

$$\tau_Z = \alpha/(m\nu_{os}). \quad (2.71)$$

Therefore, the oil production rate given by Zargar and Farouq Ali (2016) is

$$q_o = \Delta y \sqrt{kg\varphi \Delta S_o H \alpha/(m\nu_{os})}. \quad (2.72)$$

Although they noticed that chamber advancing velocity is changing along the chamber edge due to the assumption of an inverted-triangle chamber, they used a constant front velocity to replace the chamber edge advancing velocity in their calculation. This constant front velocity results in the temperature distribution ahead of the chamber edge that is constant with elevation. Additionally, constant steam chamber edge temperature is assumed here. That is, τ_Z is constant with elevation as in all previous analytical models. The integration of flow in the reservoir ahead of a steam chamber was conducted from the interface to infinity at all elevations, which is not always accurate.

In addition, they also provided another approach called the "Constant Heat Injection" method. The difference between these two approaches is how they obtain a temperature distribution ahead of the steam-chamber edge. Instead of using a front velocity to calculate temperature distribution, they used energy balance to calculate a temperature distribution in the reservoir.

$$Q'_R = Q'_{inj} - \left(Q'_{sz} + Q'_L\right) = -K_R A\left(\frac{dT}{d\xi}\right)_{\xi=0}, \tag{2.73}$$

where K_R is the thermal conductivity of reservoir and A is the interface area.

Also, temperature gradient at the chamber edge was a function of maximum advancing velocity of steam chamber (v_{max}). By setting steam injection rate constant, which means constant injection heat, they back-calculated the corresponding temperature distribution ahead of a steam chamber and maximum chamber edge advancing velocity (v_{max}). Oil production rate was obtained by global material balance as

$$q_{o(z=0)} = -\varphi \Delta S_o H v_{max} \Delta y/2. \tag{2.22}$$

Although this method is novel and different from other analytical models, it did not consider variable temperature along the chamber edge.

2.3.4 Sharma and Gates' model

Sharma and Gates (2010) discussed the multiphase flow in the mobile zone ahead of the edge of a steam chamber. Oil relative permeability was properly assumed to be correlated with oil saturation in their model. They assumed a linear relationship between oil saturation and oil relative permeability. Because of this assumption, τ can be expressed as follows based on Equation (2.15) and their modification:

$$\tau_{SG} = \alpha\Gamma(m)\Gamma(a_c+1)/[\nu_{os}\Gamma(m+a_c+1)], \tag{2.74}$$

where $\Gamma(\cdot)$ is gamma function; a_c is a parameter in Corey's coefficient expressing the relationship between relative permeability and oil saturation in the following equation:

$$k_{ro} = k_{rocw}[(1 - S_w - S_{or})/(1 - S_{wc} - S_{or})]^{a_c}, \quad (2.75)$$

where k_{ro} is relative permeability of oleic phase, k_{rocw} is the relative permeability of oleic phase at connate water saturation, S_w is water saturation, S_{wc} is connate water saturation, S_{or} is residual oil saturation.

They used Darcy's Law and local material balance as in Butler's models (Butler et al., 1981), and gave a similar final expression of oil production rate, but with a different expression for τ. Replacement of τ_B with τ_{SG} in Equation (2.56) can give the Sharma and Gates' equation as:

$$q_o = \sqrt{2\varphi\Delta S_o Hkg\tau_{SG}}\Delta y = \sqrt{2\varphi\Delta S_o Hkg\,\alpha\Gamma(m)\Gamma(a_c + 1)/[\nu_{os}\Gamma(m + a_c + 1)]}\,\Delta y. \quad (2.76)$$

Although two-phase flow was considered in their model with detailed saturation distribution ahead of a steam chamber, they did not change temperature and the integration range for τ along the chamber edge.

2.3.5 Gupta and Gittins' model

Gupta and Gittins (2012) modified Butler's Tandrain model by considering the diffusion of solvent in SA-SAGD production. They proposed that solvent distribution ahead of steam chamber can be expressed as

$$C_s = C_R + (C_e - C_R)\exp(-U\xi/D), \quad (2.77)$$

where C_s stands for solvent concentration; C_R is the solvent concentration in the original reservoir; C_e is the solvent concentration at the steam chamber edge; D is the solvent diffusion coefficient.

By adding this into analytical model, τ is modified as:

$$\tau_{GG} = UI = U\int_0^{\infty}(1 - C_s)\left(\frac{1}{\nu} - \frac{1}{\nu_R}\right)d\xi. \quad (2.78)$$

In Butler's Tandrain model (Butler and Stephens, 1981), the constant 2.0 in the final expression is replaced by 1.5 for better results. In addition, substituting Equation (2.78) into Equation (2.56) to replace τ_B by τ_{GG} can give the expression of oil flow rate proposed by Gupta and Gittins (2012) by considering solvent diffusion in SA-SAGD as:

$$q_{o(z=0)} = \Delta y\sqrt{1.5\varphi\Delta S_o Hkg\tau_{GG}}. \quad (2.79)$$

They considered the diffusion of solvent in SA-SAGD process that makes calculation of oleic phase mobility more accurate. However, they also failed to consider the varying τ_{GG} along the chamber edge.

2.3.6 Kesharvarz et al.'s model

The quasi-steady state for temperature distribution is a widely used, but simplifying assumption. Butler (1985) and Kesharvarz et al. (2016) discussed unsteady-state heat conduction in SAGD, and proposed an average between the two limiting cases: (i) quasi-steady state where the edge of a steam chamber advances at a constant velocity, and (ii) a stationary edge of a steam chamber. Kesharvarz et al. (2016) used an average value between the two cases, and applied it to the chamber-rising stage of SAGD production before the steam chamber reaches the top of the reservoir.

Butler (1985) proposed a parameter named "heat penetration depth" that is defined as

$$\gamma = \int_0^{\infty} (T - T_R)/(T_S - T_R)\, d\xi. \tag{2.80}$$

Thus,

$$(T - T_R)/(T_S - T_R) = \exp(-\xi/\gamma). \tag{2.81}$$

This equation was used in their derivation, in place of Equation (2.11) that was used for the model developed in this research.

Under the assumption of a pseudo steady state ahead of the steam-chamber edge, γ is

$$\gamma = \alpha/U, \tag{2.82}$$

which is the same as this research.

For the case where a steam-chamber edge is stationary (e.g. at the bottom of the reservoir where the steam chamber edge is attached to the production well), γ is

$$\gamma = 2\sqrt{\alpha t/\pi}, \tag{2.83}$$

where t is the operation time of SAGD production.

In Keshavarz et al.'s model, the steam chamber only grows upward during the chamber-rising stage of production. γ is

$$\gamma = 2\sqrt{\alpha\,(t - t_0)/\pi}, \tag{2.84}$$

where t_o is the time when the steam chamber reaches a certain height.

Combining Equation (2.81) and (2.84) with Equation (2.10) gives

$$I_o = \int_0^\infty \frac{1}{\nu_o} d\xi = a'\gamma/(m\nu_s), \tag{2.85}$$

where a' is a correction factor used by Kesharvarz et al. (2016), and can be obtained by history matching.

Based on Equation (2.9),

$$q_o = -kg \sin\theta\, \Delta y I_o = 2kg \sin\theta\, \Delta y\, a'\sqrt{\alpha\,(t - t_0)/\pi}/(m\nu_s), \tag{2.86}$$

where θ is the inclination angle of a steam chamber during the chamber-rising stage before it reaches the reservoir ceiling. This angle was assumed constant during the chamber-rising stage. Although they analyzed the chamber-rising stage of SAGD, instead of the horizontal expansion stage analyzed in this research, their model can also be reproduced by the general derivation with appropriate modifications and assumptions.

2.4 Summary

This chapter presented an analytical model in SAGD with consideration of variable temperature along the edge of a steam chamber on the basis of Okuno (2015). There are three main equations used in the model: local material balance, global material balance, and Darcy's law. Solution of these equations gives Equation (2.27), which expresses the relationship between chamber-edge temperature and oil-production rate. A new model for calculation of SOR with consideration of variable chamber-edge temperature was also presented.

Also, it was shown that many prior analytical models can be reproduced by the unified method along with relevant assumptions. This will greatly help those who start to learn analytical SAGD models understand the main factors involved in the problem.

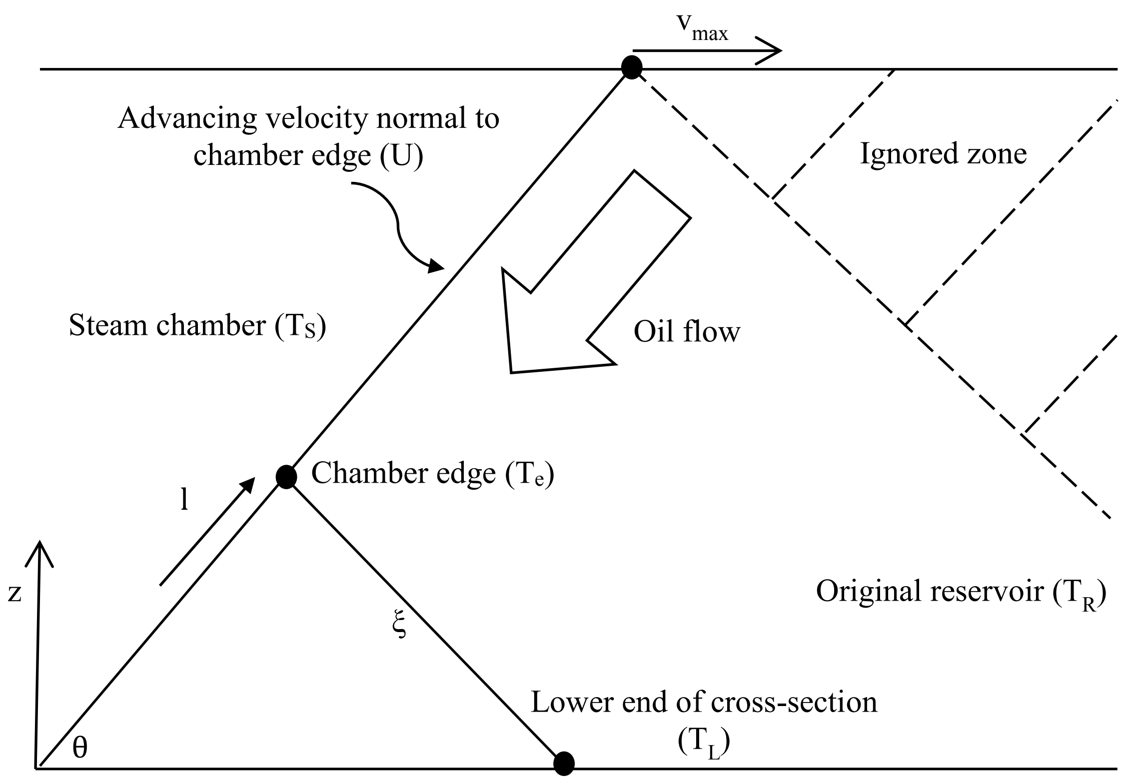

Figure 2.1 Schematic diagram of oil flow along the steam chamber edge in the SAGD process for the developed analytical model.

Steam chamber edge is assumed linear and 1-D oil flow ahead of the edge of a steam chamber is parallel to the chamber edge. There is only 1-D heat conduction through a moving boundary ahead of the edge of a steam chamber.

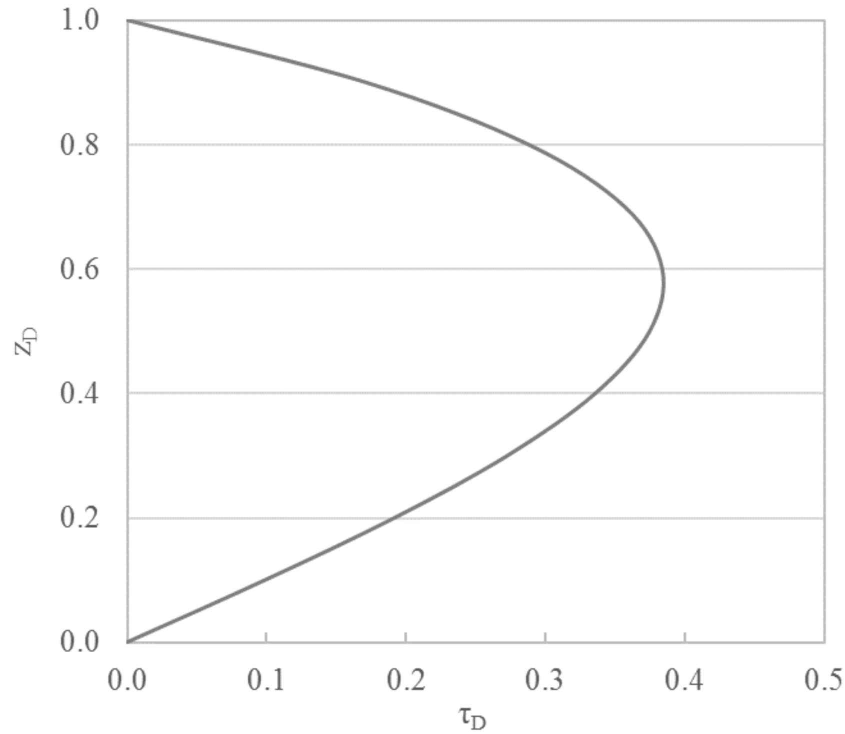

Figure 2.2 Relationship between dimensionless (τ_D) and dimensionless elevation z_D

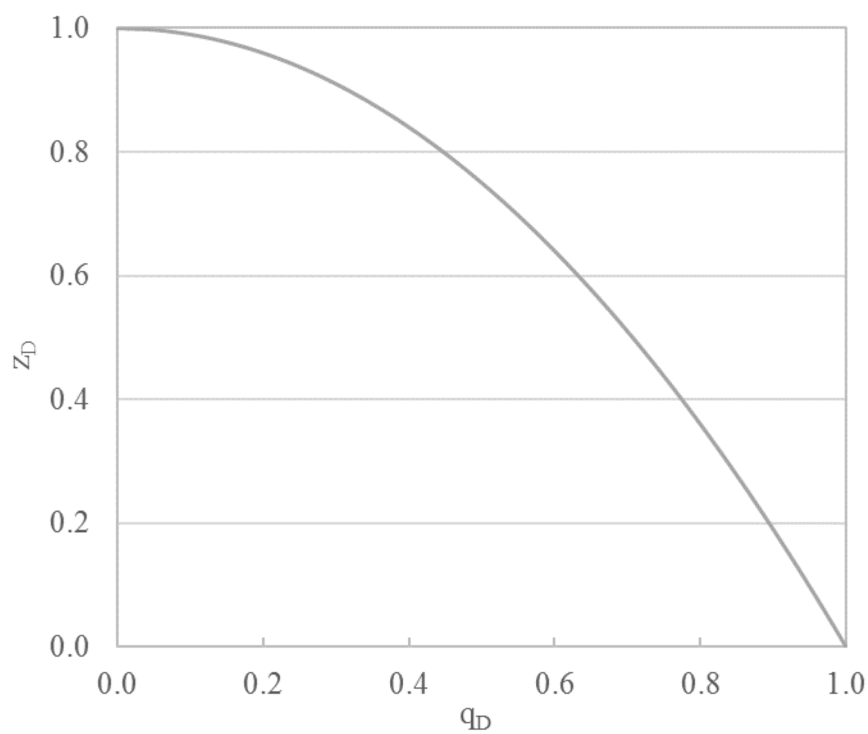

Figure 2.3 Relationship between dimension less oil flow rate (q_D) and dimensionless elevation (z_D)

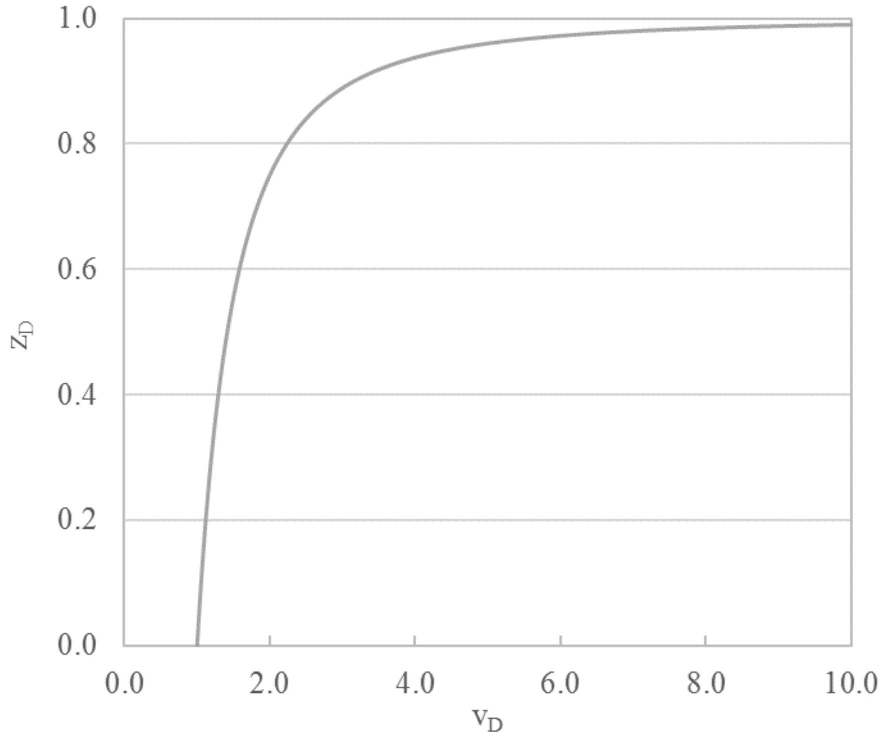

Figure 2.4 Dimensionless steam chamber edge advancing velocity (v_D) changing with dimensionless elevation (z_D) in Butler's model based on reproduction of Butler's model

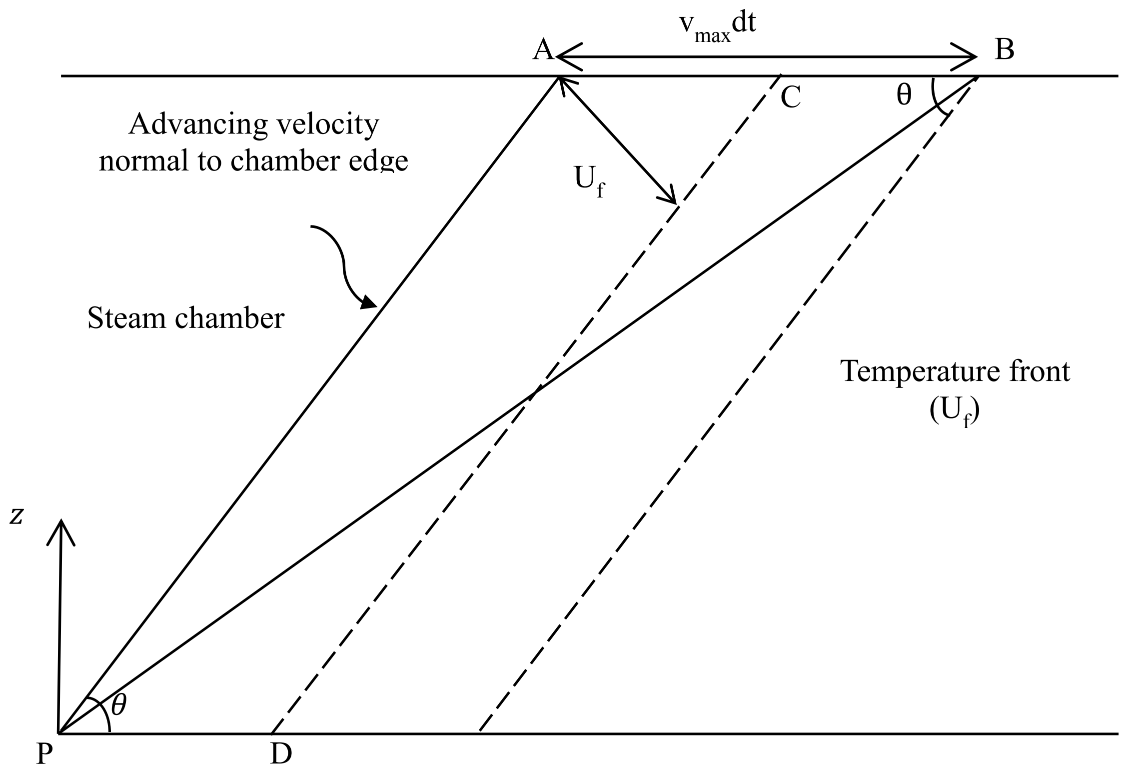

Figure 2.5 Schematic figure for the model of Zargar and Farouq Ali (2016)

CHAPTER 3 VALIDATION AGAINST SIMULATIONS

Chapter 2 showed a new analytical model to describe oil flow along the linear edge of a steam chamber in SAGD, its application for calculation of oil production rate, temperature profile along the chamber edge, and steam-oil ratio. The main purpose of this chapter is to validate the developed analytical model with numerical flow simulations of SAGD. All simulation cases are performed by use of the STARS simulator of Computer Modelling Group (CMG, 2014).

3.1 Introduction

This section contains two parts: introduction of simulation cases, and introduction of calculations of production rate and oil-phase composition along the edge of a steam chamber. The introduction of simulation cases provides all continent information regarding the simulation cases used in this chapter in CMG (2014), such as fluid models, reservoir properties, and operation strategies in all cases. The introduction of calculation includes an explanation of when calculations are conducted in each case, and how to calculate composition of oleic-phase along the edge of a steam chamber with calculated temperature along the edge.

3.1.1 Introduction of simulation cases

In order to validate the developed model, four sets of simulation models with different fluid models are used in this chapter, i.e., live bitumen, dead bitumen, compressible water dissolution in oil, and incompressible water dissolution in oil. In each set of the cases, there are three cases with three different reservoir permeabilities, i.e., 2000 mD, 4000 mD, and 6000 mD.

Tables 3.1, 3.2, and 3.3 summarize the reservoir and fluid properties used for simulation cases in this chapter, which will be explained in this section. In total, 14 cases are presented. Table 3.4 shows a comparison among the 14 simulation cases. Cases 1 and 2 are used to discuss the relationship between steam chamber shape and heat loss to the surrounding formations. The fluid model and reservoir properties are the same with Case 3, except for thermal properties of the surrounding formations.

Cases 3-5 use live bitumen with 10 mol% methane in the original oil. There is no water dissolution in the oleic phase, and water is compressible.

Cases 6-8 use dead bitumen with 0.01 mol% methane in the original reservoir. There is also no water dissolution in the oleic phase, and water is compressible.

Cases 9-14 consider water dissolution in oil. Water in Cases 9-11 are incompressible to be consistent with the assumption that oil phase is incompressible in the analytical model. Water in Cases 12-14 is compressible to see the effect of the water compressibility on simulation results.

There are three components in all simulation cases in this chapter, i.e., methane, bitumen, and water. All properties of three components, including Pc, Tc, ω and BIP, are taken from Kumar and Okuno (2015) and Venkatramani and Okuno (2016), as shown in Table 3.2. The bitumen used in case studies is modeled as a single pseudo component (Kumar and Okuno, 2015; Venkatramani and Okuno, 2016). The use of a single pseudo component to characterize bitumen simplifies phase behavior analysis for calculation of oil-phase composition.

Fluid models are controlled by K-value tables in STARS (CMG, 2014). The K value of a component is defined as the ratio of its concentration in one phase to the other phase. K values are tabulated under different temperature and pressure points, and assumed to be constant with composition in the simulations. There are two kinds of fluid models used in this chapter (Venkatramani and Okuno, 2016); one type used in Cases 1-8 where there is no water dissolution in oleic phase, and the other type used in Cases 9-14 where there is water dissolution in oleic phase. For the former, K values for methane and bitumen are calculated from the PR EOS, while K values for water are from Raoult's law. For the latter, K values for all three components are calculated from the PR EOS.

Viscosities and densities of liquid phase in STARS are calculated using the mixing rules shown below. The mixing rule used for the oleic phase viscosity is

$$\mu_o = \exp\left(\sum x_i \ln\mu_i\right), \tag{3.1}$$

where i={methane, bitumen, water}, μ_o is the viscosity of oleic phase, x_i is the mole fraction of component i in oleic phase, and μ_i is the dynamic viscosity of component i. Table 3.3 shows viscosity of components changing with temperature under the operation pressure of 35 bara.

The mixing rule used for the oleic-phase molar density is

$$1/\rho_o = \sum (x_i/\rho_i), \tag{3.2}$$

where i={methane, bitumen, water}, ρ_o is the molar density of oleic phase, and ρ_i is the molar density of component i. In the derivation, oleic phase is assumed to the incompressible. In order to make the simulation model consistence with the analytical model, bitumen is made incompressible; that is, bitumen density is constant with temperature and pressure. However, methane gas is much more compressible, and making methane-gas density constant is unreasonable. Densities of methane and water change with temperature and pressure in the simulator under the following rule:

$$\rho_i = 19955.7\exp[a_1(P - 1.01325) - a_2(T - 288.15) - 0.5a_3(T^2 - 288.15^2) \\ + a_4(P - 1.01325)(T - 288.15)], \quad (3.3)$$

where $a_1 = 3.85 \times 10^{-5}$, $a_2 = -2.00 \times 10^{-5}$, $a_3 = 8.97 \times 10^{-7}$, $a_4 = 4.79 \times 10^{-7}$ for methane; $a_1 = 0$, $a_2 = -1.674695 \times 10^{-3}$, $a_3 = -1.674695 \times 10^{-3}$, $a_4 = 0$ for water. According to this equation, methane density increases with increasing temperature under a constant pressure. Under the reservoir pressure, 35 bara, oleic-phase density equals to 992.64 kg/m^3 at steam saturation temperature, while it equals to 979.88 kg/m^3 at initial reservoir temperature. The change in oleic phase density caused by compressible methane is only 1.3%, which is deemed negligible. Therefore, use of Equation 3.5 is effective for modeling the compressible methane gas, while keeping the live oil essentially incompressible.

Reservoir properties are the same in all simulation cases except for permeability. Validation of the developed analytical model requires that the simulation cases to be compared are reasonably close to the assumptions made for the analytical model. For all simulation cases in this chapter, reservoirs are set to be homogeneous and isotropy. These case studies only simulate a half of the steam chamber. Dimensions of the simulation models are 70.0 × 37.5 m × 20.0 m in the x, y, and z directions, respectively. There are 140 × 1 × 20 grid blocks in the x, y, and z directions, respectively. The injection well is situated at the 14th layer from the top, while production well is at the 18th layer from the top in the reservoir. Both wells are located on the left edge of the reservoir model. Reservoir temperature and pressure are initially at 286.15 K and 15 bara for all simulation cases in this chapter.

In all cases in this chapter, the two-phase relative permeability models used are based on Corey's model, but are two X-shape straight lines. That is, relative permeabilities are in linear relationship with saturation as given below.

$$k_{rw} = k_{rwio}\,(S_w - S_{wc})/(1 - S_{wc} - S_{or}), \quad (3.4)$$

$$k_{ro} = k_{rocw}\,(1 - S_w - S_{or})/(1 - S_{wc} - S_{or}), \quad (3.5)$$

where k_{rw} is relative permeability of water phase, k_{rwio} is the relative permeability of water phase at irreducible oil saturation, k_{ro} is relative permeability of oleic phase, k_{rocw} is the relative permeability of oleic phase at connate water saturation, S_w is water saturation, S_{wc} is connate water saturation, and S_{or} is residual oil saturation.

The X-shape relative permeability curves are used because actual relative permeability curves for bitumen reservoirs are not well known. Therefore, this type of simplified relative permeability has been used in prior SAGD simulation studies (Sasaki, et al., 2001; Mojarad and Dehghanpour, 2016). The initial oil saturation and residual oil saturation are set to 0.75 and 0.13, respectively. In addition, the relative permeability curves used in the simulation do not change with temperature.

Operation strategy are the same in all simulation cases. At the beginning of SAGD production, reservoirs are pre-heated for six months before the start of production with both injection and production wells being closed. At the beginning of the 7th month, the injection and production wells are open. Steam of 90% quality is injected into the reservoir through the injection well at the saturation temperature 515.71 K at 35 bara. The operating pressure for all cases are 35 bara. The maximum and minimum BHP for the injection wells are 35 bara and 15 bara, respectively.

Additional constraints are set for the production well. The minimum bottom hole pressure is 15 bara, which equals to the initial reservoir pressure. The maximum surface liquid rate for the producer is 200 m^3/day. The maximum steam rate for the producer is 1.0 m^3/day to limit the production of steam. Table 3.1 lists all pertinent reservoir properties used in the simulation cases. Surrounding formation rocks have the same properties as those of reservoir rock and there is heat loss to both overburden and underlying formation rocks.

To obtain a linear steam-chamber edge in the simulation results as assumed in the analytical model, the effect of heat loss on steam chamber shape is discussed here. As mentioned before, Case 1-3 have the same fluid model and reservoir properties. However, heat loss to the surroundings is different. Case 1 only has heat loss to the overburden formation, and the overburden formation has the same thermal properties as reservoir rock. There is no heat loss to the surrounding formations in Case 2. Case 3 has heat loss to both overburden and underburden formations, and the surrounding formations have the same thermal properties as reservoir rock.

Figure 3.1 shows steam chamber shapes of different simulation cases. It shows that simulation Case 3 with heat loss to surrounding presents a linear steam chamber edge. Moreover, the comparison of these figures manifests that the S-shaped chamber edge requires no heat loss to the surroundings, especially to the overburden rock. In real reservoirs, there are heat losses to the surrounding formations, both under and overburden. These results support the use of assumption 13 and, therefore, assumption 1; i.e., steam chamber is an inverted triangle. Hence, all simulation cases used for validation in the following sections, Cases 3-14, have heat loss to the overburden and underburden formations.

3.1.2 Introduction of calculation

Analytical calculation based on simulation cases aims at validate the developed model, following the steps given in Chapter 2.1. Temperature at the midpoint of the edge of a steam chamber is used as input in Equation (2.27). This choice of input will be explained in Chapter 3.2.1 with detailed analysis based on Case 3 as an example. Oil-production rate is calculated. Chamber-edge temperatures at various elevations are also solved by using the calculated production rates and different values of z_D in Equation (2.27).

In addition, calculation results are compared with the results obtained in prior models, such as Butler's models (Butler et al., 1981; Butler and Stephens, 1981; Butler, 1994), Reis's model (1992), and Sharma and Gates' model (2010). In their calculation, the constant "m" is used in description of how bitumen viscosity changes with temperature as follows:

$$\nu_s/\nu_o = [(T - T_R)/(T_S - T_R)]^m, \quad (2.50)$$

The constant "m" in each simulation case is calculated according to APPENDIX I of this thesis.

There is an appropriate time during the operation that the developed method gives the best results. As mentioned before, the developed model focuses on the sideway-expansion stage of SAGD (Butler et al., 1981; Chung and Butler, 1988; Edmunds et al., 1994). After totally contacting the overburden and becoming stable, the steam chamber is in an inverted-triangle shape, and the edge becomes linear, which is the same as assumption 1 in the analytical model in this research. The developed model is expected to give best results at this time when the steam-chamber edge just becomes linear.

At late time in the sideway-expansion stage, water condensate accumulates ahead of a steam chamber, resulting in strong two-phase flow. Since the two-phase flow is not considered in the developed model, this generally decreases accuracy of the developed model. Also, water accumulation ahead of a steam chamber enhances heat transfer by multidimensional convective heat flux. These two factors likely make the developed model inaccurate at later times of SAGD in the sideway-expansion stage. Thus, an appropriate time for validation of the analytical model is when the steam chamber edge just becomes linear. This time is called State I in the thesis. Detailed calculation of water accumulation will be shown in Case 3.

Sensitivity analysis of four factors (i.e., two-phase flow, oil-phase flow direction, temperature distribution ahead of a steam-chamber edge, and maximum chamber-edge advancing velocity) is conducted after presentation of calculation results. The angles (θ) between the steam chamber edge and horizontal line are different at the time of State I in different cases. Thus, gravity effects on the oil flow are different. In order to analyze the effect of other factors on the developed model, calculations are also conducted for all cases when the steam chamber edge reaches the same position: when angle (θ) in all simulation cases reaches the same value, 28°, in this thesis. For the sake of discussion, when steam chamber edge reaches the common position with θ of 28°, it is referred to as State II. State II is mainly used for sensitivity analysis of different factors in different simulation cases.

Comparisons between calculation results under States I and II for each case also show that the developed model gives more accurate results under State I when steam chamber edge just becomes linear for each case. In addition, no matter when the calculation is conducted, the developed method gives the best prediction among all analytical models.

When presenting calculation results of production rate and temperature along the edge of a steam chamber in each case under States I and II, the value of angle (θ), operation time and cumulative production of bitumen are provided. Cumulative production is presented as percentage of original-oil-in-place (OOIP) and OOIP is calculated according to APPENDIX II. In addition, values of τ obtained in each model, i.e., τ at the midpoint of the edge of the steam chamber in the developed model, τ_B in Butler's models (Butler et al., 1981; Butler and Stephens, 1981; Butler, 1994) and τ_R in Reis' model (1992) are provided. In the developed model, temperature at the edge of a steam chamber and the length of cross-section are different at different elevations. Integrations of τ based on the temperature distribution ahead of the chamber edge from assumption 12 are calculated locally, resulting in a variable value of τ for different elevations. However, Butler's models (Butler et al., 1981; Butler and Stephens, 1981; Butler, 1994) integrated oil flow from the chamber edge to infinity, and used a constant chamber edge temperature which equals to T_S for integration of τ_B for all elevations. So did Reis' model (1992). Their models have a constant value of τ for all elevations. Other models simply modified the values of τ in Butler' and Reis' models and they also gave some constant values. Comparison of the values of τ indicates overestimation of oil production rate in Butler's models and Reis' model.

Moreover, with calculated temperature along the edge of a steam chamber, composition of oleic phase along the edge of a steam chamber can be obtained by flash calculation. The calculated composition of oleic phase along the edge of a steam chamber can analytically describe the fluid properties along the edge more accurately compared to previous models. This calculation can also be extended to ES-SAGD, where solvent dilution in oleic phase plays an important role in enhancing production rate.

There are three components in the reservoir and three phases on the steam chamber edge. According to Gibbs phase rule,

$$\mathrm{F} = \mathrm{N_C} - \mathrm{N_P} + 2, \tag{3.6}$$

where F is the degree of freedom, $\mathrm{N_C}$ is the number of components in the system, $\mathrm{N_P}$ is the number of phases. According to Equation (3.6), the degree of freedom along the edge of a steam chamber is 2. Thus, composition and temperature are interdependent at a certain pressure. In the developed model, there is no capillary pressure based on assumption 8 and pressure along the chamber edge equals to a constant injection pressure. The composition of the reservoir fluid under three-phase equilibrium can be solved from flash calculation at the operating pressure of 35 bara.

For example, Figure 3.2 shows the relationship between methane concentration in oleic phase and temperature under 35 bara in Case 3 which is a live bitumen case without water dissolution in oleic phase. With the help of this relationship, methane concentration along the edge of a steam chamber can be solved in Case 3. Figure 3.3 shows the relationship between water concentration in oleic phase and temperature under 35 bara in Case 9 where compressible water dissolution in oleic phase is considered. With the help of this relationship, water concentration in oil phase along the edge of a steam chamber can be solved in Case 9.

For application of the developed model, methane concentration in oleic phase in Case 3 is calculated and compared with simulation results. In addition, water dissolution in oleic phase along the edge of a steam chamber is calculated in Case 9. Results will be shown in the next section.

3.2 Calculation results in simulation cases and discussion of results

The developed analytical model is applied to fine scale simulation cases in this section. Calculation results to be shown for each simulation case include production rate, temperature along the edge of a steam chamber (T_e), and steam-oil ratio (SOR).

3.2.1 Live bitumen cases without water dissolution in oleic phase

This section shows calculation results in Cases 3-5. In these simulation cases, there is 90% bitumen and 10% methane in the original reservoir and water dissolution is not considered. All constraints are the same in Cases 3, 4 and 5 except for permeability which is 4000 mD, 2000 mD and 6000 mD, respectively. Aforementioned step-wised calculation in section 2.1 is conducted. Chamber edge temperature at the midpoint is used to predict oil production rate and the same calculation is conducted to Cases 3-5.

For Case 3, steam chamber edge reaches State I, i.e., chamber edge becomes linear, after 75 days of operation since the time when injection and production wells are open. At this time, 1160 m^3 oil has been produced; that is 11% of original oil in place (OOIP). The angle between steam chamber edge and horizontal, θ, at this time is 43°. Calculation is conducted according to the step-wise description in section 2.1. Pertinent reservoir properties required in the calculation can be found in Table 3.1. Chamber edge temperature, T_e, at the midpoint taken from simulation results is 487.7 K under State I. Oil production rate calculation results from Butler's methods (Butler et al., 1981; Butler, 1981; Butler, 1994) and Reis' method (Reis, 1992) are also provided in the Table 3.5. Calculation result for Case 3 under State I is listed in Table 3.5. Absolute and relative deviations of each analytical model's prediction results are also listed in the table. Table 3.5 shows that the developed model in this thesis gives the most accurate results compared to prior models. Calculation results for oil production rate is nearly equal to the simulation result under State I when steam chamber edge just becomes linear.

At this time, τ is 0.0848 at the midpoint from the developed model based on Equation (2.15). However, τ_B is 0.1228 according to Equation (2.51) and τ_R is 0.3070 according to Equation (2.64). Comparison between values of τ in different models indicates there are overestimation in Butler's and Reis' models (Butler et al., 1981; Butler and Stephens, 1981; Butler, 1994; Reis, 1992).

Because the developed model matches the simulation well under State I, chamber edge temperature calculation is conducted under State I. Temperature along the edge of a steam chamber obtained from calculation based on the developed model and that from simulation results are shown in Figure 3.4. It is found that calculated chamber edge temperature shows a S-shape in the bottom reservoir. This will be discussed in Chapter 3.2.5. In addition, it demonstrates that chamber edge temperature is not constant along the edge, which is on the contrary to the assumption used in the prior analytical models.

Using the calculated steam chamber edge temperature in Figure 3.2 and the relationship between methane concentration in oleic phase and temperature in Figure 3.4 to calculate the methane concentration along chamber edge. Calculation results of Case 3 under State I is in Figure 3.5. It can be seen that deviation appears at the same locations as deviation in chamber edge temperature calculation. Because temperature determines composition of oleic phase under a certain pressure, inaccurate temperature results in inaccurate methane concentration in oleic phase. That is, deviation in methane concentration comes from deviation in chamber edge temperature calculation.

Far Case 3, chamber edge reaches State II when angle θ is 28° after 146 days of production. At this time, cumulative bitumen production volume is 1954 m^3; that is 18% OOIP. T_e taken from the midpoint of simulation is 488.7 K. Calculation is conducted in the same way as above and results from various models are listed in Table 3.6. Comparison between oil production rates in various model shows that the developed model gives the best results. However, compared to relative deviation under State I in Table 3.5, the relative deviation in Case 3 under State II is larger. This is because of the appropriate time discussed in section 3.2. As operation goes on, there is more and more water condensate in the mobile zone ahead of steam chamber, resulting in strong two-phase flow that can not be ignored. In addition, due to the thicker mobile zone in the later stage of operation because of the slower chamber advancing velocity, flow is not parallel to steam chamber which deviates from the assumption 2 in the developed model. Thus, deviation in calculation is larger in later time of operation.

Reservoir and fluid in Case 4 are the same as Case 3 except for permeability. Permeability is 2000 mD in Case 4 while it is 4000 mD in Case 3. For Case 4, steam chamber reaches State I after 56 days of operation. At this time, cumulative bitumen produced is 494 m^3, i.e., 5% OOIP and the approximate angle θ is 68°. T_e at the midpoint of the edge from simulation is 498.0 K. Chamber edge temperature calculation result under State I is in Figure 3.6.

Calculated τ at the midpoint under State I is 0.0987 in the developed model. τ_B is 0.1258 according to Equation (2.51) and τ_R is 0.3145 according to Equation (2.64). Clearly, Butler's (Butler et al. 1981; Butler and Stephens, 1981; Butler, 1994) and Reis' (1992) analytical models are overestimating flow rate ahead of steam chamber.

Case 4 reaches State II after 264 days when cumulative bitumen production is 1930 m^3 (18% OOIP). T_e at the midpoint of the edge is 497.0 K. Calculation results of Case 4 under State I and State II are listed in Table 3.7 and Table 3.8, respectively. Comparisons between the two tables and results from various models in the two tables are the same as that of Case 3.

Permeability in Case 5 is 6000 mD and other properties are the same as Case 3. Case 5 reaches State I after 88 days of operation when cumulative bitumen production is 1700 m^3 (16% OOIP) and the approximate angle θ is 32°. T_e at the midpoint from simulation is 480.0 K. Chamber edge temperature calculation result under State I is in Figure 3.7.

Calculated τ at the midpoint of the edge under State I is 0.0825 in the developed model. τ_B is 0.1238 according to Equation (2.51) and τ_R is 0.3094 according to Equation (2.64). Comparison between these values shows overestimation in flow rate ahead of steam chamber in Butler's (Butler et al. 1981; Butler and Stephens, 1981; Butler, 1994) and Reis' (1992) equation.

After 107 days of operation, Case 5 reaches State II. At this time, cumulative production is 1987 m^3 (18% OOIP) and T_e at the midpoint is 486.0 K. Calculation results of production rate for Case 5 under State I and State II are in Table 3.9 and Table 3.10, respectively. Comparisons between the two states and results from various models in the two tables are the same as that of Case 3.

In all cases, there is deviation between calculation results and simulation. Calculation results are lower in the top of reservoir because the quasi-steady state is not accurate due to heat loss to overburden and accumulation of non-condensable gas in the upper part of the chamber. Heat loss to the overburden rock decreases the amount of heat transferred to the reservoir ahead of steam chamber. Moreover, non-condensable gas accumulates in the top of steam chamber edge since it has lower density than steam. This blocks heat from transferring to the reservoir ahead. The collaborative effects of these two reasons result in the deviation in the chamber edge temperature in the top of reservoir. For the bottom part, because of the heat loss to underlying rocks, there is deviation in the calculation of chamber edge temperature in the bottom of reservoir. Detailed analysis about reasons for deviation will be further addressed in section 3.3.

Comparison between reservoirs with different permeabilities indicates that the developed model can be applied in reservoirs with different permeabilities. However, reservoir with low permeability reaches State I within longer time and a large angle θ. This is because oil production rate is low in low permeability reservoir, so it takes longer time to reach State I and State II. In addition, development of steam chamber since the start of SAGD is more stable in low permeability reservoir and it reaches linear chamber edge more quickly with a large angle θ.

3.2.2 Dead bitumen cases without water dissolution in oleic phase

This section shows calculation results of Cases 6-8 where there is 99.99% bitumen and 0.01% methane originally in the reservoir. Water dissolution is not considered. All constraints are the same in Cases 6-8 except for permeability which is 4000 mD, 2000 mD and 6000 mD, respectively. Same calculations are conducted as that in section 3.2.1.

Case 6 reaches State I after 80 days of operation when cumulative production volume is 1190 m^3 (11% OOIP) and the approximate angle θ is 42°. T_e at the midpoint of the edge from simulation is 488.6 K. Chamber edge temperature calculation result under State I is in Figure 3.8.

Calculated τ at the midpoint under State I is 0.0870 in the developed model. τ_B is 0.1101 according to Equation (2.51) and τ_R is 0.2754 according to Equation (2.64). Clearly, Butler's (Butler et al., 1981; Butler and Stephens, 1981; Butler, 1994) and Reis' (1992) analytical models are overestimating flow rate ahead of steam chamber.

After 158 days of operation, Case 6 reaches State II. At this time, cumulative production is 2015 m^3 (19% OOIP) and T_e at the midpoint of chamber edge is 496.9 K. Calculation results of production rates for Case 6 under State I and State II are in Table 3.11 and Table 3.12, respectively. Comparisons between the two tables show the same trend as previous cases.

Case 7 reaches State I after 80 days of operation when cumulative production volume is 1190 m^3 (11% OOIP) and the approximate angle θ is 68°. T_e at the midpoint of chamber edge from simulation is 494.0 K. Chamber edge temperature calculation result under State I is in Figure 3.9.

Calculated τ at the midpoint of chamber edge under State I is 0.0932 in the developed model. τ_B is 0.1104 according to Equation (2.51) and τ_R is 0.2760 according to Equation (2.64). It can be inferred that Butler's (Butler et al., 1981; Butler and Stephens, 1981; Butler, 1994) and Reis' (1992) analytical models are overestimating flow rate ahead of steam chamber.

After 296 days of operation, Case 7 reaches State II. At this time, cumulative production is 2040 m^3 (19% OOIP) and T_e at the midpoint of the chamber edge is 502.0 K. Calculation results of production rates for Case 7 under State I and State II are in Table 3.13 and Table 3.14, respectively.

For Case 8, State I is reached after 78 days of operation. Cumulative bitumen produced is 1533 m^3 (14% OOIP) and approximate angle θ is 36°. T_e at the midpoint of the chamber edge from simulation is 488.0 K. Chamber edge temperature calculation result under State I is in Figure 3.10.

Calculated τ at the midpoint under State I is 0.0820 in the developed model. τ_B is 0.1100 according to Equation (2.51) and τ_R is 0.2751 according to Equation (2.64). Clearly, Butler's (Butler et al., 1981; Butler and Stephens, 1981; Butler, 1994) and Reis' (1992) analytical models are overestimating flow rate ahead of steam chamber.

After 114 days of operation, Case 8 reaches State II. At this time, cumulative production is 2035 m^3 (19% OOIP) and T_e at the midpoint of the chamber edge is 492.6 K. Calculation results of production rates for Case 8 under State I and State II are in Table 3.15 and Table 3.16, respectively.

Comparisons between the two tables under different states for each case show the same trend of calculation accuracy decreasing with production time as previous cases. Compared to prior models, the developed model gives the best calculation results among all analytical models.

Differences between Cases 3-5 and Cases 6-8 are the amount of methane in the reservoir. For Cases 3-5, the larger amount of methane presented in the reservoir aggravates the accumulation in the top front of chamber. Temperature in this case in the upper reservoir should be even lower than that in Cases 6-8, which is shown in Figure 3.4-Figure 3.7 and Figure 3.8-Figure 3.10. In Cases 3-5, the effect of methane on decreasing oleic phase viscosity is more significant, leading to larger production rate.

Moreover, oil production rate is higher in simulation cases with more methane in the reservoir due to the decrease in oil viscosity from dilution of methane in oleic phase. This makes that live bitumen cases reaches State I and State II quicker than dead bitumen cases.

3.2.3 Compressible water dissolution cases

In reality, there is water dissolution in the oleic phase during SAGD production. In Cases 9-11, water dissolution in the oleic phase is considered and there is 90% bitumen with 10% methane in the live bitumen in these cases. This is the set of simulations that are closest to reality. In Cases 9-11, water is compressible and has the same compressibility of water in Cases 1-8.

For Case 9, State I is reached after 78 days of operation. Cumulative production is 1706 m^3 (16% OOIP) and approximate angle θ is 35°. T_e at the midpoint of the chamber edge from simulation is 479.4 K. Chamber edge temperature calculation result under State I is in Figure 3.11.

Calculated τ at the midpoint under State I is 0.1275 in the developed model. τ_B is 0.2826 according to Equation (2.51) and τ_R is 0.7066 according to Equation (2.64). Butler's (Butler et al., 1981; Butler and Stephens, 1981; Butler, 1994) and Reis' (1992) analytical models are overestimating flow rate ahead of steam chamber.

Because there is water dissolution in oleic phase in Case 9, water dissolution can be obtained from the same procedure for calculation of methane concentration in section 3.2.1. Flash calculation for the three component system is conducted under 35 bara with consideration of water dissolution in oleic phase. The calculated relationship between water concentration in oleic phase and temperature is shown in Figure 3.3. Using this relationship and the calculated chamber edge temperature along the edge, water concentration along the chamber edge can be obtained. The calculated water concentration along chamber edge for Case 9 under State I is in Figure 3.12.

After 111 days of operation, Case 9 reaches State II. At this time, cumulative production is 2181 m^3 (20% OOIP) and T_e at the midpoint of the chamber edge is 479.4 K. Calculation results of production rates for Case 9 under State I and State II are in Table 3.17 and Table 3.18, respectively.

Case 10 is different from Case 9 in permeability. Permeability of reservoir is 2000 mD in Case 10 instead of 4000 mD in Case 9. For Case 10, State I is reached after 63 days of operation. Cumulative bitumen produced is 902 m^3 (8% OOIP) and approximate angle θ is 57°. T_e at the midpoint of the chamber edge from simulation is 487.1 K. Chamber edge temperature calculation result under State I is in Figure 3.13.

Calculated τ at the midpoint under State I is 0.1545 in the developed model. τ_B is 0.2823 according to Equation (2.51) and τ_R is 0.7059 according to Equation (2.64). Clearly, Bulter's (Butler et al., 1981; Butler and Stephens, 1981; Butler, 1994) and Reis' (1992) analytical models are overestimating flow rate ahead of steam chamber.

After 203 days of operation, Case 10 reaches State II. At this time, cumulative production is 2153 m^3 (20% OOIP) and T_e at the midpoint of the chamber edge is 500.0 K. Calculation results of production rates for Case 10 under State I and State II are in Table 3.19 and Table 3.20, respectively.

Permeability in Case 11 is 6000 mD, which is greater than that in Case 9 and Case 10. For Case 11, State I is reached after 83 days of operation. Cumulative bitumen produced is 2267m^3 (21% OOIP) and approximate angle θ is 28°. T_e at the midpoint of the chamber edge from simulation is 479.0 K. Chamber edge temperature calculation result under State I is in Figure 3.14. Comparison of production rate prediction is in Table 3.21.

Calculated τ at the midpoint under State I is 0.1253 in the developed model. τ_B is 0.2833 according to Equation (2.51) and τ_R is 0.7082 according to Equation (2.64). Clearly, Bulter's (Butler et al., 1981; Butler and Stephens, 1981; Butler, 1994) and Reis' (1992) analytical models are overestimating flow rate ahead of steam chamber.

Comparisons between the two tables under different states for Cases 9-11 show the same trend of calculation accuracy decreasing with production time as previous cases. Calculation results of oil production rate are the best compared to prior models, which shows that the developed model can be used in reservoirs with different permeabilities.

Comparison between Cases 3-5 and Cases 9-11 shows that production rate is higher when there is water dissolution in oleic phase. This is because water has low viscosity and its dilution in oleic phase help increase oil phase mobility. Higher production rate makes Cases 9-11 reach State II with shorter time than Cases 3-5. However, Cases 9-11 reach State I after longer operation time and at a smaller angle θ. This is because production rate is higher and makes steam chamber expansion since the start of operation less stable. Thus, longer time is needed to reach a linear chamber edge.

3.2.4 Incompressible water dissolution cases

In the derivation, oleic phase density is assumed constant. Water concentration in oleic phase varies a lot with temperature. Thus, change in oleic phase density caused by compressible water dissolution can be significant. In order to analyze the effect of compressible water dissolution in the developed model, this subsection deals with incompressible water and all other settings in the simulation cases are the same as simulation cases in section 3.2.3.

Case 12 has a permeability of 4000 mD. For Case 12, State I is reached after 92 days of operation. Cumulative bitumen produced is 2057 m^3 (19% OOIP) and approximate angle θ is 31°. T_e at the midpoint of the chamber edge from simulation is 480.5 K. Chamber edge temperature calculation result under State I is in Figure 3.15.

Calculated τ at the midpoint under State I is 0.1697 in the developed model. τ_B is 0.2818 according to Equation (2.51) and τ_R is 0.7046 according to Equation (2.64). Clearly, Butler's (Butler et al. 1981; Butler and Stephens, 1981; Butler, 1994) and Reis' (1992) analytical models are overestimating flow rate ahead of steam chamber.

After 103 days of operation, Case 12 reaches State II. At this time, cumulative production is 2228 m^3 (21% OOIP) and T_e at the midpoint of the chamber edge is 490.0 K. Calculation results of production rates for Case 12 under State I and State II are in Table 3.22 and Table 3.23, respectively.

Unlike Case 12, permeability in Case 13 is 2000 mD. For Case 13, State I is reached after 80 days of operation. Cumulative bitumen produced is 1175 m^3 (11% OOIP) and approximate angle θ is 48°. T_e at the midpoint of the chamber edge from simulation is 483.5 K. Chamber edge temperature calculation result under State I is in Figure 3.16.

Calculated τ at the midpoint under State I is 0.1392 in the developed model. τ_B is 0.2874 according to Equation (2.51) and τ_R is 0.7061 according to Equation (2.64). Clearly, Bulter's (Butler et al., 1981; Butler and Stephens, 1981; Butler, 1994) and Reis' (1992) analytical models are overestimating flow rate ahead of steam chamber.

After 179 days of operation, Case 13 reaches State II. At this time, cumulative production is 2164 m^3 (20% OOIP) and T_e at the midpoint is 491.3 K. Calculation results of production rates for Case 13 under State I and State II are in Table 3.24 and Table 3.25, respectively.

For Case 14, State I is reached after 99 days of operation. Cumulative bitumen produced is 2729 m^3 (25% OOIP) and approximate angle θ is 24°. T_e at the midpoint of the chamber edge from simulation is 479.7 K. Chamber edge temperature calculation result under State I is in Figure 3.17.

Calculated τ at the midpoint under State I is 0.1293 in the developed model. τ_B is 0.2831 according to Equation (2.51) and τ_R is 0.7076 according to Equation (2.64). Clearly, Butler's (Butler et al., 1981; Butler and Stephens, 1981; Butler, 1994) and Reis' (1992) analytical models are overestimating flow rate ahead of steam chamber.

After 80 days of operation, Case 14 reaches State II. At this time, cumulative production is 2349 m^3 (22% OOIP) and T_e at the midpoint is 471.5 K. Calculation results of production rates for Case 14 under State I and State II are in Table 3.26 and Table 3.27, respectively.

Comparisons between the two tables under different states for Case 12-14 show the same trend of calculation accuracy decreasing with production time as previous cases. Calculation results of oil production rate are the best compared to prior models, which shows that the developed model can be used in reservoirs with different permeabilities in incompressible water dissolution cases.

When there is compressible water diluted in oleic phase, oleic phase is compressible, which is not consistent with assumption 6 used in developed model. However, comparison between compressible water dissolution cases, i.e., Cases 9-11, and incompressible water dissolution cases, i.e., Cases 12-14 shows that the developed model can give reasonably accurate calculation results in compressible water dissolution cases.

Incompressible water dissolution cases need longer time than compressible water dissolution cases to reach State I. They also reach State I with smaller angle θ. This indicates that steam chamber expansion is not stable since the start of operation in those cases. However, Cases 12-14 reach State II faster than Cases 9-11. This is because production rate is higher in incompressible water dissolution cases, so it takes shorter time for them to produce a certain amount of bitumen inside reservoir.

3.2.5 Discussion of calculation results in simulation cases

In this section, there are many three discussions regarding to three problems in the calculation results shown above. The first is about the choice of temperature at the midpoint as input value in the calculation. The second is the reason for the S shape in the calculation results of temperature on chamber edge in the bottom reservoir. The last is why calculation results are better under State I than State II. Case 3 is chosen as a representative of all cases and is analyzed for the discussion of the aforementioned three aspects.

First, chamber edge temperature at the midpoint is chosen as input for calculation of production rate. This is based on calculation results. Calculation results of production rate in Case 3 using chamber edge temperature from simulation at different elevation as input are shown in Figure 3.18. It can be inferred that calculation result matches best with simulation results if chamber edge temperature at midpoint is used as input. This is because the developed analytical model matches best at the middle of reservoir. This will be further discussed in the sensitivity analysis in next section.

Second, calculation results of temperature along the edge in all simulation cases show a S-shape. The calculated chamber edge temperature is low in the top reservoir which matches with simulation results. It should be a stable value in the bottom reservoir. However, calculated chamber edge temperature is low in bottom of reservoir and increases at the production layer, showing a S-shape curve in the bottom of reservoir. This is because the assumptions used in the analytical model are inconsistent with simulation in bottom reservoir. As elevation decreases, deviation in assumptions and simulation increases, especially assumption 12 which assumes 1-D steady-state heat conduction ahead of steam chamber.

Figure 3.19 shows comparison between calculated temperature distribution ahead of steam chamber and temperature distribution from simulation at z=3m in Case 3. This is the elevation where calculated chamber edge temperature decreases. Figure 3.20 shows comparison between temperature distribution ahead of steam chamber in the calculation and simulation at z=1m in Case 3. This is the lowest elevation in calculation and the position where calculated chamber edge temperature increases. These two figures indicate that assumption 12 is not accurate in bottom of reservoir. However, according to the developed model, integration of oil flow rate is conducted in the perpendicular cross-section from steam chamber edge to the elevation of production well. Deviation accumulates with integration in the cross-section. As elevation decreases, the integration length deceases. Thus, under the coupling effects of inaccurate assumptions and changing integration length, calculation results of chamber edge temperature show a S-shape in the bottom of reservoir.

Third, calculation results of production rate are more accurate under State I than State II which is shown in all cases. Figure 3.21 shows calculation results of oil production rate in Case 3 at different values of angle θ. Angle θ decreases as operation goes on. It can be inferred that deviation in calculation increases as operation goes on. However, calculation results are still better than that from other models.

This increasing deviation is a result of water condensate accumulation ahead of steam chamber. Figure 3.22 shows the amount of water accumulation ahead of steam chamber changing with angle θ. Water accumulation is calculated as the following:

$$\text{Water accumulation} = \sum_{i=1}^{N}(S_w - S_{wc})\varphi(0.5 \times 1.0 \times \Delta y)\rho_w, \qquad (3.7)$$

where i is integer, N is the number of gridblocks ahead of steam chamber, S_w is water saturation in each gridblock, S_{wc} is the connate water saturation in reservoir which equals to 0.25 in all simulation cases, 0.5 is the width of each gridblock, 1.0 is the height of each gridblock and ρ_w is water density in each gridblock.

This figure clearly shows that there is increasing water condensate accumulated ahead of steam chamber edge. The existence of water makes assumptions used in analytical model deviate from simulation. A large amount of water flowing with oil ahead of steam chamber aggravates two-phase flow which is ignored in the developed model according to assumption 11. Water also makes assumption 12 which is a 1-D quasi-steady state heat conduction equation inaccurate in simulation. Water enhances heat transfer by heat convection. Thus, developed model deviates from simulation as operation goes on. Calculation results are the best under State I when steam chamber edge just becomes linear as assumed in the model.

3.3 Sensitivity analysis

Previous sections explain the developed analytical model and validation of this model. For the sake of easy description of the oil flow in SAGD production, some factors are ignored in the analytical model. Developed model ignores multiphase flow. Temperature profile ahead of the interface is obtained by one-dimensional heat conduction. However, they do affect the calculation results. In this section, discussion shows sensitivity analysis regarding to the following four factors on the accuracy of developed model: two-phase flow, temperature distribution ahead of steam chamber, oil flow direction and chamber advancing velocity.

3.3.1 Effects of two-phase flow on the developed model

In the SAGD production, there is two-phase flow, oleic phase and aqueous phase, ahead of the edge of a steam chamber flowing down to the production well. The presence of two-phase flow makes the permeability of oleic phase flow smaller than the absolute permeability of reservoir. However, the developed model does not consider two-phase flow and assumes the relative permeability of oleic phase is always one. To evaluate the multiphase flow effect on the oil flow, Bharatha et al. (2005) used the following equation:

$$k_{rave} = \int_{T_L}^{T_e} \frac{k_{ro}}{\nu_o(T-T_R)} dT \Big/ \int_{T_L}^{T_e} \frac{1}{\nu_o(T-T_R)} dT \quad (3.8)$$

Although Bharatha et al. (2005) did not consider the variable local chamber edge temperature, his method of calculating average permeability can analyze multiphase flow effect on oil flow in this research. Equation (3.8) is applied to calculate average relative permeability of oleic phase in each cross-section perpendicular to chamber edge. The variable local chamber edge temperature and variable temperature at the intersection point of the cross-section with production layer (T_L) are taken into consideration. Therefore, Equation (3.8) is rewritten as

$$k_{rave(z)} = \int_{T_{L(z)}}^{T_{e(z)}} \frac{k_{ro}}{\nu_o(T-T_R)} dT \Big/ \int_{T_{L(z)}}^{T_{e(z)}} \frac{1}{\nu_o(T-T_R)} dT \tag{3.9}$$

where z is the elevation of the starting point of the cross-section on chamber edge. Equation (3.9) is used to analyze two-phase flow in all simulation cases. Table 3.28 and Table 3.29 show the calculation results for all cases.

In Equation (3.9), calculation uses output data of temperature distribution, relative permeability and kinematic viscosity of oleic phase in ξ direction (perpendicular to steam chamber edge) ahead of steam chamber. The use of local temperature in each grid block avoids deviation brought by the assumed temperature profile ahead of chamber edge in the derivation.

Obviously, k_{rave} is smaller than one in the reservoir ahead of steam chamber due to existence of two-phase flow. In Table 3.28, there is no obvious trend observed. One of the possible reasons for this is that effects of gravity on oil drainage are different in SAGD when slopes of steam chamber in all cases are different. In order to eliminate the different effects of gravity on oil flow in SAGD process, calculation results in Table 3.29 when steam chamber slopes are the same in all cases are used to analyze the effect of two-phase flow on the accuracy of developed model.

Comparison between Cases 3-5 and Cases 6-8 shows that k_{rave} is smaller in the case with less methane in the live bitumen. Comparisons between cases with different permeabilities show that k_{rave} is smaller in the reservoir with lower permeability. This indicates that two-phase flow is more significant in these cases with less methane and lower permeability. In these cases, oil flow ahead of the chamber edge is slower and oil phase viscosity is higher. Two-phase flow is more significant.

Moreover, water dissolution in oleic phase and water compressibility will also aggravate the effect of two-phase flow on the accuracy of developed model. With water dissolved in the oleic phase, oleic phase mobility becomes lower than that without water dissolution at the same temperature. Thus, the mobile bitumen zone ahead of chamber edge is thicker and brings more deviation to the developed model. For compressible water, compressibility of water will add convective flow into the reservoir due to heat expansion. This will enhance heat transfer into the reservoir and make the two-phase flow zone ahead of chamber edge thicker, which will aggravate two-phase flow. Comparison between Table 3.28 and Table 3.29 shows that k_{rave} decreases with increasing operation time. This is because that water condensation accumulates along the edge with operation going on. There is more movable water coexists with oleic phase flow and this will result in stronger two-phase flow.

3.3.2 Effect of flow direction on the developed model

In the previous models and the developed model, oil flow along the chamber edge is assumed parallel to the chamber edge. However, the simulation results show that this is not always true inside the reservoir. This section will discuss the deviation caused by this phenomenon for the first time.

Figure 3.23 shows the flow vector of oil flow in the reservoir for Case 3 when the steam chamber edges just become linear. Arrows in the figure represent oleic phase flow direction and their lengths reflect value of oil flow in the reservoir.

In order to evaluate this effect in the analytical model, here introduce a new constant named β_θ that describes the extent to which actual oil flow direction deviates from steam chamber edge. β_θ compares the average angle of oil flow ahead of steam chamber. The average angle of oil flow at each elevation is calculated according to the following Equation (3.10) and it is calculated in the cross-section perpendicular to steam chamber edge.

$$\theta_{ave(z)} = \arctan(-\sum \text{flow in vertical direction}/\sum \text{flow in horizontal direction}) \quad (3.10)$$

where z is the elevation of the starting point of the cross-section on the chamber edge.

The inconsistency of unparalleled flow, which is recorded as β_θ, is defined as the ratio of sine of average flow angle θ_{ave} and sine of θ.

$$\beta_{\theta(z)} = \sin\theta_{ave(z)}/\sin\theta \quad (3.11)$$

The calculation results for simulation cases are shown in Table 3.30 and Table 3.31. In these tables, it can be inferred that flow is more paralleled to the chamber edge in the middle reservoir. In the bottom of reservoir, chamber edge temperature is high and chamber edge moving velocity is low. Thus, heated zone ahead of steam chamber is thick according to Equation (2.11). Oil flow direction deviates from the edge of a steam chamber in the thicker mobile zone.

Comparison between Table 3.30 and Table 3.31 shows that oil flow direction is more deviated from the chamber edge as production goes on. With time going on, production rate decreases and chamber expanding rate decreases. According to Equation (2.11), heated area ahead of steam chamber is thicker with slower chamber edge advancing velocity. Thus, movable bitumen zone is thicker at later time and oleic flow direction is more inconsistent. Due to the same reason mentioned above, calculation results in Table 3.31 are compared to analyze the effect of unparalleled flow on the accuracy of developed model.

In Table 3.31, there is no obvious trend between simulation cases with different permeabilities. However, flow ahead of the edge is more parallel in the simulation cases with more methane, water dissolution in oleic phase and compressible water. These three factors decrease the viscosity of oleic phase, increasing oil flow rate. Since oil can flow in the direction along chamber edge quickly, there is limited flow in the direction perpendicular to the chamber edge. Thus, flow is more parallel to the edge and simulation meets the assumption in the developed model better.

3.3.3 Effect of temperature profile ahead of the edge on the developed model

The temperature distribution ahead of steam chamber edge is obtained based on the assumption of one dimensional quasi-steady state conduction only heat transfer with moving boundary (Carslaw and Jaeger, 1959) for the convenience of calculation, which is not accurate in the reservoir. When using this equation as approximation, discussions about the accuracy of this equation in the different position of reservoir are conducted (Butler, 1997; Reis, 1992; Bharatha et al., 2005).

It was mentioned in the previous sections that the equation gives the best results in the middle of the reservoir while it was not accurate in the top and bottom of reservoir. In the ceiling part, there is a significant amount of heat loss to the overburden that cannot be ignored in the calculation of temperature distribution ahead of chamber edge. In the bottom part near production well, steam chamber edge is attached to the well. The interface is nearly stationary. Thus, it is not accurate.

However, no quantitative analysis has been conducted. This section will calculate the deviation caused by Equation (2.11) for the first time. A new parameter β_ξ to evaluate the inaccuracy of Equation (2.11) is introduced in the discussion here. With the help of β_ξ, Equation (3.12) can match the temperature distribution in the normal direction ahead of steam chamber edge. Calculation of β_ξ is obtained by fitting the temperature distribution to the simulation result.

$$T_{(\xi,z)} = T_R + \left[T_{e(z)} - T_R\right]\exp\left[-\beta_\xi \xi v_{(z)} \sin\theta/\alpha\right] \tag{3.12}$$

The value of β_ξ illustrates the deviation between temperature profile ahead of chamber edge obtained in Equation (2.11) and simulation results. If the temperature profile used in the derivation is the same as simulation results, β_ξ equals to one. β_ξ greater than one means that temperature ahead of chamber edge obtained in Equation (2.11) decreases slower than the simulation results. This indicates that temperature ahead of chamber edge is higher in the derivation than that in simulation results. Table 3.32 and Table 3.33 show values of β_ξ at different elevations in various simulation cases.

The results show that the temperature distribution ahead of chamber edge used in the derivation is not accurate in the top and bottom of reservoir where β_ξ is much larger than one. It corresponds to the discussion in prior papers (Reis, 1992; Bharatha et al., 2005) that Equation (2.11) can match the simulation result best in the middle of reservoir and causes deviation in the top and especially in the bottom of reservoir.

To analyze the reason for deviation in the bottom section of reservoir, Figure 3.24 - Figure 3.25 show comparisons of temperature profile obtained in the derivation and simulation results in Case 3.

In the middle of reservoir (z=9) as shown in Figure 3.24, temperature profile obtained by derivation can match the simulation result very well. On the contrary, derivation temperature profile deviates from the simulation results in the bottom reservoir as shown in Figure 3.19 and Figure 3.20. In addition, the deviation between simulation and derivation of temperature distribution ahead of chamber edge increases as distance increases. Because the normal distance under analysis is shorter in the layer with z=1m than in the layer with z=3m, deviation in the layer with z=1m is smaller than that in the layer with z=3m. Calculation results also show smaller deviation in chamber edge temperature in the layer with z=1m compared to that in the layer with z=3m.

In addition, for top of reservoir, although there is heat loss to the overburden rock, Equation (2.11) gives better description of temperature distribution ahead of steam chamber edge compared to that in bottom of reservoir. This is because that Equation (2.11) expresses temperature profile in the normal direction and ignores heat loss. Due to the angle between steam chamber edge and horizontal, the developed analytical model does not consider the ignored zone in the top of reservoir as shown in Figure 2.1. Heat loss to overburden mainly affects temperature in this ignored zone and has slightly effects on temperature profile normal to chamber edge in top of reservoir as shown in Figure 3.25. As for the ignored zone, temperature in this zone is low and nearly equal to the original reservoir temperature. Bitumen in this area has extreme high viscosity and hard to move. Thus, oil flow in this zone ignored in the analytical model does not affect the accuracy of developed model. In the bottom of reservoir, there is heat loss to the underburden. Moreover, Equation (2.11) is used to describe heat conduction in the solid. In the bottom of reservoir, there is significant oil flow ahead of chamber edge which will enhance heat transfer by convection, making Equation (2.11) less accurate.

As discussed by Butler (1985) and Keshavarz et al. (2016), the one-dimensional quasi-steady state heat conduction used in the analytical model is not accurate in the ceiling and bottom of reservoir. As they mentioned, this assumption is not accurate when steam chamber is stationary. The bottom of interface is fixed to the production well. Thus, chamber edge advancing velocity is zero at the bottom and low in the lower part of interface. There will be significant deviation caused by the quasi-steady state assumption in the bottom of reservoir. For the ceiling part, deviation is mainly result from inaccurate one-dimensional assumption. As developed in this thesis, steam chamber edge temperature is changing along the steam chamber. There is temperature gradient in the direction parallel to the edge of a steam chamber. Heat conduction will happen in two dimensions.

From Table 3.33, there is no obvious trend between simulation cases with different permeability. However, simulation cases with more methane show slightly larger value of β_ξ, which means temperature profile ahead of chamber edge is more different between simulation and derivation. This is because there is little methane ahead of chamber edge and the thermal diffusivity stays nearly constant in cases with little methane, which is the same as the constant thermal diffusivity used in the analytical model. In the cases with a lot of methane, the distribution of methane ahead of chamber edge varies and this will affect the thermal diffusivity of reservoir, resulting in inaccurate temperature distribution ahead of chamber edge in the derivation.

In addition, simulation cases with water dissolution in oleic phase have smaller β_ξ. In cases without water dissolution, β_ξ is greater than one, which means temperature ahead of chamber is higher in derivation than that in simulation. The existence of water in oleic phase boosts heat transfer and increases temperature ahead of steam chamber. Thus, deviation between derivation and simulation is decreased.

Comparisons between Cases 9-11 and Cases 12-14 show that simulation case with compressible water has smaller β_ξ. Zhou et al. (2016) can explain this. With the injection of steam, reservoir temperature ahead of steam chamber rises. This will cause the compressible water to expand and transfer heat by convection into the reservoir. In Cases 12-14, water is incompressible. Thus, heat transfer is impaired compared to that in Cases 9-11 with compressible water, resulting in slower heating ahead of chamber edge. Temperature increases slowly ahead of the chamber edge. This corresponds to the calculation result of β_ξ in Table 3.32.

Comparison between Table 3.32 and Table 3.33 show that Equation (2.11) is more accurate in the later time. This is because that Equation (2.11) is used for heat transfer by conduction only and ignores heat convection. According to Sharma and Gates (2011), heat convection plays an important role in SAGD especially along the chamber edge. Production rate decreases with increasing operation time. Fast flow ahead of steam chamber will enhance heat transfer via convection. Thus, Equation (2.11) is more accurate at later stage of SAGD when flow rate is lower.

3.3.4 Effect of maximum chamber-edge advancing velocity on the developed model

The maximum chamber-edge advancing velocity (v_{max}) is an important parameter used in the analytical model. This thesis discusses the effect of the accuracy of maximum chamber advancing velocity on the accuracy of analytical model for the first time. In the previous calculations, this data is obtained based on the global material balance on the reservoir with given production rate. There are possibilities that this value is not accurate. This section presents the effect of different values of v_{max} on calculation of temperature profile along steam chamber edge. Calculations will be conducted in the same simulation case (Case 3) with different values of v_{max}. Figure 3.26 shows the calculation results.

Figure 3.26 shows that the value of v_{max} does not affect the calculation results of chamber edge temperature in the upper part of reservoir while affects the results in the bottom part. Based on Equation (2.11) attached again as follows,

$$(T - T_R)/(T_e - T_R) = \exp(-U\xi/\alpha) = \exp(-\xi v \sin\theta/\alpha). \quad (2.11)$$

The lower end of integration of τ, i.e., T_L, is calculated by Equation (2.14) and this value depends on the value of v_{max}.

$$T_{L(z)} = T_R + [T_{e(z)} - T_R]\exp[-v_{(z)} z \tan\theta/\alpha]. \quad (2.14)$$

For top of reservoir, the calculation of T_L gives results very close to the initial reservoir temperature (T_R). In addition, a different value of v_{max} only results in the nearly same value of T_L. Therefore, different values of v_{max} do not affect calculation results of chamber edge temperature in the upper part of reservoir. On the other hand, for bottom of reservoir, different values of v_{max} give different temperature profiles ahead of steam chamber, changing the calculation results.

3.4 SOR calculation results in the simulation cases

According to the analytical model developed in this thesis, reservoir inside steam chamber is under steam temperature. That is to say $T_{ceiling}$, temperature at the contact area between steam chamber and overburden formations, equals to steam chamber temperature (T_S). Thus, Equation (2.44) is used to calculate the SOR value for all simulation.

$$Q'_{OB} = 2M_{over}(T_S - T_R)\Delta y\sqrt{\alpha v_{max} W_S/\pi}. \tag{2.44}$$

SOR calculation results for all fine scale simulations are shown in Table 3.34. It is shown that developed methods give accurate calculation results compared to the simulation results and better results than that obtained from calculation described in section 2.3.

Temperature at most of the contact area between steam chamber and overburden rock is at steam injection temperature (T_S) in all simulation cases. For example, Figure 3.27 is taken from Case 9 that is closest to the real reservoir situation. Figure 3.27 shows temperature distribution in the reservoir and it clearly shows that $T_{ceiling}$ equals to T_S. Accumulation of methane happens near the interface. Only for a limited contact area, temperature is lower than steam temperature (T_S) due to accumulation of methane. Thus, it is reasonable to let $T_{ceiling}$ equals to T_S in the calculation.

3.5 Discussion about SOR calculation results in simulation cases

According to Equation (2.28), heat loss consists four parts.

$$Q'_{inj} = Q'_{SC} + Q'_{AC} + Q'_{OB} + Q'_{PO}. \tag{2.28}$$

Table 3.35 shows the fraction of each term in the total heat loss for all simulation cases. In Table 3.35, if fraction of Q'_{AC} is higher in a case, fraction of Q'_{OB} is higher. For each category of simulation cases, fraction of Q'_{AC} and Q'_{OB} is the highest in the reservoir with high permeability and lowest in the reservoir with low permeability. For example, among Cases 3, 4 and 5, Q'_{AC} and Q'_{OB} is highest in the Case 5 with 6000 mD permeability and lowest in the Case 4 with 2000 mD permeability. This trend can be explained by Equation (2.40) and Equation (2.44).

$Q'_{AC} = \sum_{i=1}^{N_L} 2M_R\left[T_{e(z)} - T_{L(z)}\right]\alpha h_i \Delta y/(z\tan\theta).$ (2.40)

$Q'_{OB} = dQ_{OB}/dt = 2M_{over}(T_s - T_R)\Delta y\sqrt{\alpha v_{max} W_S/\pi}.$ (2.44)

As mentioned before, calculations are conducted at the time when steam chamber edge just becomes linear. The angle (θ) between steam chamber and horizontal is larger in the reservoir with lower permeability and width of steam chamber (W_S) is smaller. Values of tanθ in the three simulation cases are listed in Table 3.36. tanθ is larger in higher permeability reservoir, making value of Q'_{AC} lower.

Figure 3.28 shows the value of $\left[T_{e(z)} - T_{L(z)}\right]$ in Equation (2.40). It seems that $\left[T_{e(z)} - T_{L(z)}\right]$ is highest in low permeability Case 4 and lowest in high permeability Case 5. However, the effect of difference in $\left[T_{e(z)} - T_{L(z)}\right]$ on the result of Equation (2.40) is less than the effect of difference in tanθ. Thus, fraction of Q'_{AC} is lower in the low permeability cases.

Moreover, production rate is lower in the low permeability reservoir, resulting in lower steam chamber advancing velocity (v_{max}). Smaller W_S and v_{max} result in lower Q'_{OB} according to Equation (2.40). Thus, there is such trend that fraction of Q'_{AC} and Q'_{OB} is higher in the high permeability reservoirs.

3.6 Summary

The developed model in Chapter 2 is validated in this chapter in various simulation cases. It was shown that the developed model gave accurate calculation results of oil production rate among all the analytical models tested in the case studies. When steam chamber edge just becomes linear (i.e., State I), calculation results of oil production rate are accurate. SOR calculation also gave reasonably-accurate results for the simulation cases tested in this chapter.

The temperature profile along the edge of a steam chamber can be obtained by the developed model. Flash calculation at T_e and the operating pressure gives the oleic phase along the edge of a steam chamber. However, the temperature profile is not accurate for the top and bottom parts of the reservoir, making the resulting composition inaccurate there. Sensitivity analysis of four factors: two-phase flow, 1-D quasi-steady state heat conduction, inconsistent flow direction and v_{max} were conducted to explain the deviation of calculation results from simulation results.

Table 3.1 Reservoir properties used in all simulation cases

Property	Value
Porosity	0.33
Initial oil saturation	0.75
Initial water saturation	0.25
Residual oleic phase saturation	0.13
Residual liquid saturation	0.38
k_{rocw}	1
k_{rwio}	0.3
k_{rg} at connate liquid saturation	0.3
Exponent for calculating relative permeability for all phases	1
Initial reservoir temperature T_R, K	286.15
Temperature of injected steam, K	515.71
Initial reservoir pressure, bara	15
Steam quality	0.9
Steam Latent Heat, J/kg	1.75×10^6
Maximum BHP for injector, bara	35
Minimum BHP for producer, bara	15
Horizontal well length, m	37.5
Maximum surface liquid rate for producer, m^3/day	200
Maximum steam rate for producer, m^3/day	1
Permeability for Case 1,2, 3, 6, 9 & 12, mD	4000
Permeability for Case 4, 7, 10 & 13, mD	2000
Permeability for Case 5, 8, 11 & 14, mD	6000
Rock heat capacity, kJ/(m^3·K)	2600
Rock thermal conductivity, J/(m·day·K) (Butler, 1997)	6.60×10^5
Bitumen thermal conductivity, J/(m·day·K) (Butler, 1997)	1.15×10^4
Gas thermal conductivity, J/(m·day·K) (Yazdani et al. 2011)	2892
Water thermal conductivity, J/(m·day·K) (CMG, 2014)	1.50×10^5

Table 3.2 Component properties used in the EOS model for all cases

Component	MW, g/mol	Tc, K	Pc, bar	ω
Methane	16.04	190.60	46.00	0.0080
Bitumen	530.00	847.17	10.64	1.0406
Water	18.01	647.10	220.64	0.3433

Table 3.3 Component viscosity table

Temperature, °C	Temperature, K	Oil viscosity, cp	Methane viscosity, cp	Water viscosity, cp
10	283.15	2457801.75	38.54	1.3117
30	303.15	114116.11	22.59	0.798
50	323.15	10642.80	14.15	0.5453
70	343.15	1650.00	9.36	0.4028
90	363.15	422.00	6.48	0.3144
110	383.15	133.00	4.66	0.2555
130	403.15	58.70	3.46	0.2141
150	423.15	31.00	2.65	0.1835
170	443.15	18.30	2.07	0.1603
190	463.15	12.50	1.66	0.1421
210	483.15	9.24	1.35	0.1275
230	503.15	7.31	1.12	0.1155
250	523.15	6.10	0.94	0.1055

Table 3.4 Comparison of simulation cases

Case	Methane concentration initially in the bitumen	Permeability, mD	Heat loss	Water dissolution in oleic phase	Water compressibility
1	10%	4000	Overburden	No	Compressible
2	10%	4000	No heat loss	No	Compressible
3	10%	4000	Over and underburden	No	Compressible
4	10%	2000	Over and underburden	No	Compressible
5	10%	6000	Over and underburden	No	Compressible
6	0.01%	4000	Over and underburden	No	Compressible
7	0.01%	2000	Over and underburden	No	Compressible
8	0.01%	6000	Over and underburden	No	Compressible
9	10%	4000	Over and underburden	Yes	Compressible
10	10%	2000	Over and underburden	Yes	Compressible
11	10%	6000	Over and underburden	Yes	Compressible
12	10%	4000	Over and underburden	Yes	Incompressible
13	10%	2000	Over and underburden	Yes	Incompressible
14	10%	6000	Over and underburden	Yes	Incompressible

Table 3.5 Comparison of production rate of Case 3 under State I

Calculation is conducted after 75 days of production when chamber edge just becomes linear. Cumulative bitumen production equals to 1160 m^3 (11% OOIP) and approximate angle θ is 43°.

	Production rate, m^3/day	Absolute deviation	Relative deviation
Simulation	12.8751	–	–
This research	12.8219	-0.0532	-0.0041
Butler et al. (1981)	19.0218	6.1466	0.4774
Tandrain	16.4733	3.5982	0.2795
Lindrain	15.3358	2.4607	0.1911
Reis (1992)	15.0380	2.1629	0.1680

Table 3.6 Comparison of production rate of Case 3 under State II.

This is the result after 146 days of production when chamber edge reaches the common position where the approximate angle θ is 28°. Cumulative bitumen production is to 1954 m^3 (18% OOIP).

	Production rate, m^3/day	Absolute deviation	Relative deviation
Simulation	9.8986	–	–
This research	12.9863	3.0877	0.3119
Butler et al. (1981)	19.0218	9.1232	0.9217
Tandrain	16.4733	6.5747	0.6642
Lindrain	15.3358	5.4372	0.5493
Reis (1992)	15.038	5.1394	0.5192

Table 3.7 Comparison of production rate of Case 4 under State I

Calculation is conducted after 56 days of production when chamber edge just becomes linear. Cumulative bitumen production equals to 494 m^3 (5% OOIP) and approximate angle θ is 68°.

	Production rate, m^3/day	Absolute deviation	Relative deviation
Simulation	9.8850	–	–
This research	9.9843	0.0992	0.0100
Butler et al. (1981)	13.3618	3.4768	0.3517
Tandrain	11.5717	1.6866	0.1706
Lindrain	10.7726	0.8876	0.0898
Reis (1992)	10.5634	0.6784	0.0686

Table 3.8 Comparison of production rate of Case 4 under State II

This is the result after 264 days of production when chamber edge reaches the common position where the approximate angle θ is 28°. Cumulative bitumen production is to 1930 m^3 (18% OOIP).

	Production rate, m^3/day	Absolute deviation	Relative deviation
Simulation	5.3231	–	–
This research	9.8055	4.4824	0.8421
Butler et al. (1981)	13.3618	8.0387	1.5102
Tandrain	11.5717	6.2486	1.1739
Lindrain	10.7726	5.4495	1.0237
Reis (1992)	10.5634	5.2403	0.9844

Table 3.9 Comparison of production rate of Case 5 under State I

Calculation is conducted after 88 days of production when chamber edge just becomes linear. Cumulative bitumen production equals to 1700 m^3 (16% OOIP) and approximate angle θ is 32°.

	Production rate, m^3/day	Absolute deviation	Relative deviation
Simulation	14.8918	–	–
This research	14.8863	-0.0056	-0.0004
Butler et al. (1981)	23.3191	8.4273	0.5659
Tandrain	20.1949	5.3031	0.3561
Lindrain	18.8005	3.9086	0.2625
Reis (1992)	18.4354	3.5435	0.2380

Table 3.10 Comparison of production rate of Case 5 under State II

This is the result after 107 days of production when chamber edge reaches the common position where the approximate angle θ is 28°. Cumulative bitumen is to 1987 m^3 (18% OOIP).

	Production rate, m^3/day	Absolute deviation	Relative deviation
Simulation	13.5729	–	–
This research	15.5271	1.9542	0.1440
Butler et al. (1981)	23.3191	9.7462	0.7181
Tandrain	20.1949	6.6220	0.4879
Lindrain	18.8005	5.2276	0.3851
Reis (1992)	18.4354	4.8625	0.3583

Table 3.11 Comparison of production rate of Case 6 under State I

Calculation is conducted after 80 days of production when chamber edge just becomes linear. Cumulative bitumen production equals to 1190 m^3 (11% OOIP) and approximate angle θ is 42°.

	Production rate, m^3/day	Absolute deviation	Relative deviation
Simulation	12.0261	–	–
This research	12.1143	0.0881	0.0073
Butler et al. (1981)	17.9188	5.8926	0.4900
Tandrain	15.5181	3.4920	0.2904
Lindrain	14.4466	2.4204	0.2013
Reis (1992)	14.1660	2.1399	0.1779

Table 3.12 Comparison of production rate of Case 6 under State II

This is the result after 158 days of production when chamber edge reaches the common position where the approximate angle θ is 28°. Cumulative bitumen production is to 2015 m^3(19% OOIP)

	Production rate, m^3/day	Absolute deviation	Relative deviation
Simulation	9.2217	–	–
This research	13.0184	3.7967	0.4117
Butler et al. (1981)	17.9188	8.6971	0.9431
Tandrain	15.5181	6.2964	0.6828
Lindrain	14.4466	5.2249	0.5666
Reis (1992)	14.1660	4.9443	0.5362

Table 3.13 Comparison of production rate of Case 7 under State I

Calculation is conducted after 56 days of production when chamber edge just becomes linear. Cumulative bitumen production equals to 490 m^3 (5% OOIP) and approximate angle θ is 68°.

	Production rate, m^3/day	Absolute deviation	Relative deviation
Simulation	9.2073	–	–
This research	9.2324	0.0251	0.0027
Butler et al. (1981)	12.8024	3.5951	0.3905
Tandrain	11.0872	1.8799	0.2042
Lindrain	10.3216	1.1143	0.1210
Reis (1992)	10.1212	0.9139	0.0993

Table 3.14 Comparison of production rate of Case 7 under State II

This is the result after 296 days of production when chamber edge reaches the common position where the approximate angle θ is 28°. Cumulative bitumen production is to 2040 m^3(19% OOIP).

	Production rate, m^3/day	Absolute deviation	Relative deviation
Simulation	4.9987	–	–
This research	9.5263	4.5276	0.9058
Butler et al. (1981)	12.8024	7.8037	1.5611
Tandrain	11.0872	6.0885	1.2180
Lindrain	10.3216	5.3229	1.0649
Reis (1992)	10.1212	5.1225	1.0248

Table 3.15 Comparison of production rate of Case 8 under State I

Calculation is conducted after 78 days of production when chamber edge just becomes linear. Cumulative bitumen production equals to 1533 m^3 (14% OOIP) and approximate angle θ is 36°.

	Production rate, m^3/day	Absolute deviation	Relative deviation
Simulation	14.9829	–	–
This research	14.9469	-0.0360	-0.0024
Butler et al. (1981)	22.0513	7.0684	0.4718
Tandrain	19.0970	4.1141	0.2746
Lindrain	17.7783	2.7954	0.1866
Reis (1992)	17.4331	2.4502	0.1635

Table 3.16 Comparison of production rate of Case 8 under State II

This is the result after 114 days of production when chamber edge reaches the common position where the approximate angle θ is 28°. Cumulative bitumen production is to 2035 m^3 (19% OOIP).

	Production rate, m^3/day	Absolute deviation	Relative deviation
Simulation	12.9764	–	–
This research	15.4737	2.4973	0.1924
Butler et al. (1981)	22.0513	9.0749	0.6993
Tandrain	19.097	6.1206	0.4717
Lindrain	17.7783	4.8019	0.3700
Reis (1992)	17.4331	4.4567	0.3434

Table 3.17 Comparison of production rate of Case 9 under State I

Calculation is conducted after 78 days of production when chamber edge just becomes linear. Cumulative bitumen production equals to 1706 m^3 (16% OOIP) and approximate angle θ is 35°.

	Production rate, m^3/day	Absolute deviation	Relative deviation
Simulation	15.7448	–	–
This research	15.7745	0.0297	0.0019
Butler et al. (1981)	28.8601	13.1153	0.8330
Tandrain	24.9936	9.2488	0.5874
Lindrain	23.2677	7.5230	0.4778
Reis (1992)	22.8159	7.0711	0.4491

Table 3.18 Comparison of production rate of Case 9 under State II

This is the result after 111 days of production when chamber edge reaches the common position where the approximate angle θ is 28°. Cumulative bitumen production is to 2181 m^3 (20% OOIP).

	Production rate, m^3/day	Absolute deviation	Relative deviation
Simulation	13.2412	–	–
This research	17.4461	4.2049	0.3176
Butler et al. (1981)	28.8601	15.6189	1.1796
Tandrain	24.9936	11.7524	0.8876
Lindrain	23.2677	10.0265	0.7572
Reis (1992)	22.8159	9.5747	0.7231

Table 3.19 Comparison of production rate of Case 10 under State I

Calculation is conducted after 63 days of production when steam chamber just becomes linear. Cumulative bitumen production equals to 902 m^3 (8% OOIP) and approximate angle θ is 57°.

	Production rate, m^3/day	Absolute deviation	Relative deviation
Simulation	12.3095	–	–
This research	12.2209	-0.0886	-0.0072
Butler et al. (1981)	20.3964	8.0869	0.6570
Tandrain	17.6638	5.3543	0.4350
Lindrain	16.4441	4.1346	0.3359
Reis (1992)	16.1248	3.8152	0.3099

Table 3.20 Comparison of production rate of Case 10 under State II

This is the result after 203 days of production when chamber edge reaches the common position where the approximate angle θ is 28°. Cumulative bitumen production is to 2153 m^3(20% OOIP).

	Production rate, m^3/day	Absolute deviation	Relative deviation
Simulation	6.9187	–	–
This research	14.1834	7.2647	1.0500
Butler et al. (1981)	20.3964	13.4777	1.9480
Tandrain	17.6638	10.7451	1.5531
Lindrain	16.4441	9.5254	1.3768
Reis (1992)	16.1248	9.2061	1.3306

Table 3.21 Comparison of production rate of Case 11 under State I

Calculation is conducted after 83 days of production when chamber edge just becomes linear. Cumulative bitumen production equals to 2267 m^3 (21% OOIP) and approximate angle θ is 28°.

	Production rate, m^3/day	Absolute deviation	Relative deviation
Simulation	19.0745	–	–
This research	19.1843	0.1098	0.0058
Butler et al. (1981)	35.3852	16.3107	0.8551
Tandrain	30.6445	11.5700	0.6066
Lindrain	28.5285	9.4540	0.4956
Reis (1992)	27.9745	8.9000	0.4666

Table 3.22 Comparison of production rate of Case 12 under State I

Calculation is conducted after 92 days of production when chamber edge just becomes linear. Cumulative bitumen production equals to 2057 m^3 and approximate angle θ is 31°.

	Production rate, m^3/day	Absolute deviation	Relative deviation
Simulation	15.8977	–	–
This research	15.8838	-0.0139	-0.0009
Butler et al. (1981)	28.8181	12.9204	0.8127
Tandrain	24.9572	9.0595	0.5699
Lindrain	23.2339	7.3362	0.4615
Reis (1992)	22.7827	6.8850	0.4331

Table 3.23 Comparison of production rate of Case 12 under State II

This is the result after 103 days of production when chamber edge reaches the common position where the approximate angle θ is 28°. Cumulative bitumen production is to 2228 m^3 (21% OOIP).

	Production rate, m^3/day	Absolute deviation	Relative deviation
Simulation	15.3420	–	–
This research	17.9392	2.5972	0.1693
Butler et al. (1981)	28.8181	13.4761	0.8784
Tandrain	24.9572	9.6152	0.6267
Lindrain	23.2339	7.8919	0.5144
Reis (1992)	22.7827	7.4407	0.4850

Table 3.24 Comparison of production rate of Case 13 under State I

Calculation is conducted after 80 days of production when chamber edge just becomes linear. Cumulative bitumen production equals to 1175 m^3 (11% OOIP) and approximate angle θ is 48°.

	Production rate, m^3/day	Absolute deviation	Relative deviation
Simulation	11.6255	–	–
This research	11.6614	0.0360	0.0031
Butler et al. (1981)	20.3994	8.7739	0.7547
Tandrain	17.6664	6.0409	0.5196
Lindrain	16.4465	4.8210	0.4147
Reis (1992)	16.1271	4.5017	0.3872

Table 3.25 Comparison of production rate of Case 13 under State II

This is the result after 179 days of production when chamber edge reaches the common position where the approximate angle θ is 28°. Cumulative bitumen production to 2164 m^3 (20% OOIP).

	Production rate, m^3/day	Absolute deviation	Relative deviation
Simulation	8.4646	–	–
This research	12.8508	4.3862	0.5182
Butler et al. (1981)	20.3994	11.9348	1.4100
Tandrain	17.6664	9.2018	1.0871
Lindrain	16.4465	7.9819	0.9430
Reis (1992)	16.1271	7.6625	0.9052

Table 3.26 Comparison of production rate of Case 14 under State I

Calculation is conducted after 99 days of production when chamber edge just becomes linear. Cumulative bitumen production equals to 2729 m^3 (25% OOIP) and approximate angle θ is 24°.

	Production rate, m^3/day	Absolute deviation	Relative deviation
Simulation	19.3967	–	–
This research	19.4815	0.0847	0.0044
Butler et al. (1981)	35.3716	15.9749	0.8236
Tandrain	30.6327	11.2360	0.5793
Lindrain	28.5175	9.1208	0.4702
Reis (1992)	27.9637	8.5670	0.4417

Table 3.27 Comparison of production rate of Case 14 under State II

This is the result after 80 days of production when chamber edge reaches the common position where the approximate angle θ is 28°. Cumulative bitumen production is to 2349 m^3 (22% OOIP).

	Production rate, m^3/day	Absolute deviation	Relative deviation
Simulation	21.7744	–	–
This research	17.3645	-4.4099	-0.2025
Butler et al. (1981)	35.3716	13.5972	0.6245
Tandrain	30.6327	8.8583	0.4068
Lindrain	28.5175	6.7431	0.3097
Reis (1992)	27.9637	6.1893	0.2842

Table 3.28 k_{rave} at different elevations in various simulation cases under State I when steam chamber edge just becomes linear

z, m	Case 3	Case 4	Case 5	Case 6	Case 7	Case 8	Case 9	Case 10	Case 11	Case 12	Case 13	Case 14
17	0.91	1.00	0.97	0.80	1.00	0.88	0.95	0.96	1.00	0.99	0.98	1.00
16	0.98	0.18	0.96	0.82	0.95	0.89	0.94	0.66	0.97	0.99	0.99	0.76
15	0.97	0.99	0.93	0.92	0.51	0.89	0.89	0.97	0.91	0.87	0.87	0.88
14	0.88	0.98	0.91	0.93	0.74	0.85	0.87	0.75	0.86	0.87	0.84	0.86
13	0.91	0.99	0.91	0.88	0.98	0.92	0.81	0.78	0.77	0.87	0.87	0.84
12	0.92	0.93	0.92	0.90	0.96	0.91	0.82	0.82	0.79	0.87	0.88	0.86
11	0.91	0.90	0.92	0.90	0.92	0.90	0.81	0.83	0.83	0.86	0.85	0.85
10	0.91	0.91	0.92	0.90	0.94	0.92	0.82	0.82	0.79	0.85	0.80	0.85
9	0.91	0.92	0.91	0.90	0.89	0.91	0.81	0.81	0.80	0.84	0.85	0.85
8	0.90	0.90	0.92	0.91	0.90	0.92	0.76	0.80	0.80	0.82	0.82	0.83
7	0.90	0.89	0.89	0.91	0.89	0.91	0.73	0.79	0.79	0.82	0.84	0.82
6	0.90	0.91	0.90	0.91	0.90	0.90	0.72	0.78	0.79	0.82	0.82	0.82
5	0.90	0.89	0.91	0.91	0.89	0.90	0.72	0.72	0.72	0.81	0.81	0.82
4	0.91	0.91	0.89	0.91	0.90	0.90	0.73	0.75	0.75	0.80	0.80	0.80
3	0.88	0.91	0.90	0.88	0.90	0.90	0.73	0.76	0.75	0.79	0.78	0.79
2	0.89	0.91	0.91	0.90	0.90	0.91	0.75	0.74	0.77	0.78	0.80	0.78
1	0.89	0.92	0.92	0.90	0.88	0.91	0.77	0.75	0.79	0.78	0.79	0.79

Table 3.29 k_{rave} at different elevations in various simulation cases under State II when steam chamber edge slopes are the same

z, m	Case 3	Case 4	Case 5	Case 6	Case 7	Case 8	Case 9	Case 10	Case 11	Case 12	Case 13	Case 14
17	0.99	0.99	0.97	0.93	0.94	0.91	1.00	1.00	1.00	0.97	1.00	0.93
16	0.86	0.86	0.92	0.82	0.73	0.80	0.95	0.82	0.97	0.97	0.84	0.87
15	0.89	0.84	0.89	0.81	0.73	0.80	0.75	0.68	0.91	0.86	0.79	0.94
14	0.89	0.83	0.88	0.81	0.75	0.90	0.79	0.64	0.86	0.85	0.80	0.95
13	0.88	0.84	0.87	0.82	0.78	0.90	0.74	0.70	0.77	0.85	0.77	0.90
12	0.88	0.84	0.90	0.81	0.81	0.89	0.77	0.68	0.79	0.82	0.79	0.88
11	0.87	0.84	0.89	0.89	0.83	0.85	0.74	0.65	0.83	0.82	0.77	0.86
10	0.86	0.84	0.90	0.89	0.84	0.90	0.77	0.63	0.79	0.83	0.77	0.86
9	0.89	0.84	0.89	0.88	0.84	0.89	0.75	0.62	0.80	0.82	0.78	0.88
8	0.88	0.84	0.88	0.88	0.75	0.84	0.73	0.60	0.80	0.83	0.77	0.85
7	0.87	0.83	0.90	0.86	0.76	0.91	0.71	0.67	0.79	0.81	0.76	0.84
6	0.87	0.82	0.90	0.84	0.84	0.90	0.69	0.64	0.79	0.80	0.75	0.83
5	0.86	0.84	0.90	0.81	0.84	0.90	0.68	0.60	0.72	0.80	0.74	0.83
4	0.88	0.81	0.89	0.89	0.85	0.90	0.64	0.63	0.75	0.79	0.73	0.82
3	0.87	0.86	0.89	0.88	0.86	0.91	0.73	0.57	0.75	0.80	0.74	0.80
2	0.89	0.86	0.89	0.90	0.87	0.91	0.71	0.60	0.77	0.79	0.74	0.80
1	0.91	0.88	0.92	0.92	0.90	0.92	0.77	0.70	0.79	0.78	0.73	0.80

Table 3.30 β_θ at different elevations in various simulation cases under State I when steam chamber edge just becomes linear

z, m	Case 3	Case 4	Case 5	Case 6	Case 7	Case 8	Case 9	Case 10	Case 11	Case 12	Case 13	Case 14
17	-0.13	-0.10	-0.13	-1.16	-0.99	-0.42	-0.07	-0.04	-0.03	-0.27	-0.07	-0.11
16	0.98	-1.08	1.34	0.81	-1.07	1.46	1.28	1.17	1.82	1.48	1.20	1.11
15	0.52	1.07	0.80	1.06	1.04	1.34	1.20	1.00	1.12	1.18	1.10	0.59
14	1.01	1.05	0.64	0.68	1.03	1.14	0.53	0.94	0.66	0.47	0.44	1.10
13	0.88	0.98	0.61	0.99	1.04	0.66	0.98	0.90	1.24	0.51	0.74	1.39
12	0.81	0.99	0.61	0.95	1.04	0.78	0.60	0.93	1.04	0.54	0.67	0.54
11	0.80	1.03	0.62	0.95	1.01	0.95	0.88	0.97	0.71	0.56	0.64	0.60
10	0.80	1.06	0.62	0.93	1.04	0.73	0.62	0.98	0.95	0.55	0.98	0.57
9	0.81	1.02	0.64	0.91	1.06	0.91	0.75	0.96	0.68	0.53	0.63	0.52
8	0.79	1.04	0.64	0.87	1.03	0.68	0.88	0.91	0.71	0.94	0.96	0.89
7	0.74	1.06	0.81	0.81	1.06	0.75	0.84	0.89	0.69	0.74	0.57	0.52
6	0.68	1.03	0.72	0.74	1.02	0.76	0.79	0.92	0.66	0.51	0.70	0.52
5	0.64	1.04	0.64	0.68	1.04	0.74	0.75	0.90	0.70	0.53	0.79	0.51
4	0.62	0.96	0.71	0.61	0.95	0.70	0.70	0.78	0.64	0.56	0.82	0.67
3	0.71	0.84	0.62	0.72	0.82	0.65	0.63	0.64	0.59	0.58	0.76	0.48
2	0.55	0.67	0.53	0.57	0.67	0.56	0.54	0.52	0.52	0.60	0.62	0.76
1	0.38	0.34	0.40	0.40	0.48	0.44	0.37	0.41	0.31	0.46	0.46	0.64

Table 3.31 β_θ at different elevations in various simulation cases under State II when steam chamber edge slopes are the same

z, m	Case 3	Case 4	Case 5	Case 6	Case 7	Case 8	Case 9	Case 10	Case 11	Case 12	Case 13	Case 14
17	-0.22	-0.11	-0.18	-1.35	-1.97	-1.95	-0.23	-0.28	-0.03	-0.10	-0.15	-0.18
16	1.77	1.31	0.98	1.44	1.52	1.74	0.61	1.21	1.82	0.99	1.15	1.65
15	0.82	0.99	0.95	1.14	1.09	1.26	1.48	1.19	1.12	0.95	0.73	1.44
14	0.75	0.85	0.93	0.99	0.93	0.78	0.86	1.02	0.66	0.76	0.62	0.47
13	0.73	0.78	1.01	0.92	0.85	0.82	1.12	0.83	1.24	0.51	0.82	0.48
12	0.74	0.75	0.68	0.87	0.79	0.90	0.78	0.80	1.04	1.11	0.59	0.50
11	0.79	0.73	0.83	0.73	0.74	0.94	0.95	0.79	0.71	0.98	0.71	1.14
10	0.83	0.72	0.67	0.75	0.70	0.77	0.71	0.77	0.95	0.67	0.89	0.79
9	0.68	0.71	0.74	0.77	0.68	0.86	0.77	0.74	0.68	1.00	0.57	0.54
8	0.69	0.70	0.82	0.77	0.68	0.83	0.78	0.71	0.71	0.67	0.57	0.82
7	0.71	0.70	0.66	0.74	0.68	0.69	0.76	0.67	0.69	0.78	0.59	0.98
6	0.72	0.70	0.66	0.72	0.67	0.69	0.72	0.68	0.66	0.77	0.61	0.91
5	0.71	0.68	0.65	0.70	0.66	0.67	0.69	0.67	0.70	0.66	0.65	0.61
4	0.65	0.68	0.65	0.66	0.64	0.65	0.65	0.65	0.64	0.53	0.76	0.68
3	0.64	0.62	0.63	0.64	0.61	0.62	0.61	0.60	0.59	0.48	0.58	0.75
2	0.56	0.55	0.58	0.56	0.54	0.57	0.55	0.52	0.52	0.43	0.48	0.42
1	0.41	0.39	0.41	0.39	0.35	0.39	0.33	0.36	0.31	0.56	0.44	0.37

Table 3.32 β_ξ at different elevations in various simulation cases under State I when steam chamber edge just becomes linear

z, m	Case 3	Case 4	Case 5	Case 6	Case 7	Case 8	Case 9	Case 10	Case 11	Case 12	Case 13	Case 14
17	1.13	4.32	1.26	1.48	6.84	1.48	1.08	0.69	1.28	1.21	0.93	1.29
16	1.32	6.22	1.32	1.30	6.95	1.14	1.33	1.18	1.63	1.70	1.43	1.75
15	1.12	5.54	1.14	0.97	6.03	1.08	1.17	1.22	1.22	1.19	1.15	1.29
14	0.92	4.89	1.08	0.99	5.37	1.00	1.14	0.94	1.12	1.20	1.15	1.08
13	0.93	4.63	1.06	0.89	4.85	0.98	1.00	0.89	0.99	1.12	1.02	1.03
12	0.94	4.36	1.06	0.89	4.56	0.94	1.06	0.88	1.01	1.09	1.09	1.07
11	0.95	4.20	1.08	0.91	4.52	0.92	0.99	0.88	1.05	1.09	1.00	1.07
10	0.96	4.06	1.10	0.93	4.55	0.99	1.07	0.89	1.01	1.10	0.99	1.08
9	0.97	4.32	1.12	0.95	4.55	0.98	1.04	0.91	1.09	1.13	1.02	1.11
8	1.00	4.50	1.15	0.99	5.00	1.06	1.05	0.94	1.10	1.10	1.02	1.10
7	1.04	4.80	1.12	1.05	5.34	1.08	1.08	1.00	1.13	1.15	1.12	1.16
6	1.12	5.58	1.19	1.13	6.27	1.11	1.11	1.09	1.18	1.23	1.18	1.17
5	1.21	6.45	1.28	1.24	7.26	1.16	1.16	1.12	1.14	1.23	1.26	1.16
4	1.34	8.24	1.27	1.40	9.29	1.23	1.22	1.31	1.17	1.25	1.38	1.10
3	1.41	10.65	1.45	1.51	12.01	1.34	1.33	1.68	1.25	1.29	1.60	1.19
2	1.79	13.44	1.86	1.84	15.23	1.58	1.55	2.09	1.42	1.53	1.83	1.43
1	2.80	23.63	2.39	2.86	26.25	2.09	1.77	2.37	1.39	2.61	2.50	2.59

Table 3.33 β_ξ at different elevations in various simulation cases under State II when steam chamber edge slopes are the same

z, m	Case 3	Case 4	Case 5	Case 6	Case 7	Case 8	Case 9	Case 10	Case 11	Case 12	Case 13	Case 14
17	1.04	0.80	1.17	1.37	1.13	1.45	0.98	0.69	1.28	0.98	0.83	1.33
16	1.25	1.19	1.35	1.14	1.07	1.22	1.36	0.99	1.63	1.42	1.24	2.00
15	1.13	1.02	1.09	1.01	0.95	1.04	0.99	0.83	1.22	1.06	1.05	1.33
14	1.05	0.95	1.00	0.96	0.89	0.98	0.96	0.76	1.12	0.97	0.97	1.39
13	1.01	0.92	0.97	0.95	0.87	0.95	0.88	0.76	0.99	0.95	0.92	1.30
12	1.00	0.92	1.02	0.95	0.86	0.94	0.92	0.75	1.01	0.89	0.93	1.26
11	1.01	0.93	1.00	0.96	0.87	0.97	0.89	0.75	1.05	0.91	0.92	1.16
10	1.01	0.94	1.06	0.98	0.90	0.99	0.94	0.76	1.01	0.96	0.92	1.20
9	1.08	0.97	1.06	1.00	0.93	1.01	0.95	0.77	1.09	0.95	0.97	1.25
8	1.10	1.00	1.08	1.02	0.96	1.07	0.97	0.79	1.10	1.01	0.99	1.25
7	1.13	1.04	1.17	1.05	1.00	1.11	0.99	0.85	1.13	1.02	1.01	1.27
6	1.17	1.09	1.19	1.11	1.07	1.15	1.01	0.88	1.18	1.04	1.04	1.30
5	1.21	1.22	1.24	1.19	1.15	1.21	1.04	0.92	1.14	1.06	1.08	1.34
4	1.36	1.30	1.32	1.28	1.33	1.28	1.09	1.05	1.17	1.09	1.17	1.26
3	1.48	1.65	1.44	1.40	1.63	1.39	1.23	1.17	1.25	1.14	1.38	1.27
2	1.89	2.22	1.64	1.76	2.15	1.57	1.39	1.45	1.42	1.39	1.92	1.54
1	2.18	2.88	1.75	2.14	2.81	1.71	1.73	2.38	1.39	2.42	3.34	2.59

Table 3.34 Results of SOR calculation in all simulation cases

Case number	Simulation result	Developed method		Reis' method	
		Result	Relative deviation	Result	Relative deviation
3	4.10	3.83	-0.07	3.54	-0.14
4	3.18	3.33	0.05	3.20	0.01
5	4.49	4.04	-0.10	3.76	-0.16
6	4.17	3.90	-0.06	3.60	-0.14
7	3.24	3.35	0.03	3.20	-0.01
8	4.32	3.92	-0.09	3.57	-0.17
9	4.02	3.87	-0.04	3.59	-0.11
10	3.55	3.49	-0.02	3.34	-0.06
11	4.37	3.95	-0.10	3.67	-0.16
12	4.61	4.03	-0.13	3.82	-0.17
13	4.22	3.78	-0.10	3.62	-0.14
14	4.72	4.11	-0.13	3.93	-0.17

Table 3.35 Fraction of each term in Equation (2.28) for simulation cases when using T_e along the interface from simulation

Case	Q'_{PO}	Q'_{SC}	Q'_{AC}	Q'_{OB}
3	7.91%	48.39%	16.46%	27.24%
4	9.10%	55.64%	11.69%	23.58%
5	7.49%	45.81%	18.06%	28.64%
6	7.77%	47.49%	17.23%	27.51%
7	9.03%	55.22%	12.34%	23.41%
8	7.73%	47.26%	17.67%	27.33%
9	7.82%	47.82%	16.92%	27.45%
10	8.68%	53.06%	13.24%	25.03%
11	7.67%	46.88%	17.64%	27.81%
12	7.51%	45.95%	18.00%	28.54%
13	8.02%	49.02%	15.93%	27.03%
14	7.37%	45.08%	18.68%	28.86%

Table 3.36 Different value of tanθ in Cases 3, 4 and 5

Case	tanθ	1/tanθ
3	0.9264	1.0794
4	2.4522	0.4078
5	0.6245	1.6013

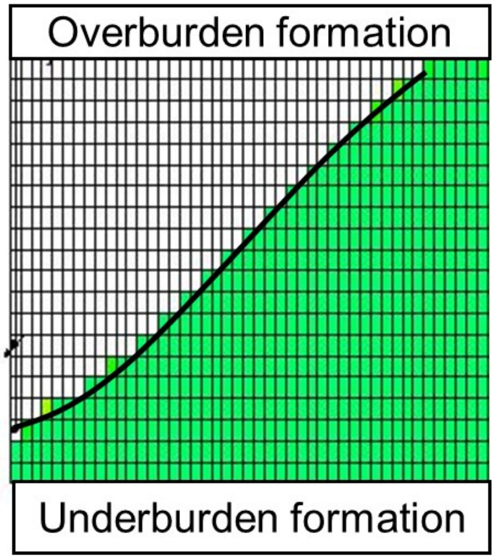

a)

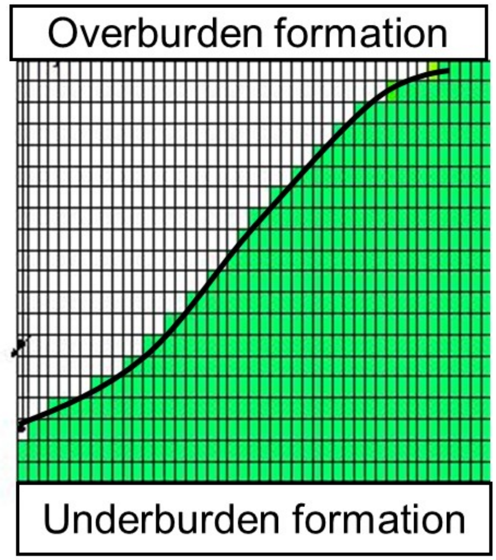

b)

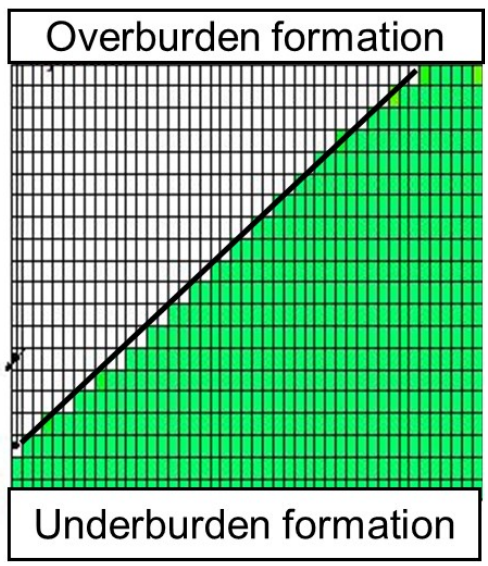

c)

Figure 3.1 Comparison of stream chamber shapes in Cases 1, 2 and 3.

a) Case 1 without underburden heat loss in the middle; b) Case 2 without all heat loss on the right; c) Case 3 with heat loss to both overburden and underburden;

In the above figure, white means that gas saturation is greater than zero in these grid blocks, i.e., inside steam chamber. Green means that gas saturation equals to zero in these grid blocks, i.e., ahead of steam chamber. Comparison of these cases and figures manifests that S-shaped chamber requires no heat loss to overburden.

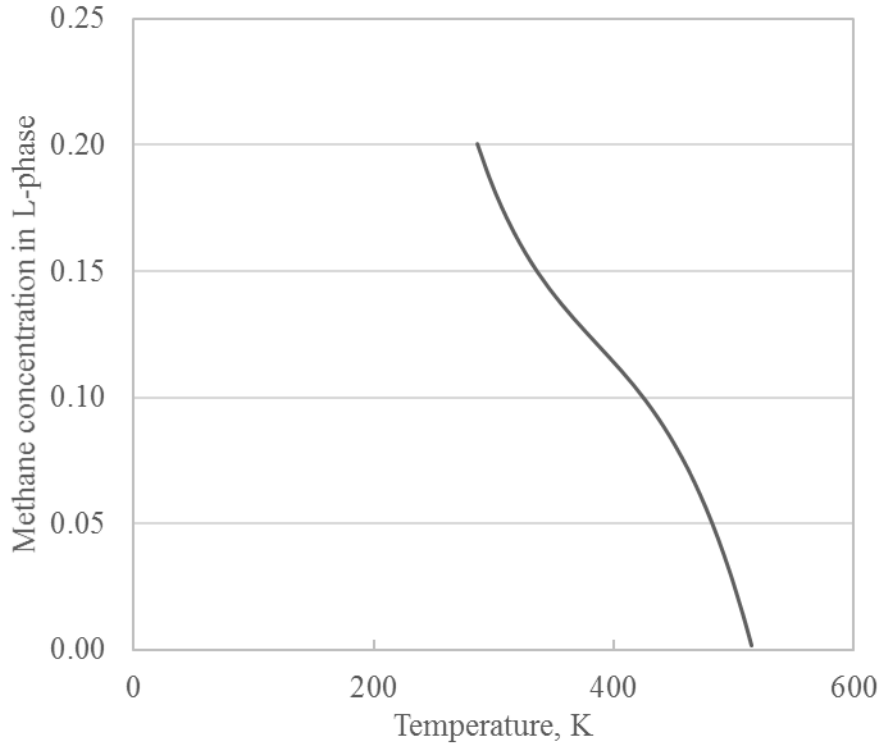

Figure 3.2 Relationship between methane concentration in oleic phase and temperature in Case 3 under 35 bara.

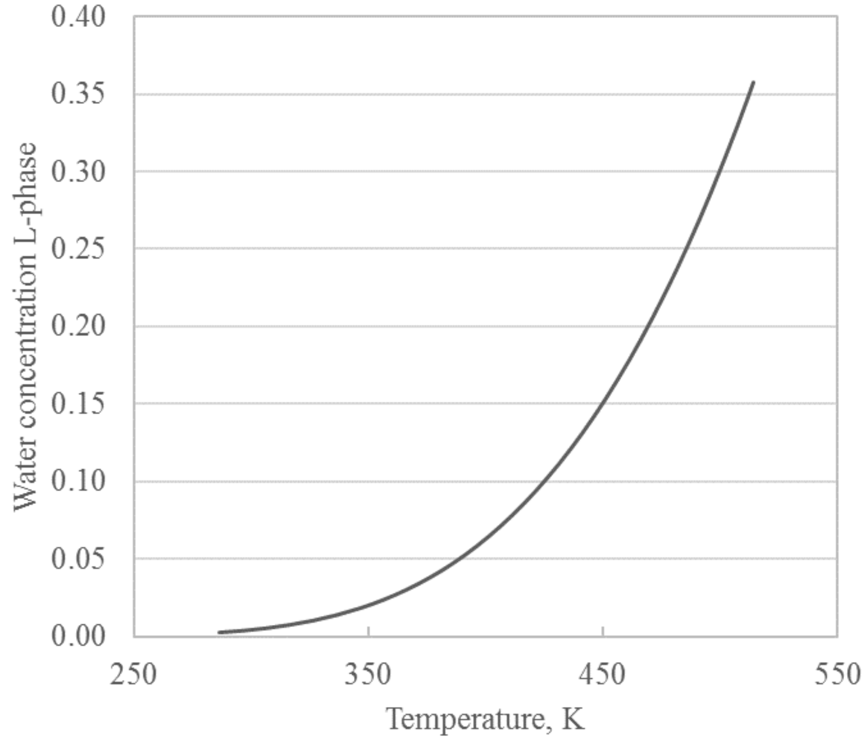

Figure 3.3 Relationship between water concentration in oleic phase and temperature in Case 9 when there is water dissolution in oleic phase

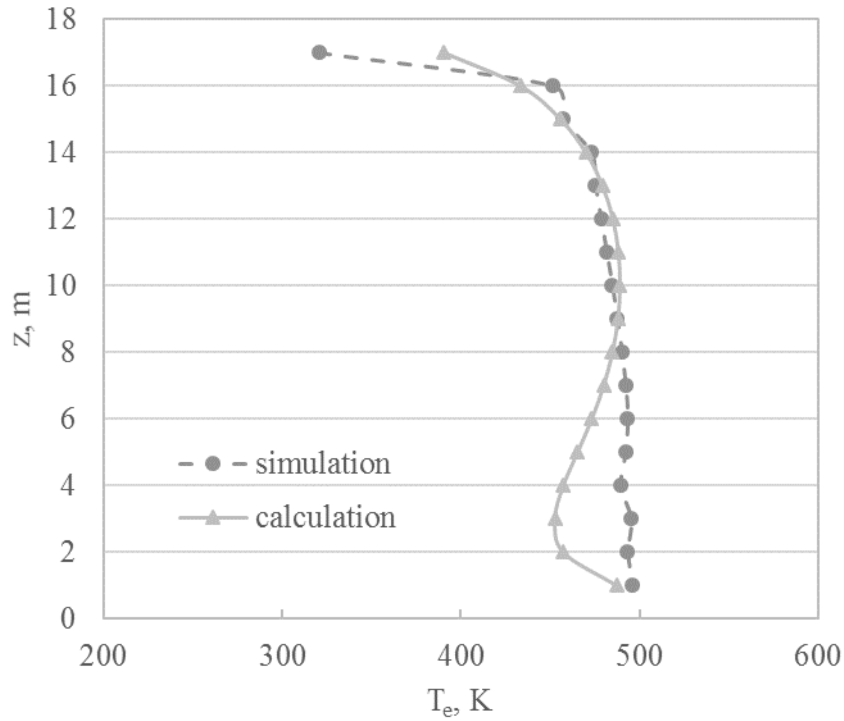

Figure 3.4 Comparison of simulation and calculation chamber edge temperature along the interface in Case 3 when steam chamber edge just becomes linear.

Original live bitumen has 90% dead bitumen and 10% methane. Reservoir permeability is 4000 mD. Compared to Case 6, chamber edge temperature in to top is even lower due to the accumulation of non-condensable gas (methane) inside the upper part of steam chamber. There is still deviation in the lower part of reservoir due to the inaccuracy of temperature description ahead of steam chamber edge in the bottom reservoir.

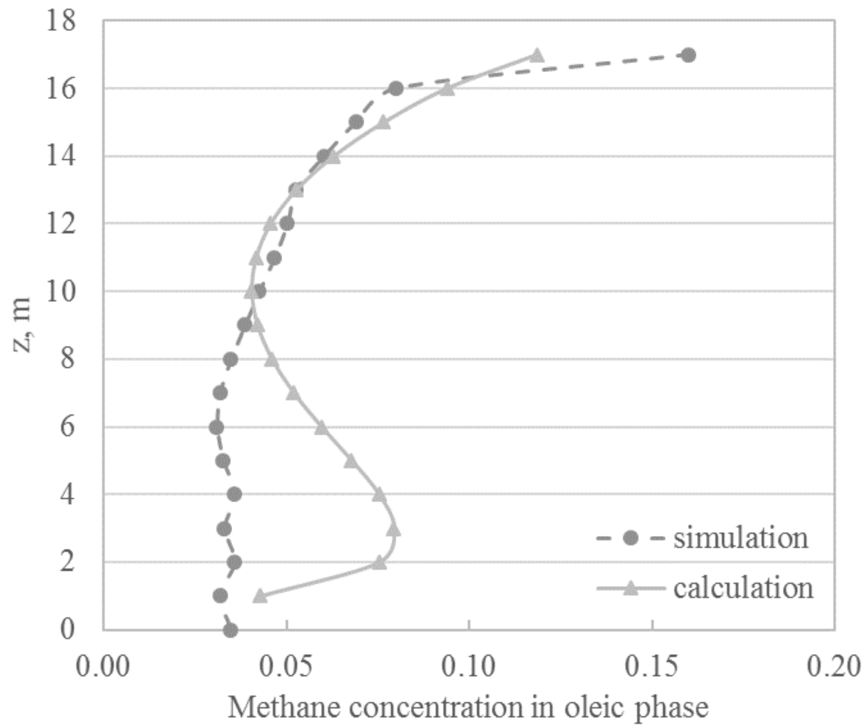

Figure 3.5 Comparison of simulation and calculation methane mole fraction in oleic phase along the interface in Case 3 when steam chamber edge just becomes linear.

Original live bitumen has 90% dead bitumen and 10% methane. Reservoir permeability is 4000 mD. The amount of methane (non-condensable gas) is calculated based on the calculated steam chamber edge temperature according to flash calculation under operation pressure (35 bara). It is higher in the upper reservoir and decreases along the edge. This corresponds to the methane accumulation mentioned before.

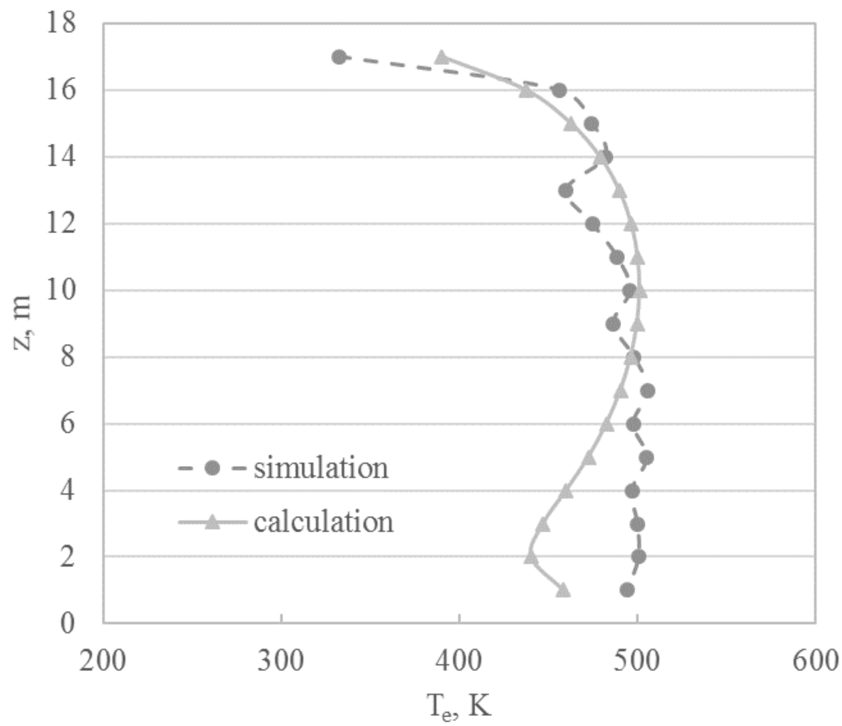

Figure 3.6 Comparison of simulation and calculation chamber edge temperature along the interface in Case 4 when steam chamber edge just becomes linear.

Original live bitumen has 90% dead bitumen and 10% methane. Reservoir permeability is 2000 mD. Compared to Case 7, chamber edge temperature in to top is even lower due to the accumulation of non-condensable gas (methane) inside the upper part of steam chamber. There is still deviation in the lower part of reservoir due to the inaccuracy of temperature description ahead of steam chamber edge in the bottom reservoir.

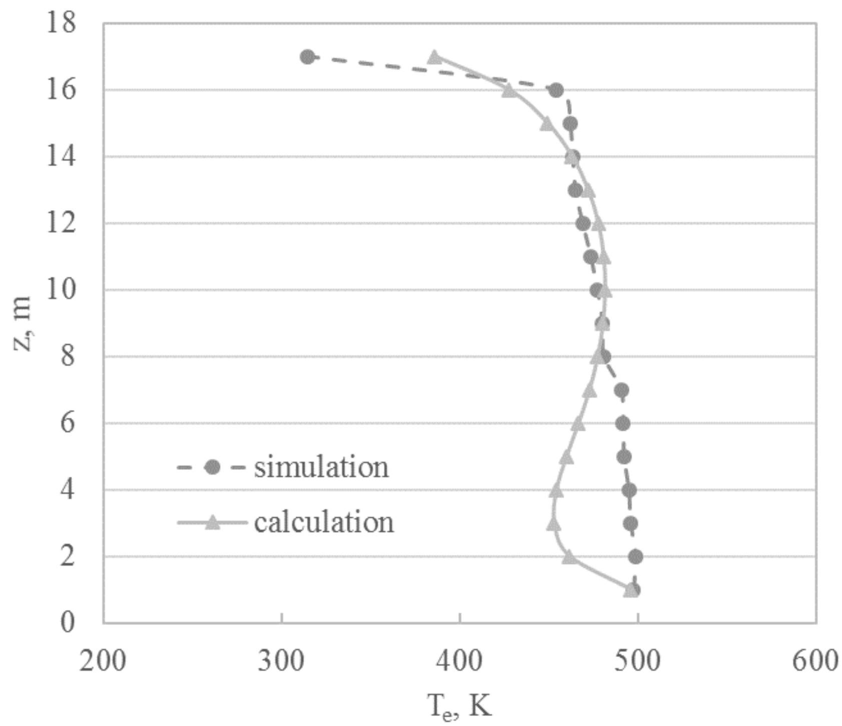

Figure 3.7 Comparison of simulation and calculation chamber edge temperature along the interface in Case 5 when steam chamber edge just becomes linear.

Original live bitumen has 90% dead bitumen and 10% methane. Reservoir permeability is 6000 mD. Compared to Case 8, chamber edge temperature in to top is even lower due to the accumulation of non-condensable gas (methane) inside the upper part of steam chamber. There is still deviation in the lower part of reservoir due to the inaccuracy of temperature description ahead of steam chamber edge in the bottom reservoir.

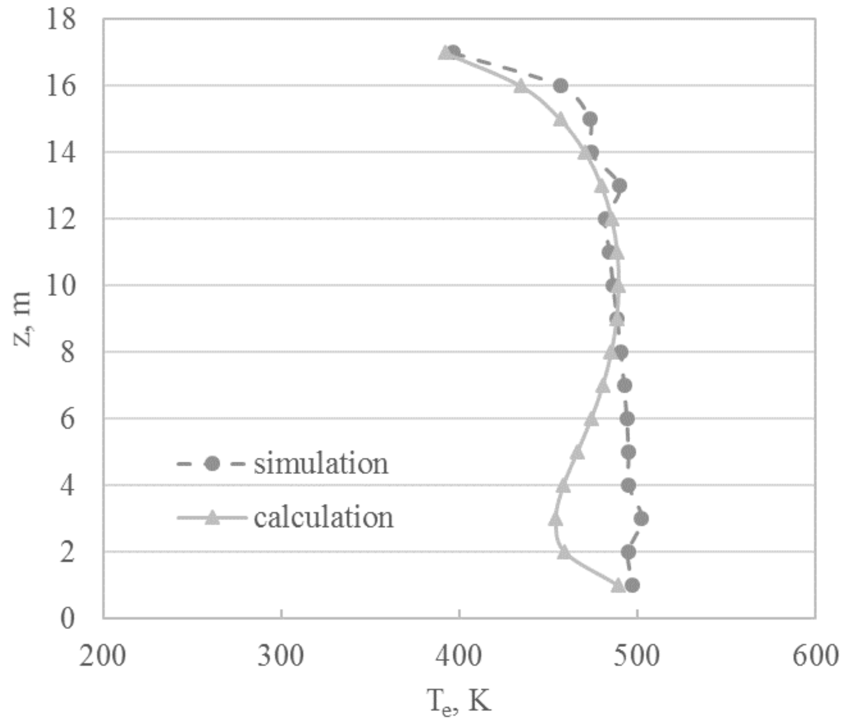

Figure 3.8 Comparison of simulation chamber edge temperature and calculated chamber edge temperature along the interface in Case 6 when steam chamber edge just becomes linear.

There is 99.99% bitumen and 0.01% methane in the live bitumen. Reservoir permeability is 4000 mD. The results show larger deviation in the bottom section of reservoir and this is because of the inaccuracy of temperature profile ahead of steam chamber edge used in derivation.

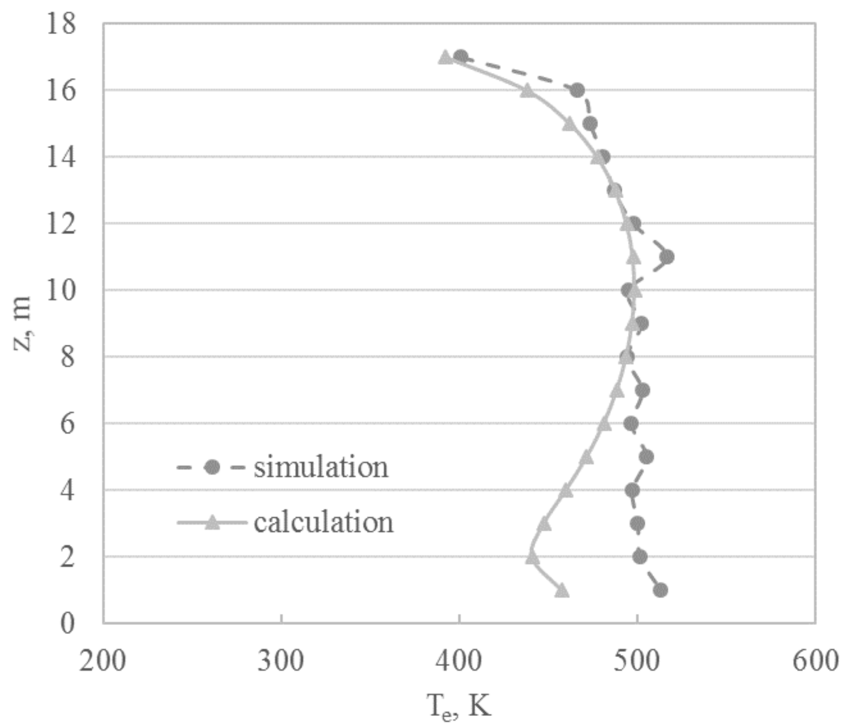

Figure 3.9 Comparison of simulation chamber edge temperature and calculated chamber edge temperature along the interface in Case 7 when steam chamber edge just becomes linear.

There is 99.99% bitumen and 0.01% methane in the live bitumen. The permeability of this reservoir is 2000 mD. The results show larger deviation in the bottom section of reservoir and this is because of the inaccuracy of temperature profile ahead of steam chamber edge used in derivation.

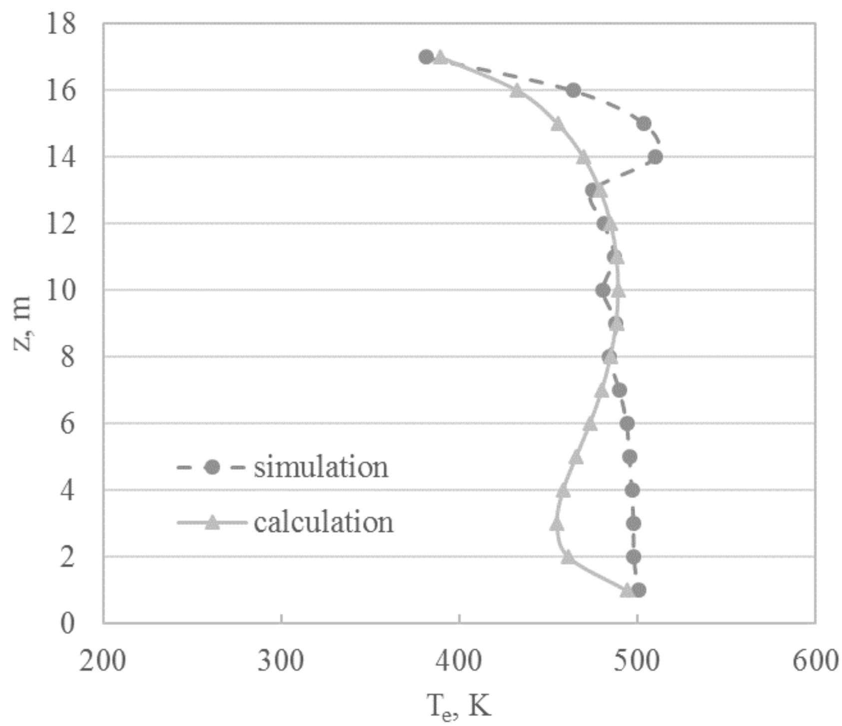

Figure 3.10 Comparison of simulation chamber edge temperature and calculated chamber edge temperature along the interface in Case 8 when steam chamber edge just becomes linear.

There is 99.99% bitumen and 0.01% methane in the live bitumen. The permeability of this reservoir is 6000 mD. The results show larger deviation in the bottom section of reservoir and this is because of the inaccuracy of temperature profile ahead of steam chamber edge used in derivation.

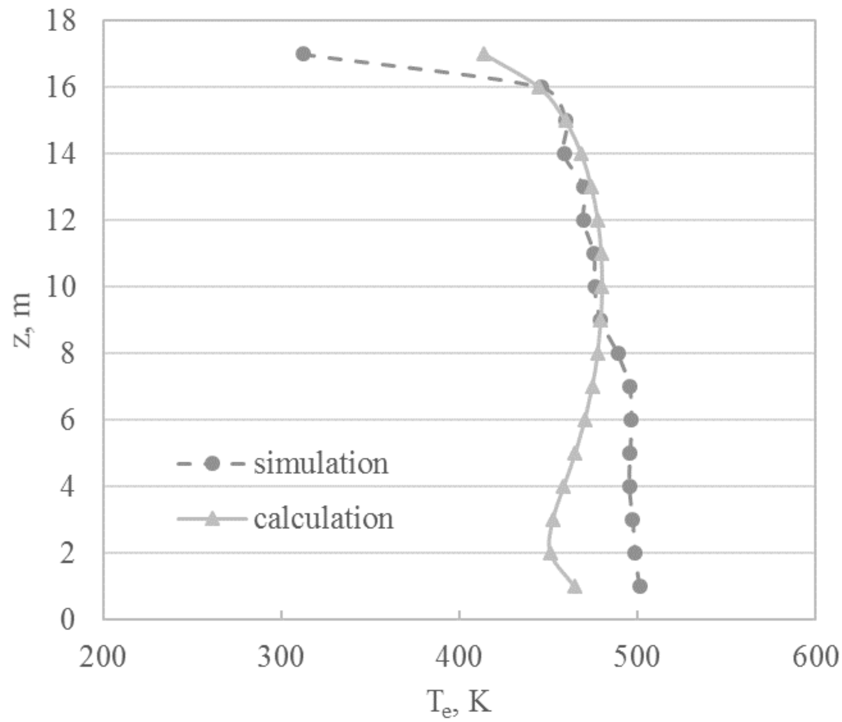

Figure 3.11 Comparison of simulation chamber edge temperature and calculated chamber edge temperature along the interface in Case 9 when steam chamber edge just becomes linear. Original live bitumen in the reservoir has 90% bitumen and 10% methane. There is compressible water dissolved in the oleic phase. Reservoir permeability is 4000 mD. There is also deviation in the calculation of chamber edge temperature at upper and bottom part.

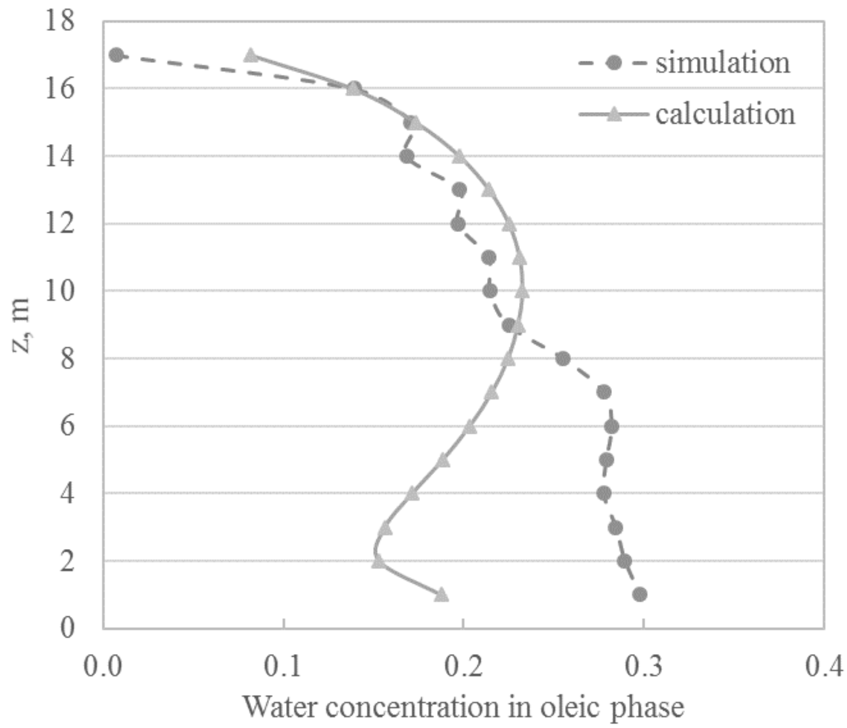

Figure 3.12 Comparison of simulation water mole fraction in the oleic phase and calculated water mole fraction along the interface in Case 9 with 90% bitumen and 10% methane originally in the reservoir.

There is compressible water dissolved in the oleic phase. Reservoir permeability is 4000 mD. Calculation result is not accurate because of the inaccurate calculation results of chamber edge temperature.

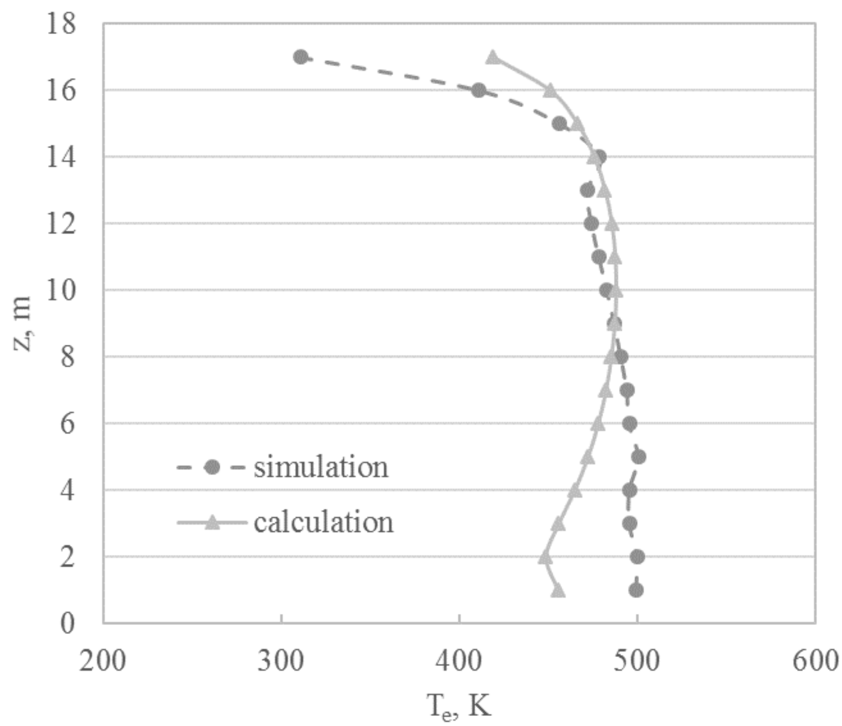

Figure 3.13 Comparison of simulation chamber edge temperature and calculated chamber edge temperature along the interface in Case 10 when steam chamber edge just becomes linear. Original live bitumen in the reservoir has 90% bitumen and 10% methane. There is compressible water dissolved in the oleic phase. Reservoir permeability is 2000 mD. There is also deviation in the calculation of chamber edge temperature at upper and bottom part.

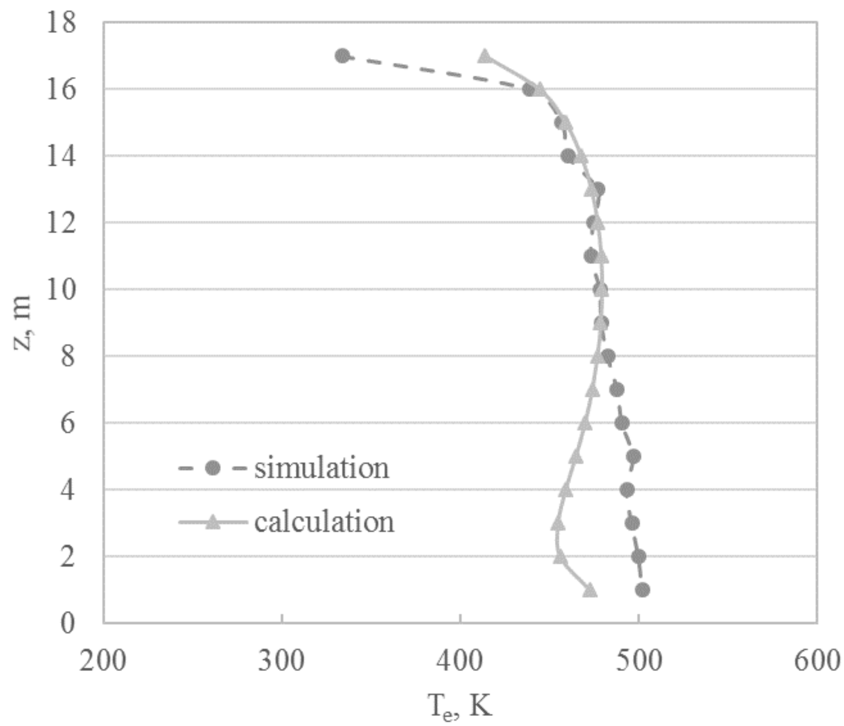

Figure 3.14 Comparison of simulation chamber edge temperature and calculated chamber edge temperature along the interface in Case 11 when steam chamber edge just becomes linear. Original live bitumen in the reservoir has 90% bitumen and 10% methane. There is compressible water dissolved in the oleic phase. Reservoir permeability is 6000 mD. There is also deviation in the calculation of chamber edge temperature at upper and bottom part.

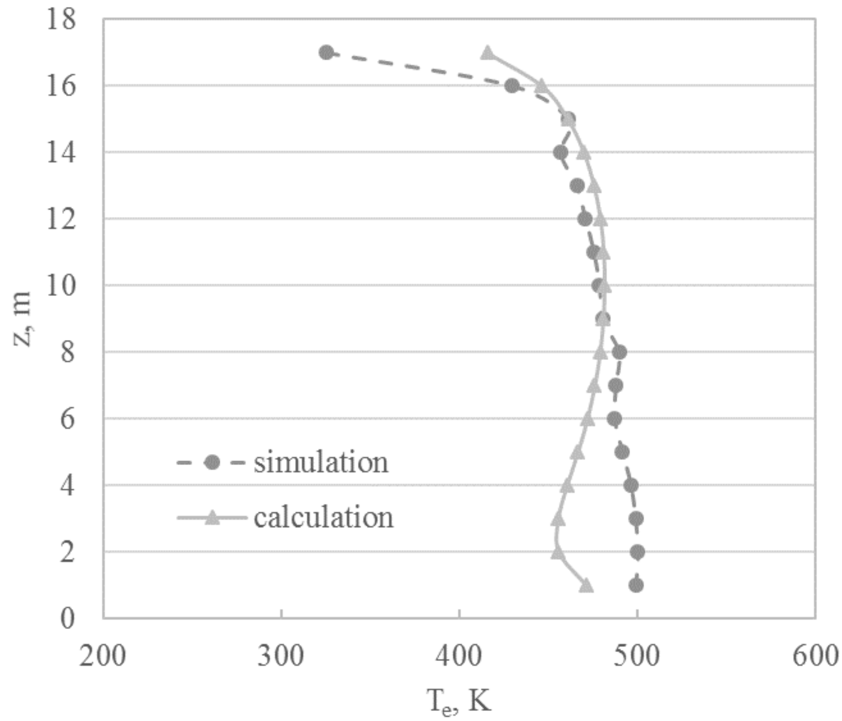

Figure 3.15 Comparison of simulation chamber edge temperature and calculated chamber edge temperature along the interface in Case 12 when steam chamber edge just becomes linear. Original live bitumen in the reservoir has 90% bitumen and 10% methane. Water dissolution in oleic phase is considered and water is incompressible in this case. Reservoir permeability is 4000 mD. There is also deviation in the calculation of chamber edge temperature at upper and bottom part.

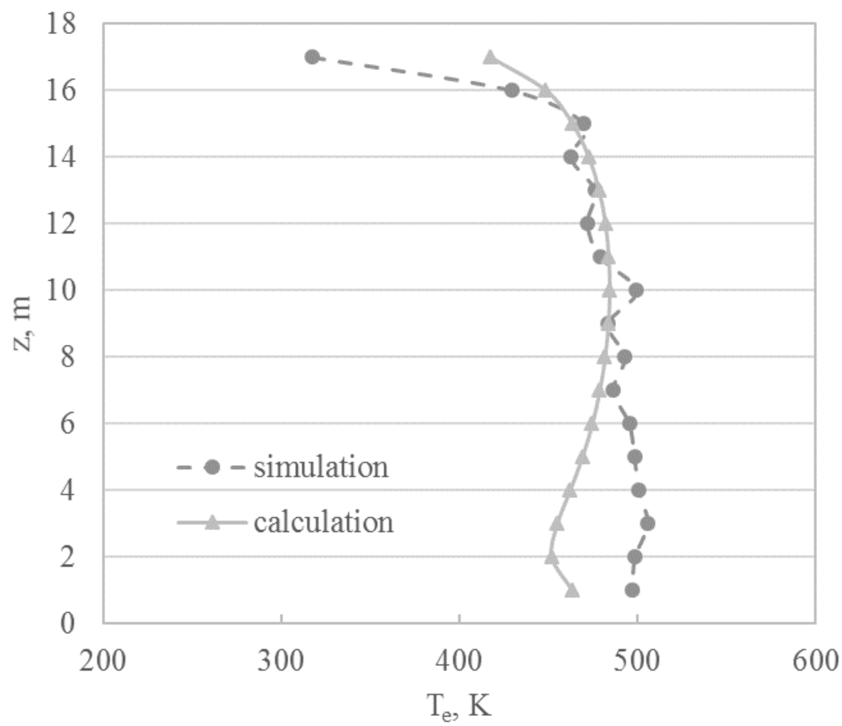

Figure 3.16 Comparison of simulation chamber edge temperature and calculated chamber edge temperature along the interface in Case 13 when steam chamber edge just becomes linear. Original live bitumen in the reservoir has 90% bitumen and 10% methane. Water dissolution in oleic phase is considered and water is incompressible in this case. Reservoir permeability is 2000 mD. There is also deviation in the calculation of chamber edge temperature at upper and bottom part.

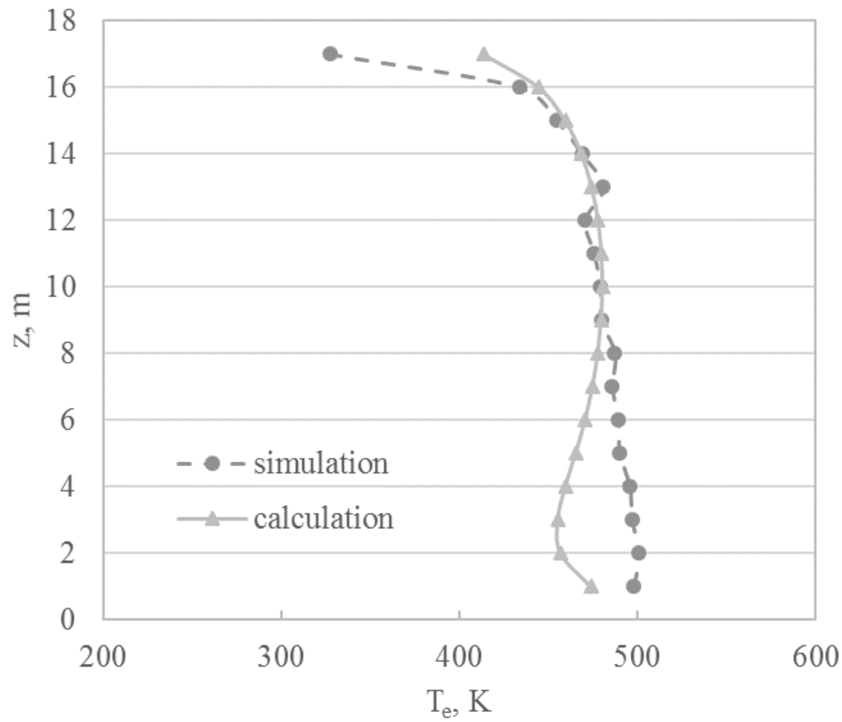

Figure 3.17 Comparison of simulation chamber edge temperature and calculated chamber edge temperature along the interface in Case 14 when steam chamber edge just becomes linear. Original live bitumen in the reservoir has 90% bitumen and 10% methane. Water dissolution in oleic phase is considered and water is incompressible in this case. Reservoir permeability is 6000 mD. There is also deviation in the calculation of chamber edge temperature at upper and bottom part.

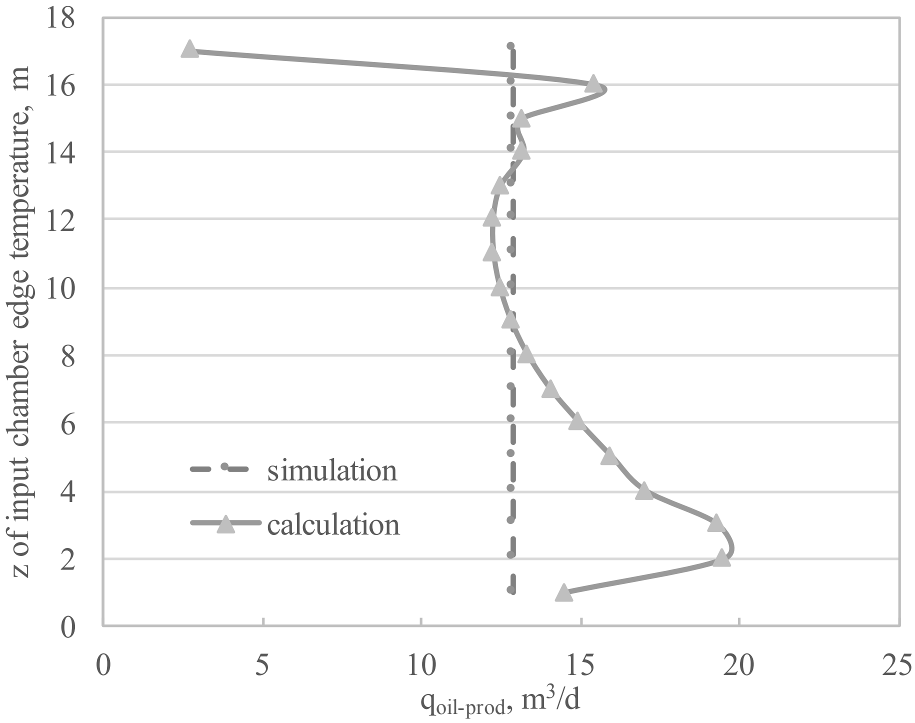

Figure 3.18 Calculation results of oil production rate using chamber edge temperature from different elevation

Chamber edge temperatures at different elevation in the simulation results are used to calculate oil production rate and compared in the above figure. It indicates that using chamber edge temperature at midpoint of steam chamber edge gives the best calculation results.

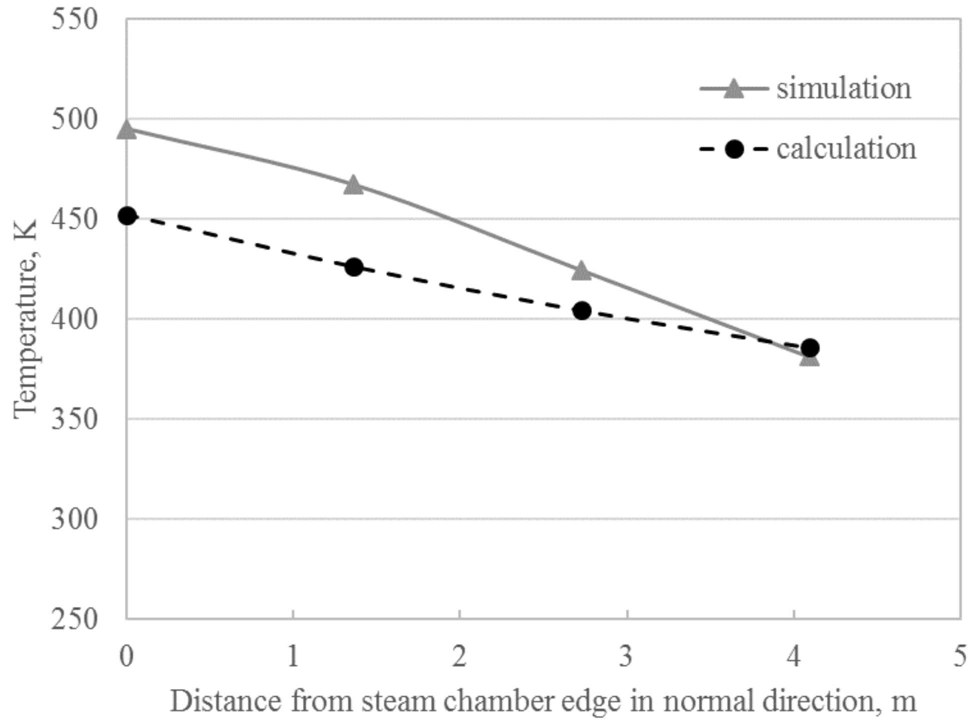

Figure 3.19 Temperature distribution ahead of chamber edge at the point where z=3m in Case 3

This is the layer with the maximum deviation in the calculation of chamber edge temperature. There is large deviation between the temperature profile used in the derivation and the simulation results in the bottom reservoir. This will result in deviation in calculation result and affect the accuracy of developed method.

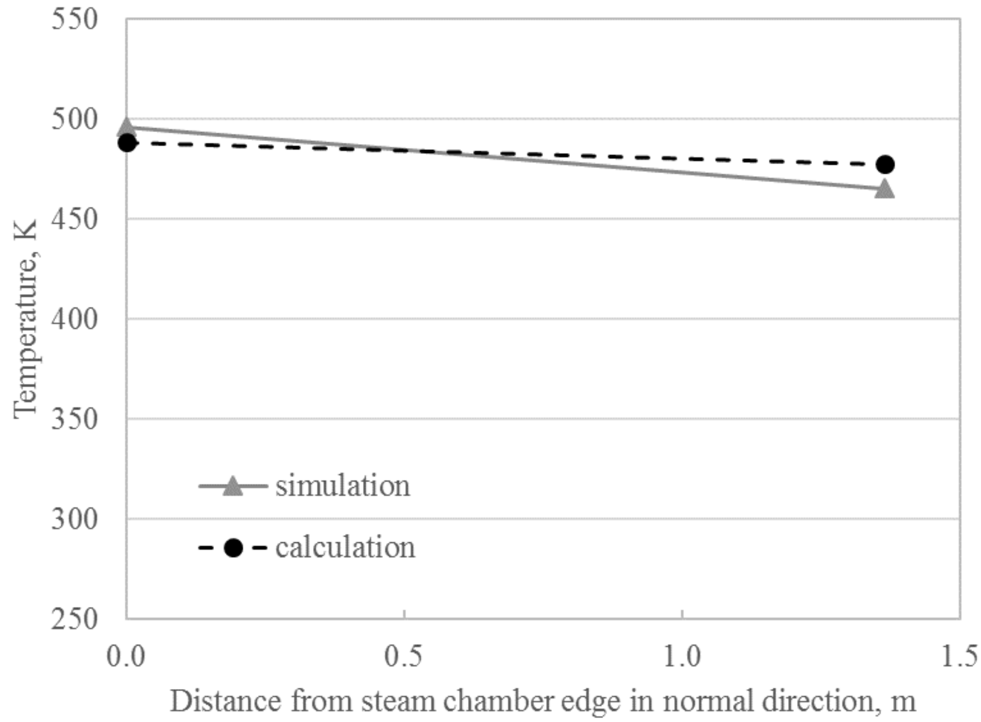

Figure 3.20 Temperature distribution ahead of chamber edge at the point where z=1m in Case 3

The temperature profile obtained in the analytical model gives better result in describing temperature distribution ahead of the edge than layer with z equal to 3 and this corresponds to the better accuracy in calculation result of chamber edge temperature. This manifests the importance of temperature distribution ahead of steam chamber edge to the accuracy of calculation results.

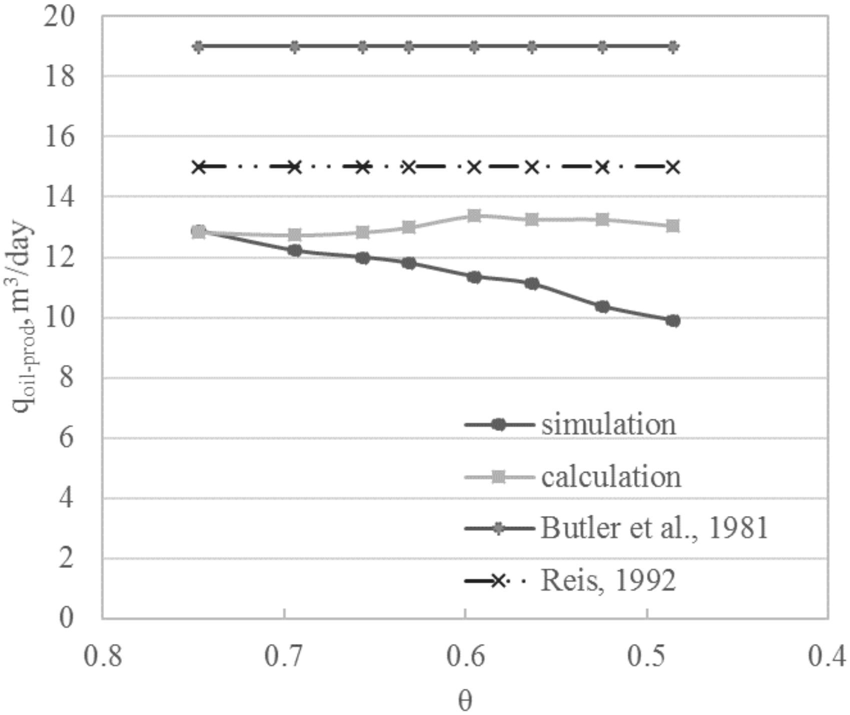

Figure 3.21 Calculation result from the developed model in Case 3 at different time

Calculation results of Case 3 at different time are compared to simulation results. It can be inferred that the developed model gives best results when steam chamber edge just becomes linear, i.e., under State I.

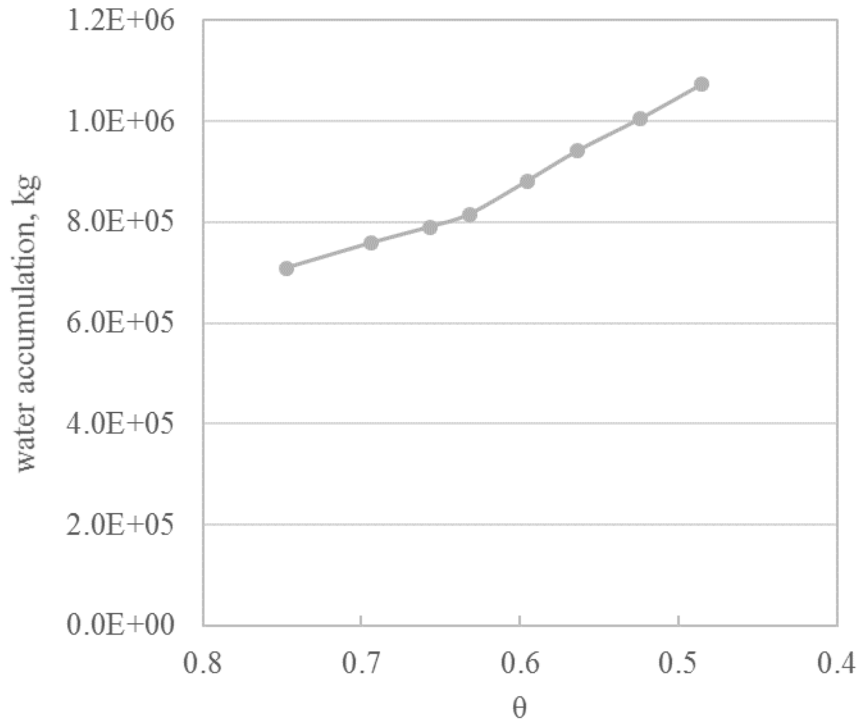

Figure 3.22 Water accumulation ahead of steam chamber in Case 3 as operation goes on. As operation goes on, angle θ decreases and water condensate accumulates ahead of steam chamber.

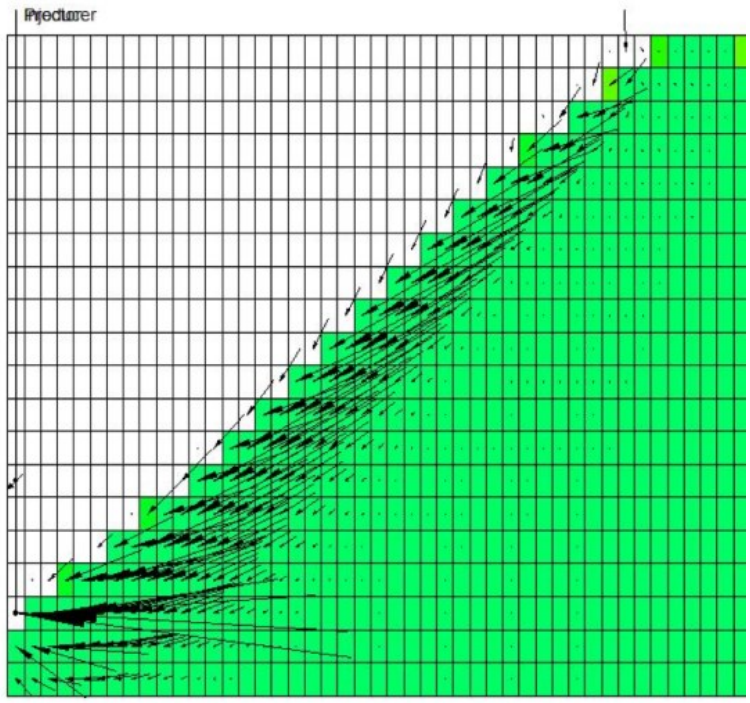

Figure 3.23 Flow vector inside the reservoir for Case 3.

This figure shows simulation result of Case 3 from CMG (2014). In the above figure, vapor phase saturation in white grid blocks are greater than one; that is, white grid blocks are inside steam chamber. Vapor phase saturation in green grid blocks are zero; that is, green grid blocks are ahead of steam chamber. The flow vector is parallel to the steam chamber edge in the upper reservoir. Chamber edge temperature increases along the edge as depth increases and the mobile bitumen region ahead of the edge is wider in the bottom layer. Because of this, flow is not parallel to the chamber edge in the bottom reservoir.

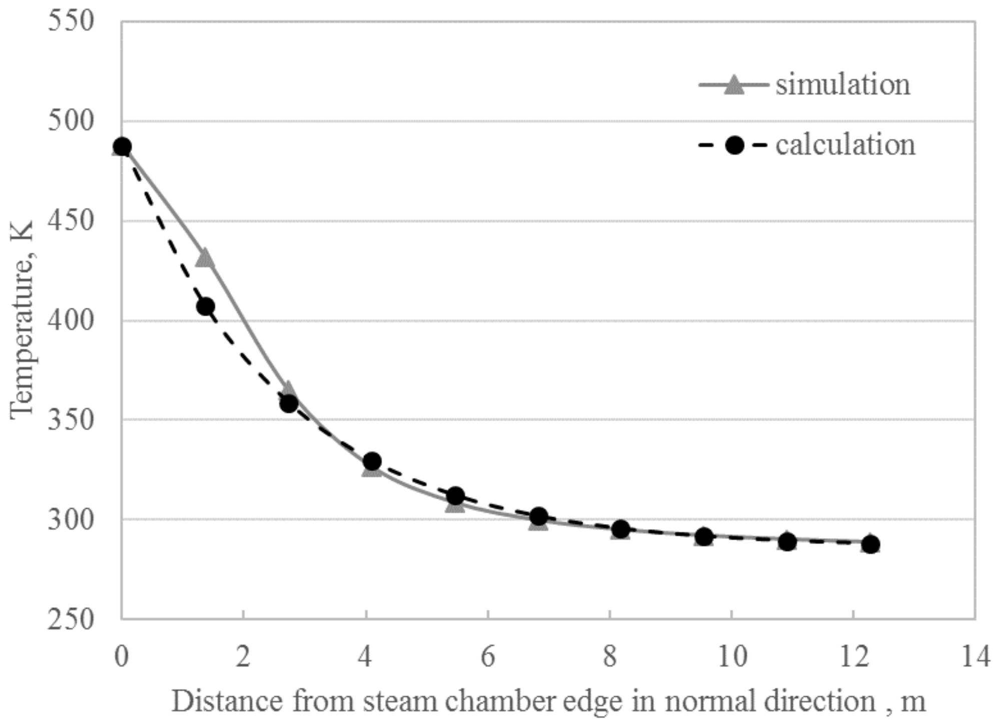

Figure 3.24 Temperature distribution ahead of chamber edge at the point where z=9m in Case 3

This is the layer which is chosen to predict oil production rate with Equation (2.27). Temperature profile used in derivation can describe the simulation result well in the middle part of reservoir.

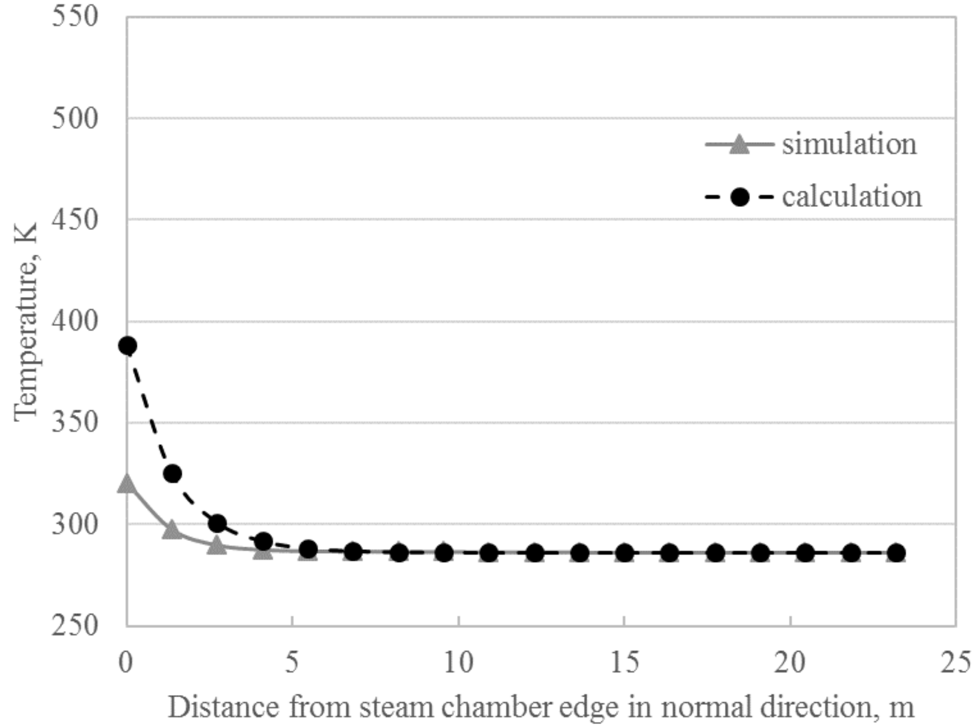

Figure 3.25 Temperature distribution ahead of chamber edge at the point where z=17m in Case 3. The temperature profile used in derivation cannot describe the simulation result in the upper reservoir but gives better temperature profile than that in the bottom layers. Therefore, the deviation in the calculation of upper reservoir is smaller than that in the bottom reservoir.

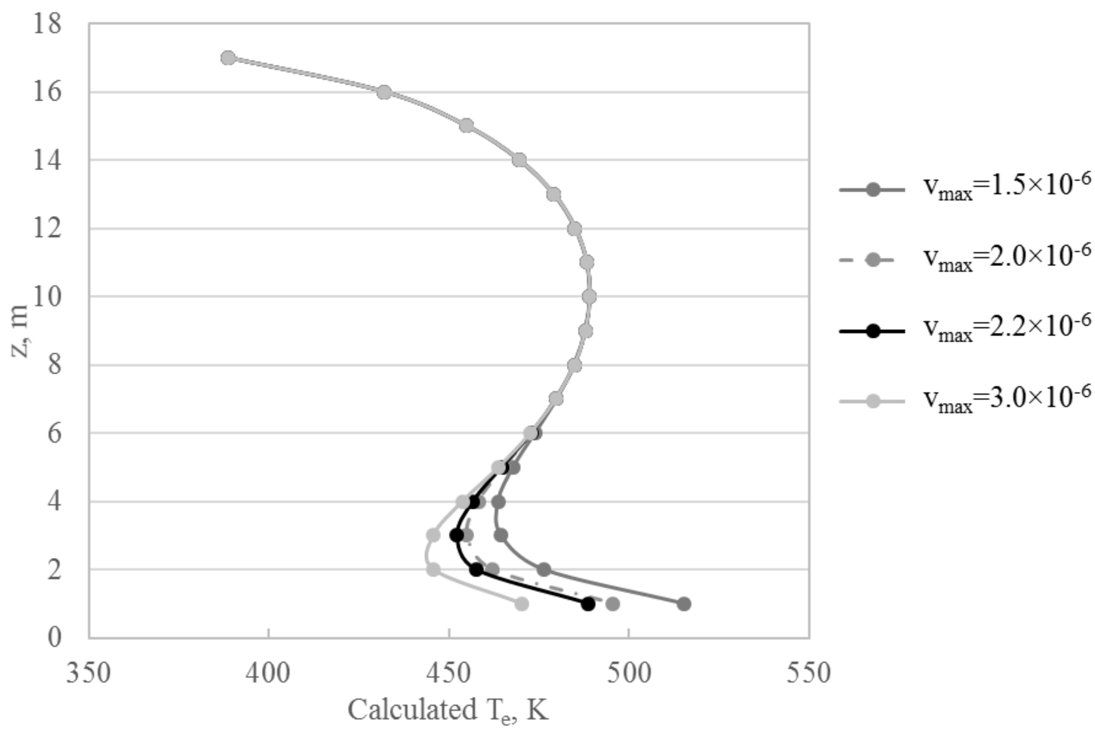

Figure 3.26 Comparison of calculated chamber edge temperature along the interface in Case 3 using different maximum chamber edge advancing velocities.

The accuracy of chamber edge advancing velocity largely affects the calculation results in the bottom reservoir while has little effect on the calculation in upper reservoir.

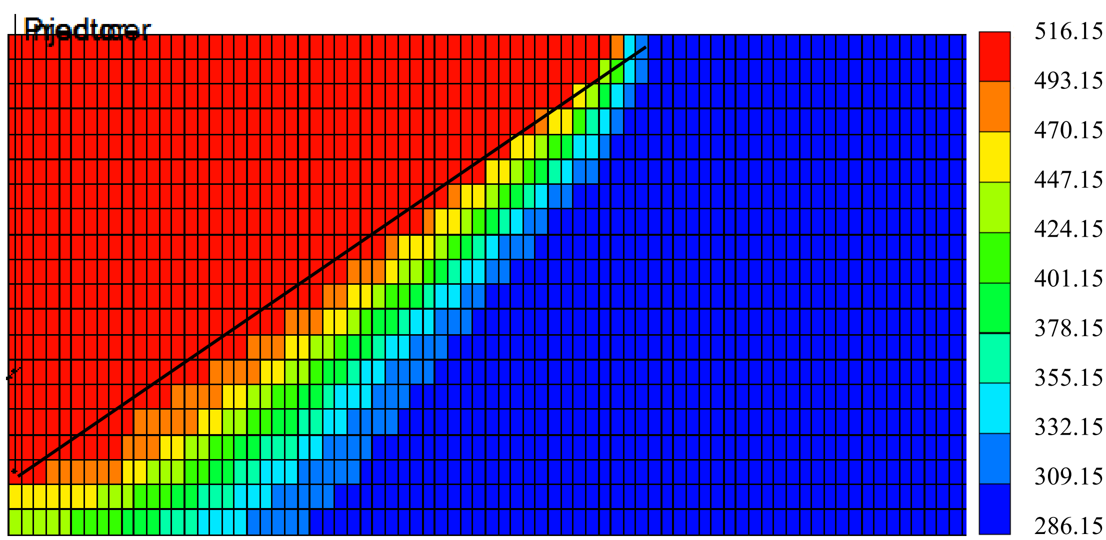

Figure 3.27 Temperature distribution in the reservoir

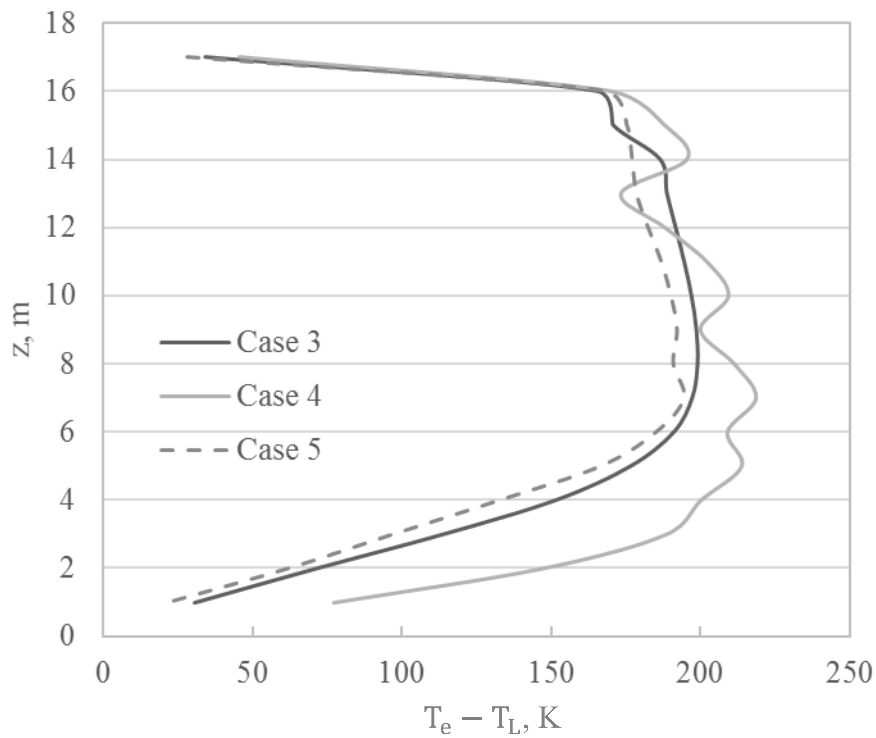

Figure 3.28 Comparison of values of [$T_{e(z)}$-$T_{L(z)}$] in Case 3, 4 and 5

CHAPTER 4 APPLICATION IN FIELD OPERARIONS

The developed model is based on the widely-used set of simplifying assumptions for analytical solution of SAGD, such as single-phase flow, 1-D flow along the edge of a steam chamber, pseudo-steady-state heat transfer, and homogeneity of the reservoir. However, the previous chapter showed that it gives more accurate results than previous analytical models. In this chapter, the developed model is applied to three field operations: Surmont project, Hilda Lake project and Hangingstone project. Calculation results of production rate, temperature along the edge of the steam chamber and SOR in these three projects are presented in this chapter. Deviations in the calculation results from field data are analyzed and discussed.

4.1 Calculation of production rate and steam chamber edge temperature

Steam chamber shape is assumed to be a whole inverted triangle with its vertex attached at the production well as shown in Figure 4.1. In Chapter 2 and 3, all derivation and validation are conducted in half of reservoir. In order to use the developed model in the field operations, some changes need to be done and new equations as listed as follows.

The developed model uses Equation (2.27) to estimate bitumen production rate ahead of one side of a steam chamber. It can be written as follows when applied in field operations:

$$q_{prod} = 2\sqrt{\tau k g H \varphi \Delta S_O \Delta y^2 / \left[2 z_D \left(1 - {z_D}^2\right)\right]}, \tag{4.1}$$

where $\tau_{(z)} = \int_{T_{L(z)}}^{T_{e(z)}} \alpha / [\nu_o (T - T_R)]\, dT$, $z_D = z/H$.

From this equation, it is known that there are some data of each project needed in the calculation. Other than reservoir properties and fluid properties, it needs to know cumulative bitumen production to calculate steam chamber expansion and to locate the position of steam chamber edge. One steam chamber edge temperature (T_e) is needed and this can be obtained from an observation well that is laterally separated from production well. The steam chamber edge temperature can be read from the observation data at the point that steam chamber edge intersects with the observation well. Oil production rate from field data is needed to compare the calculation results of developed model.

To obtain a steam chamber edge temperature (T_e), we need to locate steam chamber edge and the intersection point of steam chamber edge and observation well. Steam chamber is assumed an inverted-triangle as shown in Figure 4.1 in the thesis. With known cumulative bitumen production (Q_o), width of steam chamber (W_S) can be obtained by the following equation:

$$Q_o = \varphi \Delta S_o H W_S \Delta y/2. \quad (4.2)$$

Derivative of the above equation in term of time gives the calculation of v_{max} in field operations.

$$v_{max} = \frac{d(W_S/2)}{dt} = q_{oil-prod}/(\varphi \Delta S_o H \Delta y). \quad (4.3)$$

With the calculated chamber width (W_S), according to similar triangle rule, the position of intersection of steam chamber edge and observation well can be obtained by

$$0.5W_S/(0.5W_S - L) = H/(H - z). \quad (4.4)$$

In the annual reports of each project, depth of production well and temperature along the observation well is given. With known value of "z" in the above equation, elevation of the intersection point is known. With temperature data of observation well, steam chamber edge temperature (T_e) at that intersection point can be read.

In Equation (4.1), T_L is needed. In the developed model in Chapter 2.1, T_L can be calculated by Equation (2.14):

$$T_L = T_R + (T_e - T_R)\exp[-v_{max} z^2 \tan\theta/(H\alpha)]. \quad (2.14)$$

Thus, at the beginning of calculation, T_L is assumed equal to initial reservoir temperature (T_R). Then, calculation of Equation (4.1) will give a production rate. Using this production rate in Equation (2.14) to calculate T_L and taking the new T_L into Equation (4.1) to calculate a new production rate. Repeat above steps until the difference between new calculated production rate and previous calculated production rate is less than 0.1 m^3/day. Figure 4.2 shows the iterative procedure for calculation of oil production rate. Moreover, with calculated oil production rate, temperature along the edge of a steam chamber can be solve by Equation (4.1).

According to the aforementioned steps for validation, calculation is conducted in the following three filed operations, Surmont Project, Hangingstone Project, and Hilda Lake Project since they have enough data required for validation. Table 4.1 shows data used in validation and comparison of calculation results with field data for these three projects.

Values of parameters used in calculation for Surmont project are from ConocoPhillips annual report to ERCB (2008) while heat capacities of reservoir and overburden formations are from Gates and Chakrabarty (2006). There are heat capacity values for Surmont project. Since Surmont project locates in the Athabasca area, values for Athabasca reservoir analysis provided in Gates and Chakrabarty (2006) are used.

Values of parameters used in calculation for Hangingstone project are from JACOS annual reports to ERCB (2011, 2012). Heat capacities of reservoir and overburden formation are from Miura and Wang (2012).

Values of parameters used in calculation for Hilda Lake project are from Shell annual report to EUB (2008) while heat capacities of reservoir and overburden are from Edmunds and Peterson (2007). Although the heat capacities in Edmunds and Peterson (2007) are not for Hilda Lake, these two values are for a project in Cold Lake area where Hilda Lake project locates.

Moreover, developed analytical model requires a chamber edge temperature to calculate production rate. Validation against simulation results mentioned that the temperature distribution ahead of steam chamber edge used in the thesis is not accurate in the bottom and top of reservoir due to different reasons. From validation with simulation cases, it was found that using chamber edge temperature at the midpoint gives the best calculation results. However, in the field, there are limited observation wells and thermocouple data. Most observation wells have small lateral distance with production well, making it almost impossible to find the chamber edge temperature at the midpoint.

Because most observation wells locate near production wells, only the chamber edge temperature at the bottom of reservoir can be obtained. Butler (1985) and Kesharvarz et al. (2016) discussed the unsteady state heat conduction in the SAGD. They mentioned that there are two different situations in the heat transfer ahead of steam chamber. At the midpoint, heat transfer can be treated as quasi-steady state conduction and temperature distribution can be expressed as

$$(\mathrm{T}-\mathrm{T_R})/(\mathrm{T_e}-\mathrm{T_R}) = \exp(-\mathrm{U}\xi/\alpha) = \exp(-\xi \mathrm{v}\sin\theta/\alpha). \tag{4.5}$$

When the interface is stationary, temperature distribution is

$$(\mathrm{T}-\mathrm{T_R})/(\mathrm{T_S}-\mathrm{T_R}) = \exp[-2\mathrm{U}\xi/(\pi\alpha)]. \tag{4.6}$$

As steam chamber is assumed an inverted triangle. Chamber edge advancing velocity increases linearly with elevation and is low at the bottom of reservoir. For bottom, the second equation may better describe temperature distribution ahead of steam chamber. Thus, there are two calculation results shown in Table 4.1. “Current theory” shows the results obtained when temperature distribution ahead of chamber is expressed as Equation (2.12), while “Current theory-stationary” shows the results obtained when temperature distribution ahead of chamber is expressed as Equation (4.6). However, it is found that "Current theory-stationary" gives worse results. This may be because that although we get chamber edge temperature data in the bottom of reservoir, the steam chamber edge movement still cannot be ignored. Thus, results shown in "Current theory" should be used for better calculation results.

From Table 4.1, it is found that developed model gives good calculation results in oil production rate. In addition, all prior models input static parameters to calculate oil production rate. The developed model uses real-time temperature, which gives real-time oil production rate.

In addition, steam chamber edge temperature (T_e) along the interface is calculated based on the developed method for all three field operations. Results are shown in Figure 4.3, Figure 4.4 and Figure 4.5 for Surmont project, Hangingstone project and Hilda Lake project respectively. From calculation results, it is clearly shown that steam chamber edge temperature (T_e) is not constant along the interface. T_e is low in the top part and increase to a higher temperature quickly.

4.2 Discussion on deviation in production rate calculation

From calculation results shown in the previous section, there are larger deviations in production rate calculation for Surmont and Hilda Lake project. Hangingstone project has good production rate result. SOR calculation also shows similar trend. There are several possible reasons for deviation and will be discussed here.

4.2.1 Reservoir heterogeneity

In the annual reports of three field operations, there is geology information about each reservoir. Figure 4.6, 4.7 and 4.8 are geology analysis for Surmont project (ConocoPhillips, 2008), Hangingstone project (JACOS, 2012) and Hilda Lake project (Shell, 2008), respectively. It can be inferred that there are less mud and shale barriers and nodules in the continuous bitumen zone in the Hangingstone project compared to the other two projects. According to Gotawala and Gates (2010), there are mud and shale barriers, calcite nodules and tight sand zones in the reservoir, leading to heterogeneous reservoir. This will affect development of steam chamber and heat transfer inside reservoir, resulting in lower temperature at the ceiling of steam chamber. From Figure 4.6, Figure 4.7 and Figure 4.8, it can be inferred that reservoir in the Hangingstone project is most homogeneous among the three projects. Existence of barriers make reservoir heterogeneous, which is different from the homogeneous reservoir assumed in the analytical model. Barriers will also block downward movement of oil flow to the production well, impairing production rate. Moreover, during steam chamber expansion, barriers are heated, resulting in higher SOR. Existence of barriers in the reservoir is not considered in the developed analytical model, which results in deviation in production rate calculation.

4.2.2 Effective length

In the ideal SAGD operation, steam chamber develops along the whole well pair. However, this is not always true in the field operations. Due to various reasons (Zhang et al., 2005; Gotawala and Gates, 2009; Gotawala and Gates, 2010), such as reservoir heterogeneity and well completion, non-uniform steam chamber develops along the well. Using a wrong well length in calculation will definitely lead to an inaccurate calculation result. Using "effective length" to represent the ratio of the length of well where steam chamber evolves to well length.

$$\text{Effective length} = L_{SC}/L, \tag{4.7}$$

where L_{SC} is the length of well where steam chamber evolves, L is the total length of the horizontal well pair.

Calculations are conducted with different value of effective length and results for "Hilda Lake, Cold Lake" project are shown in Table 4.2. According to the calculation results, steam chamber evolves at 70% of well length.

In addition, the annual report of "Hilda Lake, Cold Lake" project (Shell, 2008) mentioned that steam chamber does not evolve along the whole well pair. There are four observation wells along the well pair and one of them did not detect steam chamber since the beginning of operation. This statement supports the calculation results in Table 4.2.

Calculations with different effective length are also conducted for the other two projects. Unlike Hilda Lake project, calculation results with 1.0 effective length give the best production rate for Surmont project and Hangingstone project. Calculation with a low effective length gives a high oil production rate. This indicates that steam chamber evolves along the whole well pair. Deviation in calculation results and field measurement may be caused by other possible reasons.

Based on the above discussion, deviation between oil production rates from calculation and field measurement can be a sign of problems in operation, such as non uniform steam chamber development along the well. Problems in operation will make field operations more different from the ideal case used in analytical model, which will lead to inaccurate calculation results of production rate. Thus, the developed analytical model can be used as a sign of problems.

4.2.3 Operation time

As mentioned in the validation against simulation cases, the developed analytical model gives best results when steam chamber edge just becomes linear. As operation time becomes long, deviation in calculation results increases due to accumulation of water condensation ahead of the edge of a steam chamber.

For Surmont project, calculation is conducted after operating for ten years. Operation time of calculation for Hangingstone and Hilda Lake are eight years and eleven years respectively. Among these three projects, Hangingstone project has the least operation time and best accuracy in calculation. On the contrary, Hilda Lake project has the longest operation time and worst accuracy in calculation.

4.3 Calculation of SOR

SOR calculations for all three cases are conducted as aforementioned. As mentioned in Chapter 4.1, heat capacity values for each field operations are not directly taken from their reports and are inaccurate. Heat capacity used in the SOR calculation for Surmont project is not found. Since Surmont project is in Athabasca region, average heat capacity in Athabasca can be found in the literature (Gates and Chakrabarty, 2006) and is used in the SOR calculation for Surmont project. Heat capacity values of Hangingstone project are from Miura and Wang (2012). Hilda Lake project locates in Cold Lake region. Heat capacity of Hilda Lake project used in the calculation is from another project locating in Cold Lake region. Thus, heat capacity in Hangingstone project is more reliable among the three field operations. Heat capacity of bitumen (M_o) equals to 2.09×10^3 J/(kgK).

According to the energy balance in Equation (2.28):

$$Q'_{inj} = Q'_{SC} + Q'_{AC} + Q'_{OB} + Q'_{PO}. \tag{2.28}$$

There are four terms in the calculation of SOR. Calculation for Q'_{SC}, Q'_{AC} and Q'_{OB} should be twice as much as that in Chapter 2. This is because that there is only half of a steam chamber in the derivation in Chapter 2 while there is a full steam chamber in the field operations in Chapter 4. The calculation of Q'_{PO} are not affected. Calculation results of instantaneous SOR for field operations with a full steam chamber are listed in Table 4.3 in the column "SOR using T_S". Calculation results are calculated by using T_S as the temperature at the contacting area of steam chamber and overburden are shown. The usage of T_S will be discussed in next section. It shows that there is some deviation in the SOR calculation results.

Equation (2.28) shows that the heat injected is consisted of four terms. Percentage of each term in the SOR calculation in the three field operations are presented in Table 4.4. Comparison between Table 3.35, which shows the percentages in simulation cases, and Table 4.4 shows that heat loss to overburden is more significant in field operations. This may be the reason for inaccurate SOR calculation results. Discussion of the calculation of heat loss to overburden in field operations will be shown in next section.

4.4 Sensitivity analysis of SOR calculation in field operations

Unlike the accurate SOR value obtained in simulation cases, Table 4.3 shows that there is some deviation between the calculation results of SOR and field data in field operations. This section will focus on discussion of these two possible reasons for the inaccurate SOR calculation results in field operations.

From Equation (2.47) and Equation (2.48), it can be inferred that heat capacity values are important in the calculation of SOR. In field operations, heat capacity values of reservoir are average properties of a huge reservoir which may not represent the local properties. Sensitivity analysis of heat capacity values on SOR calculation will be conducted in this section. Moreover, as mentioned in the previous section, heat loss to overburden in the calculation results is more significant in the field operations than that in simulation cases. Calculated SOR using different $T_{ceiling}$ are different. The inaccurate SOR value may be caused by the inaccurate $T_{ceiling}$. Investigation is conducted into the effect of the value of $T_{ceiling}$ on SOR calculation.

4.4.1 Heat capacity

As mentioned before, heat capacity values used in the calculation are not reliable in the Surmont and Hilda Lake projects. Calculation results are not satisfying in these two projects. Sensitivity analysis of heat capacity values on the calculation results of SOR are conducted in these two field operations.

Figure 4.9 and Figure 4.10 show how SOR calculation results change with heat capacity values of reservoir and overburden in Surmont project and Hilda Lake project respectively. “Ratio” in the x-axis expresses the ratio of heat capacity values used to heat capacity in Table 4.1. Line “SOR using T_S” is the calculation result using steam temperature as temperature at the contact area between steam chamber and overburden ($T_{ceiling}$). Line “SOR using $T_{e(ceiling)}$” uses calculated steam chamber edge temperature (T_e) as temperature at the contact area between steam chamber and overburden ($T_{ceiling}$). These two figures indicate that heat capacity values of reservoir and overburden will largely affect SOR calculation results.

Figure 4.11 and Figure 4.12 show how SOR calculation results change with heat capacity of reservoir in Surmont project and Hilda Lake project respectively. Heat capacity of overburden (M_{over}) remains constant as the value in Table 4.1. “Ratio” in the x-axis is the ratio of heat capacity of reservoir (M_R) used to heat capacity of reservoir (M_R) from literature in Table 4.1. Line “SOR using Ts” and line “SOR using $T_{e(ceiling)}$” have the same meaning as those in Figure 4.9. They show that heat capacity of reservoir will affect SOR calculation results.

Figure 4.13 and Figure 4.14 show how SOR calculation results change with heat capacity of overburden (M_{over}) in Surmont project and Hilda Lake project while heat capacity of reservoir (M_R) remains constant as the value in Table 4.1. “Ratio” in the x-axis is the ratio of heat capacity of reservoir (M_{over}) used to heat capacity of reservoir (M_{over}) from literature in Section 4.3. Line “SOR using Ts” and line “SOR using $T_{e(ceiling)}$” have the same meaning as those in Figure 4.9. The indicate the heat capacity of overburden will affect SOR calculation results since it determines heat loss to overburden.

From Figure 4.9-4.14, it can be inferred that heat capacity of reservoir and overburden play an important role in the calculation of SOR, especially heat capacity of reservoir (M_R). Inaccurate heat capacity values will lead to inaccurate SOR values. Heat capacity of reservoir (M_R) is used on the calculation of two terms, Q'_{AC} and Q'_{SC}, in Equation (2.28). Table 4.4 shows that Q'_{AC} and Q'_{SC} compromise nearly 60% of Q'_{inj}, making heat capacity value of reservoir vital in the calculation of SOR. Heat capacity of overburden (M_{over}) determines the calculation of Q'_{OB}, which composes around 35% of Q'_{inj} according to Table 4.4. It also affects SOR calculation results.

However, real reservoirs are heterogeneous. Heat capacity values are based on the core sample tested, which may not represent the heat capacity for the large reservoir. There is a high possibility that deviation in SOR calculation are from the inaccurate heat capacity values.

Compared to the heat capacity values used in the other two projects, heat capacity values in Hangingstone project is more reliable. Thus, following discussion about deviation in SOR results will only concern Hangingstone project.

4.4.2 $T_{ceiling}$ used in SOR calculation

Real reservoirs are heterogeneous. According to Gotawala and Gates (2010), there are mud and shale barriers, calcite nodules and tight sand zones in the reservoir, leading to heterogeneous reservoir. This will affect development of steam chamber and heat transfer inside reservoir, resulting in lower temperature at the ceiling of steam chamber. Thus, temperature at the contact area between steam chamber and overburden formation ($T_{ceiling}$) does not equals to steam temperature (T_S) all over the contact area.

$$Q'_{OB} = 2M_{over}\left(T_{ceiling} - T_R\right)\Delta y\sqrt{\alpha v_{max} W_S/\pi}. \tag{2.43}$$

Equation (2.38) shows that the choice of temperature ($T_{ceiling}$) at the contact area between steam chamber and overburden formation will affect calculation of SOR. It is mentioned that temperature at the contact area in the simulation cases is at steam temperature (T_S). However, reservoir is heterogeneous in the field operations. Temperature inside steam chamber equals to steam saturation temperature under injection pressure in the homogeneous reservoir in simulation cases. Due to heterogeneity, temperature inside steam chamber is not as uniform as that in simulation cases. It is hard to know the temperature at the contact area in the field operations. Sensitivity analysis is conducted in the Hanging-stone project in Figure 4.15. Figure 4.15 shows how SOR changes with different choice of temperature at the bottom of overburden formation. The highest temperature in Figure 4.15 is steam injection temperature and lowest is calculated chamber edge temperature (T_e) at the top of reservoir. It shows that calculated SOR equals to SOR in the report when 447.15 K is used in calculation, which is lower than the steam temperature (T_S).

4.5 Summary

The developed model was applied for three field operations with data from field measurements. Calculation results in terms of production rate gave the most accurate values with the developed model. A large deviation between calculation results and field data, if observed, can be used as an indicator for potential operation problems, such as non-uniform chamber development along the horizontal-well pair.

There was some deviation in the calculation results from field data in terms of SOR. According to the analysis in this chapter, part of the reasons likely comes from reservoir heterogeneity. Reservoirs are assumed to be homogeneous in the analytical model, which is not always accurate due to the variability of sand quality in bitumen reservoirs. First, shale and mud barriers require extra heat, yet little bitumen will be produced from them. Second, temperature is not uniform inside steam chamber due to heterogeneity. These two factors lead to inaccurate SOR calculation results.

Table 4.1 Comparison of calculation results from field data

	ConocoPhillips Surmont	JACOS Hangingstone	Shell Hilda Lake, Cold Lake
Well Pair	A	I	I1/P1
T_R, K	288.15	293.15	293.15
T_S, K	498.15	533.15	518.15
ρ_o, kg/m^3	880	980	880
H, m	30	25	25
Δy, m	850	500	1000
φ	0.33	0.35	0.35
α, m^2/s	7.00×10^{-7}	7.00×10^{-7}	7.00×10^{-7}
k, m^2	5.00×10^{-12}	5.00×10^{-12}	5.00×10^{-12}
Average k_{ro}	0.2	0.3	0.2
ΔS_o	0.67	0.67	0.51
v_s, m^2/s	3.41×10^{-6}	4.28×10^{-6}	3.41×10^{-6}
m	4	4	4
Corey's parameter, a	4	2	3
M_R, J/(m^3·K)	2.60×10^{6}	2.35×10^{6}	2.56×10^{6}
M_{over}, J/(m^3·K)	2.60×10^{6}	2.38×10^{6}	2.47×10^{6}
Steam Quality	98%	97%	95%
Latent Heat, J/kg	1.84×10^{6}	1.66×10^{6}	1.74×10^{6}
Input T_e, K	398.27	532.15	435.87
z_D	0.7183	0.0687	0.1749
SOR	4	4	3.2
CSOR	3.5	3.5	3.4
Oil flow rate q_o, m^3/d			
Butler et al. (1981)	379	229	366
Tandrain	329	199	317
Lindrain	306	185	295
Reis (1992)	300	181	290
Current theory-stationary	110	121	155
Current theory	87	119	137
Field data	36	55	46

Table 4.2 Calculation results of production rate with different effective lengths in Hilda Lake project

Effective length	1.0	0.9	0.8	0.7
Current theory, m^3/d	137	104	72	45

Table 4.3 Calculation of SOR for field operations

Operation	T_S, K	SOR using T_S	SOR from report
Surmont	498.15	3.0	4.0
Hangingstone	533.15	4.6	4.0
Hilda Lake	518.15	4.6	3.2

Table 4.4 Fraction of each term in the energy balance equation in field operations

	Q'_{PO}	Q'_{SC}	Q'_{AC}	Q'_{OB}
Surmont	7.13%	45.55%	13.72%	33.60%
Hangingstone	6.74%	32.91%	24.07%	36.28%
Hilda Lake	5.41%	42.15%	18.79%	33.65%

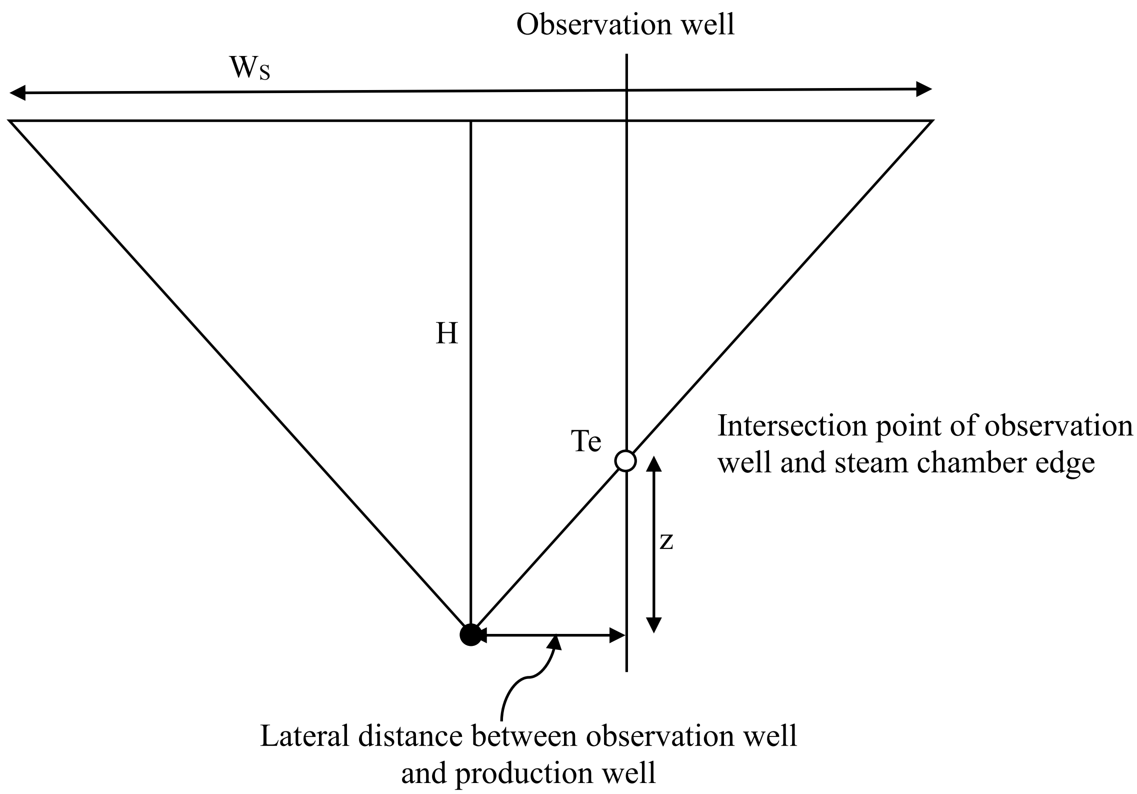

Figure 4.1 Schematic figure to explain how to get a steam chamber edge temperature T_e from observation well data

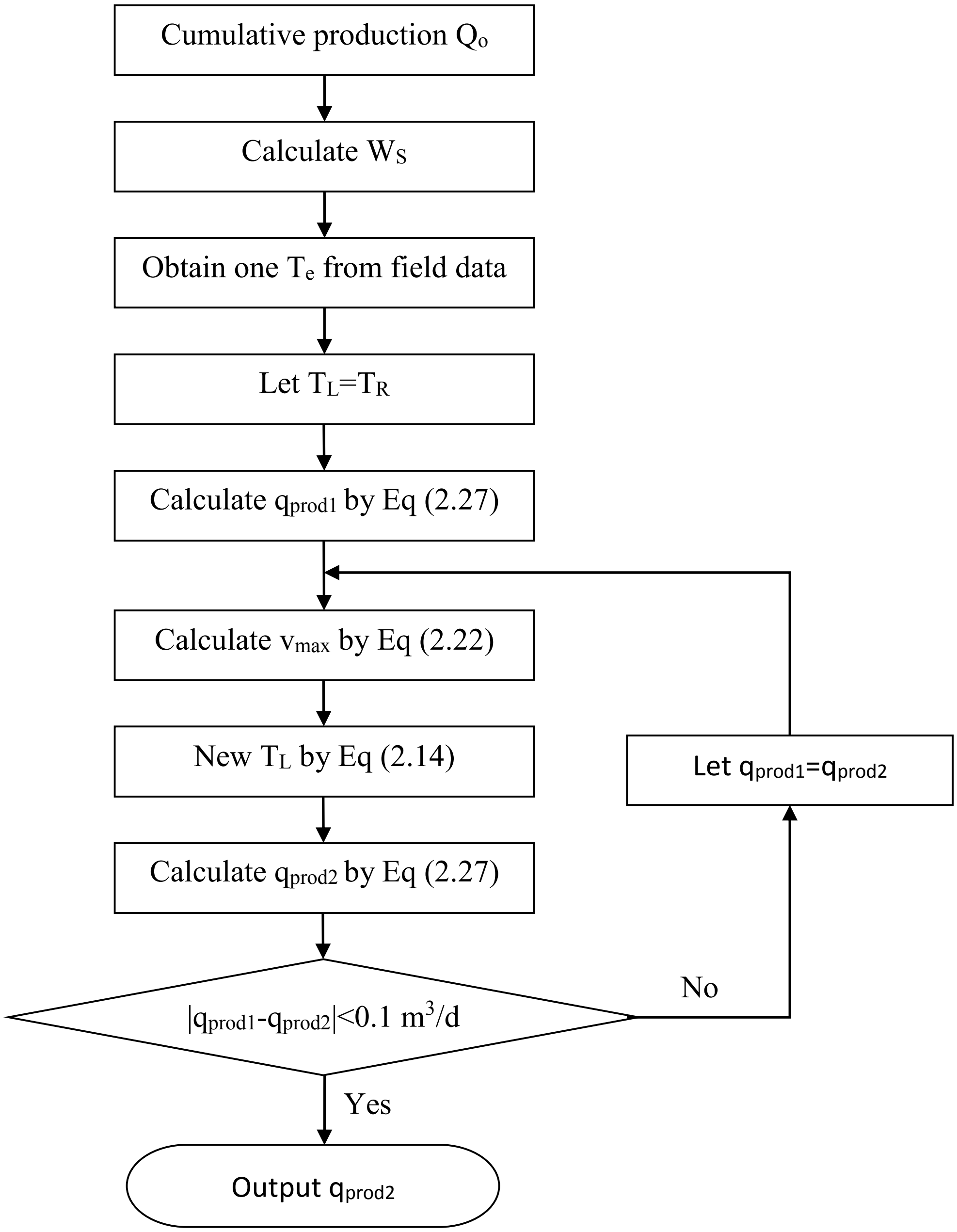

Figure 4.2 Flowchart of the iterative procedure for oil production calculation in field operations

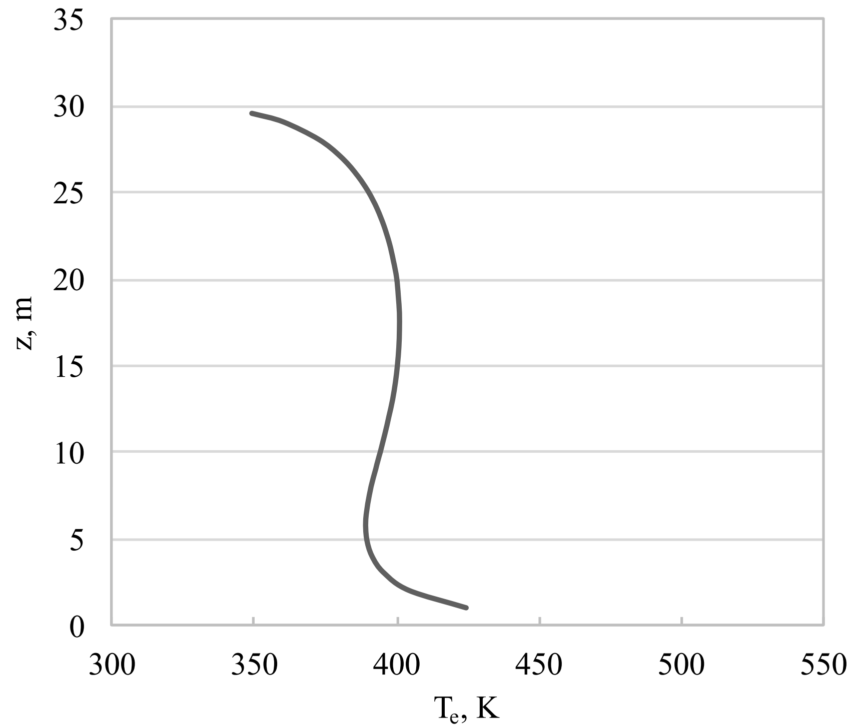

Figure 4.3 Steam chamber edge temperature (T_e) calculation results of Surmont project

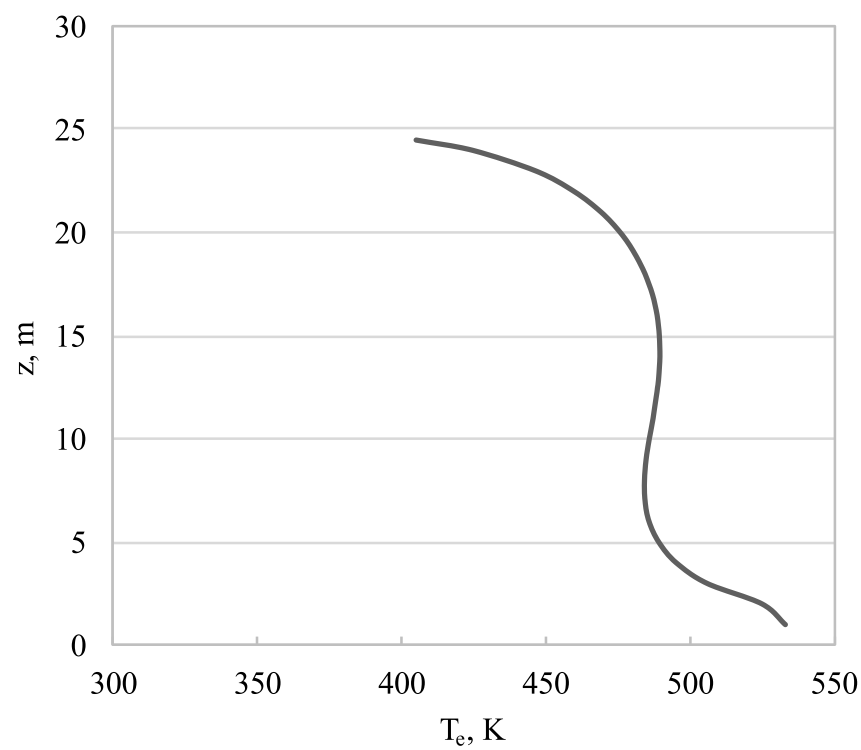

Figure 4.4 Steam chamber edge temperature (T_e) calculation results of Hangingstone project

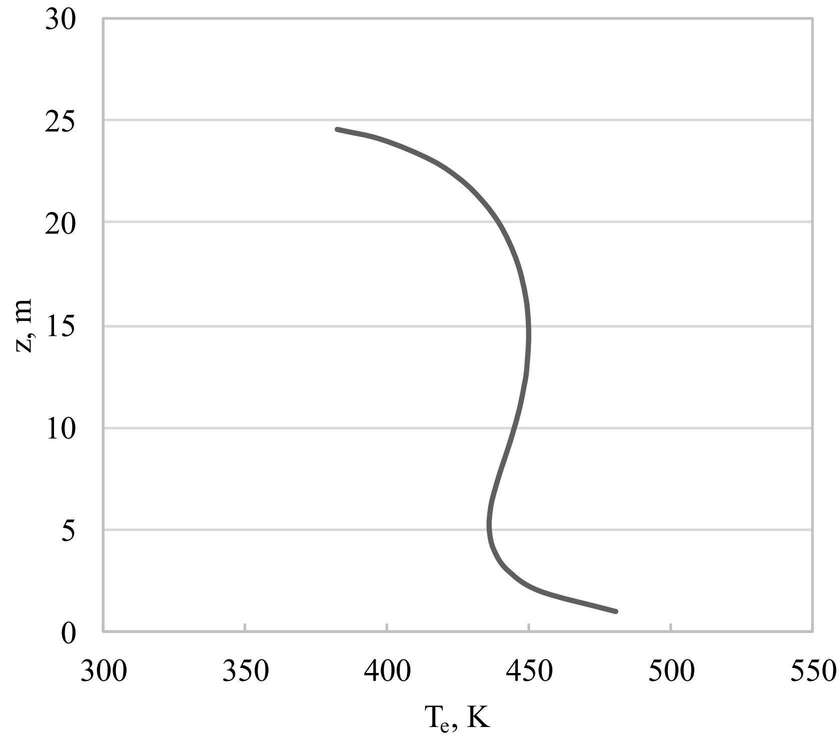

Figure 4.5 Steam chamber edge temperature (T_e) calculation results of Hilda Lake project

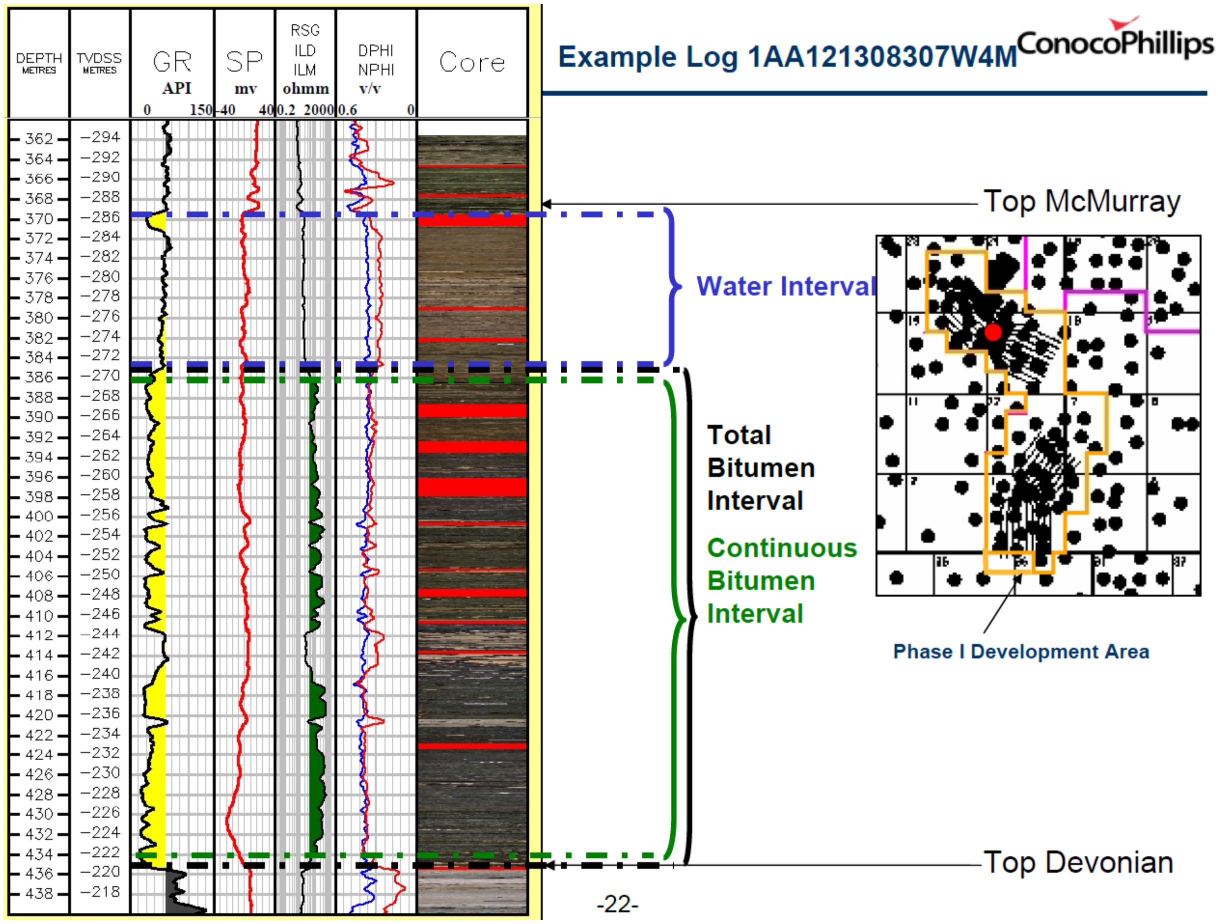

Figure 4.6 Analysis regarding heterogeneity from "Conoco Phillips Surmont SAGD presentation and data to ERCB (2008)."

It seems that continuous bitumen interval is thick, but there are some barriers. Courtesy of ConocoPhillips Surmont SAGD presentation to ERCB (2008).

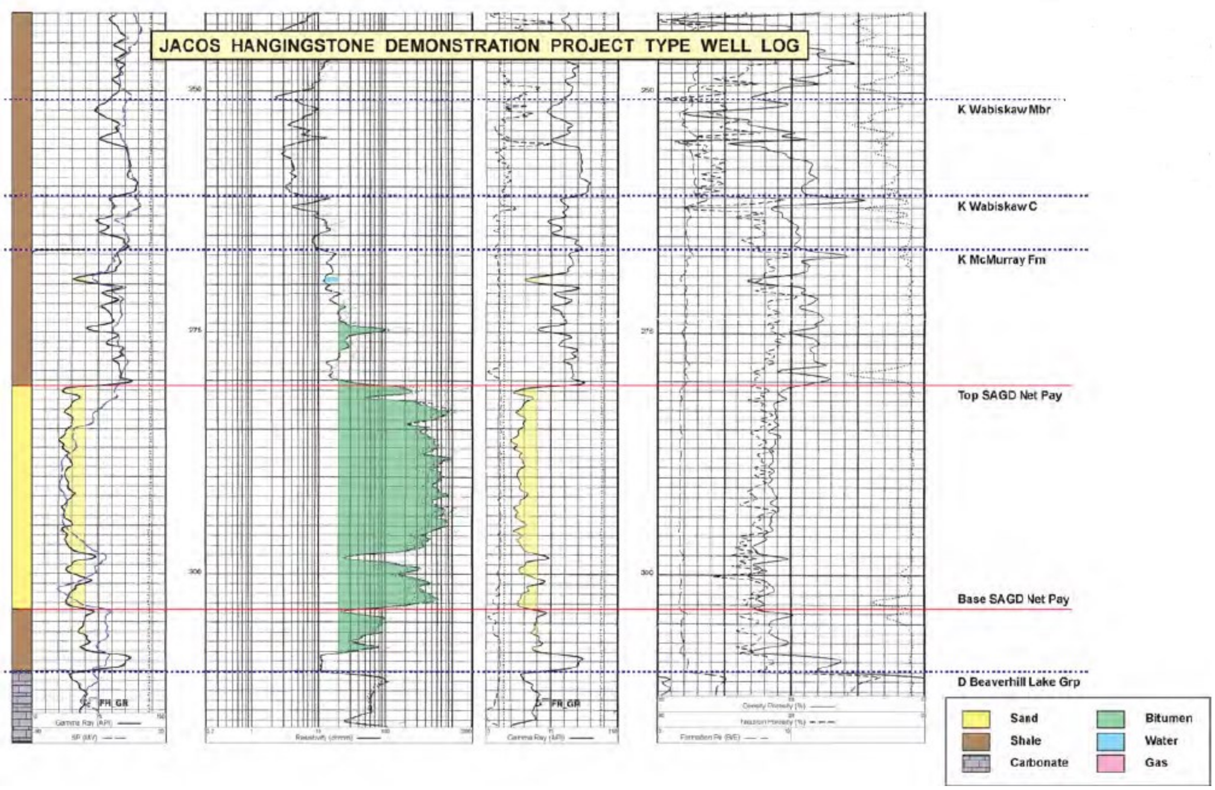

Figure 4.7 Analysis regarding heterogeneity from “JACOS Hangingstone SAGD project progress report presentation to ERCB (2012)”.

It seems that there is a thick zone of continuous bitumen. Courtesy of JACOS Hangingstone SAGD project progress report presentation to ERCB (2012).

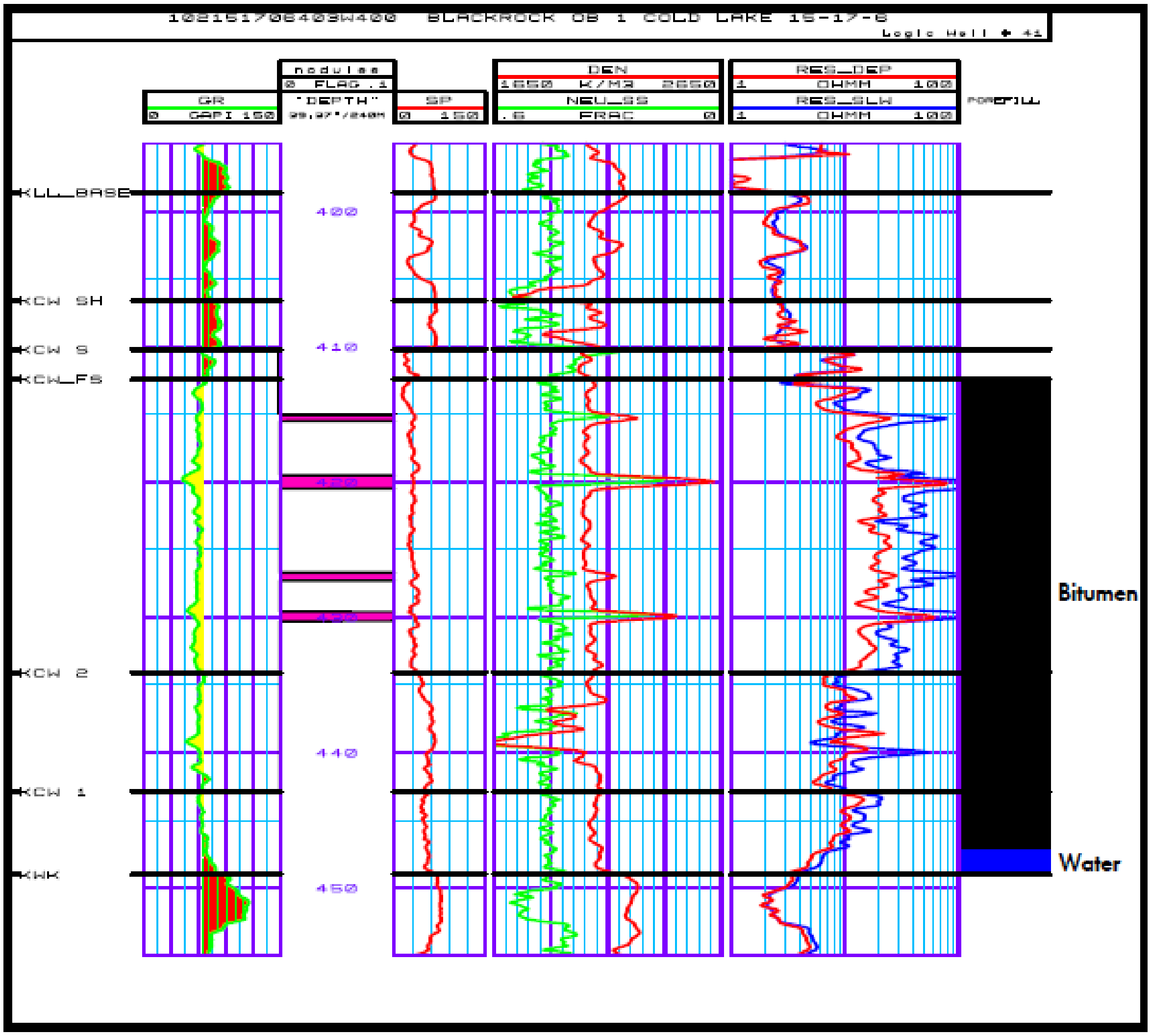

Figure 4.8 Well log from "Shell Canada Hilda Lake Pilot SAGD project annual presentation to EUB (2008)."

There are nodules in the pay zone. Courtesy of Shell Canada Hilda Lake Pilot SAGD project annual presentation and data to EUB (2008).

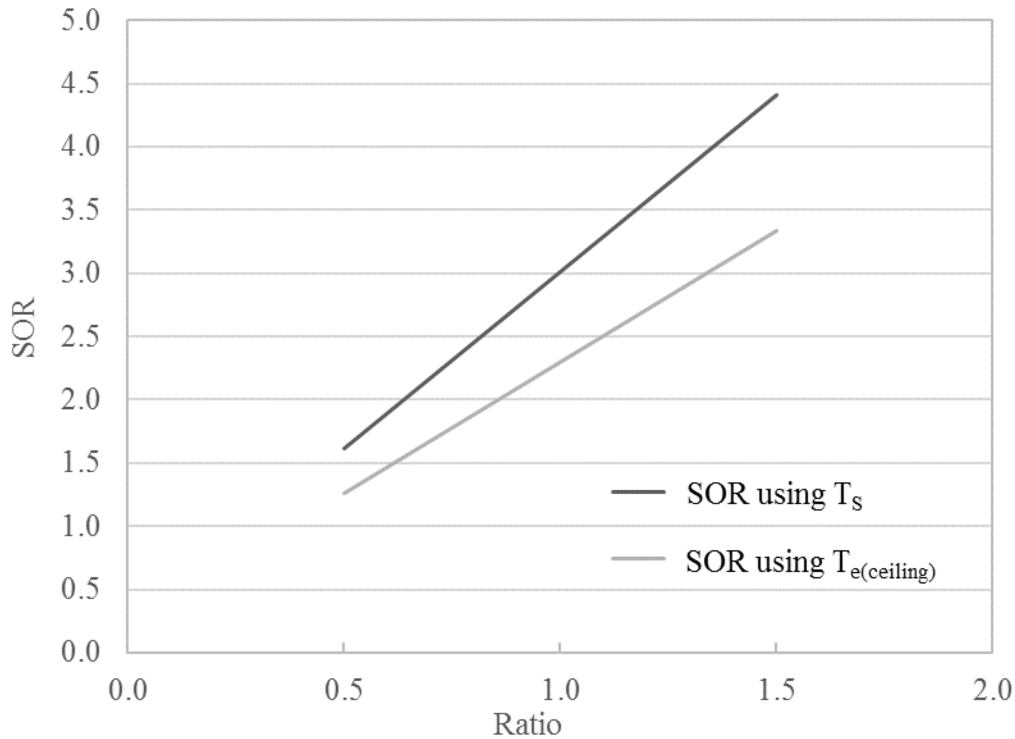

Figure 4.9 Sensitivity analysis of heat capacity values on SOR in the Surmont project

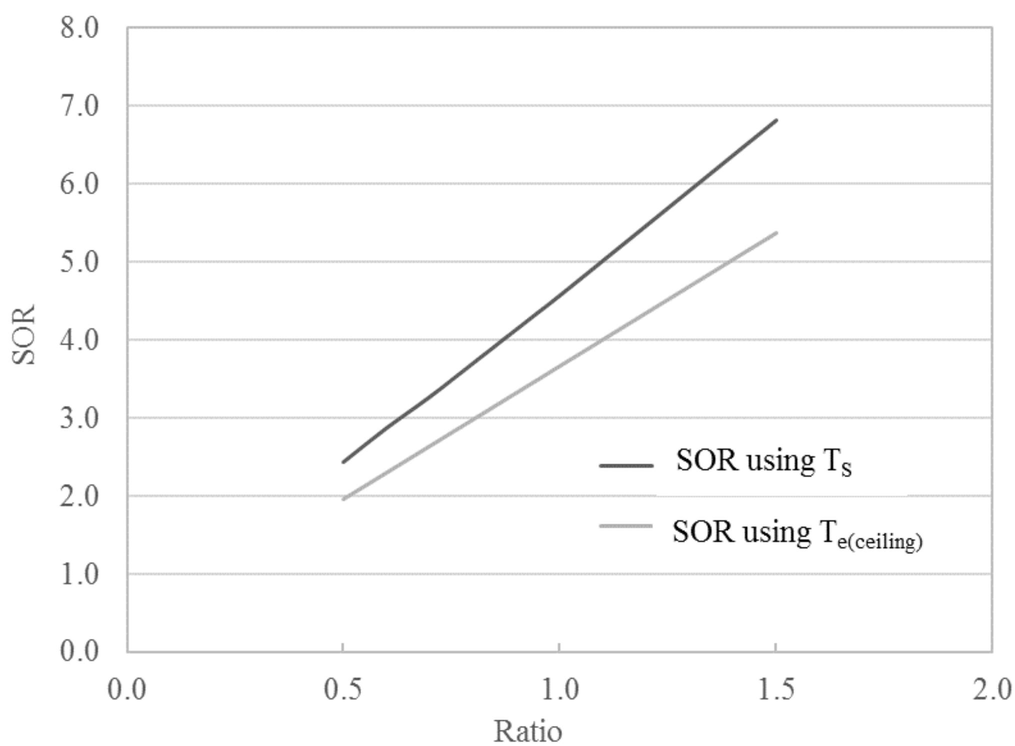

Figure 4.10 Sensitivity analysis of heat capacity values on SOR in the Hilda Lake project

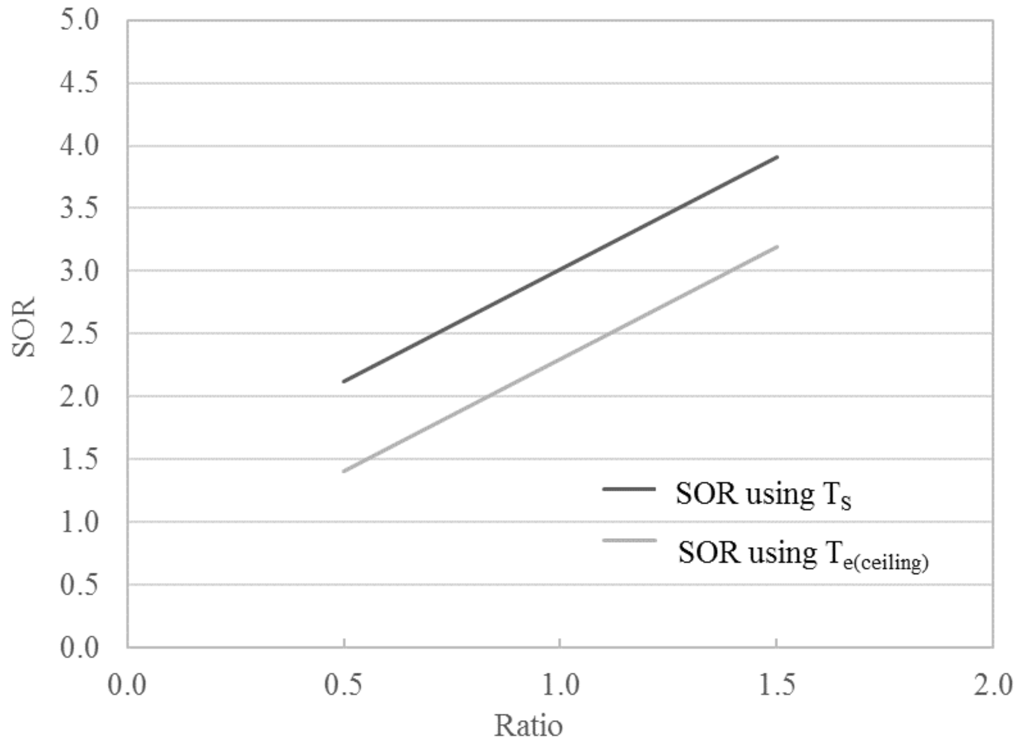

Figure 4.11 Sensitivity analysis of heat capacity of reservoir on SOR in the Surmont project

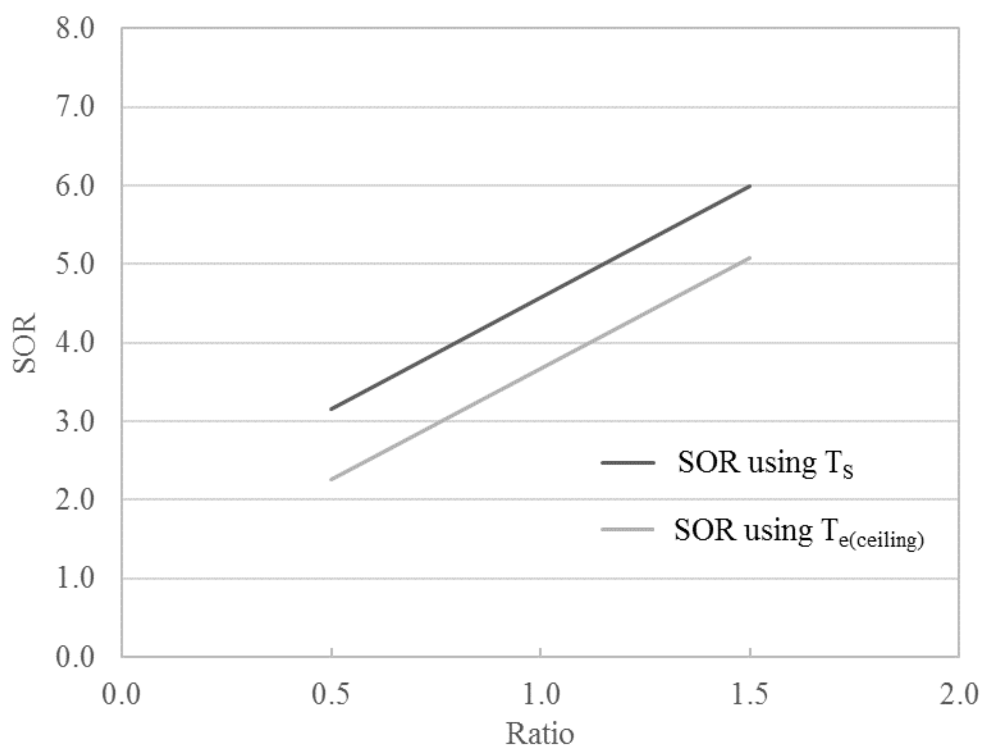

Figure 4.12 Sensitivity analysis of heat capacity of reservoir on SOR in the Hilda Lake project

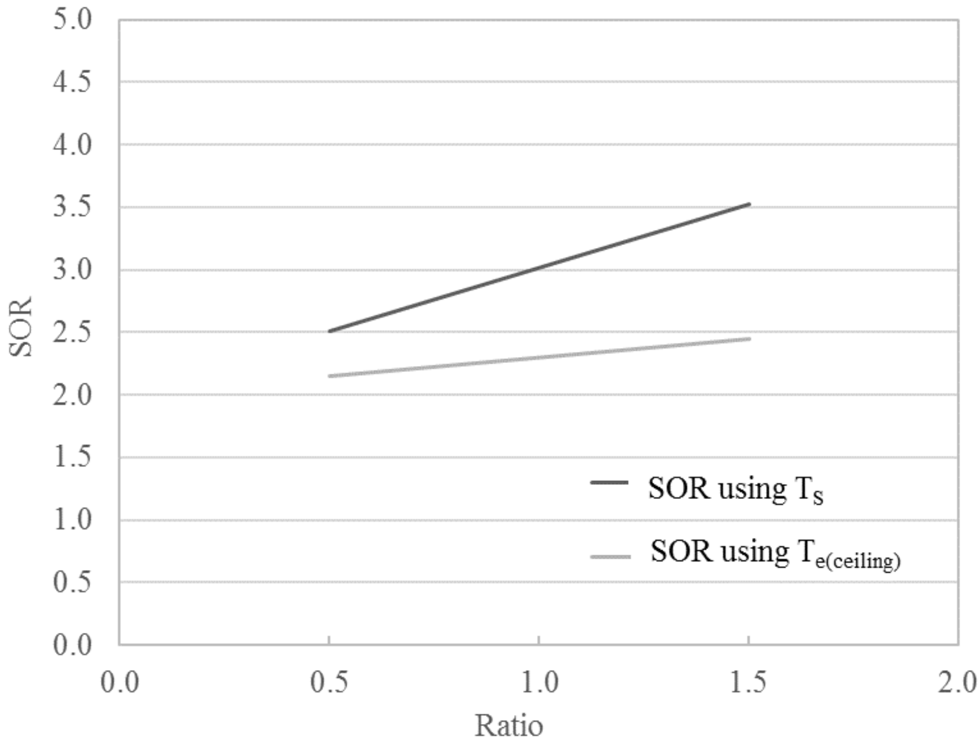

Figure 4.13 Sensitivity analysis of heat capacity of overburden on SOR in the Surmont project

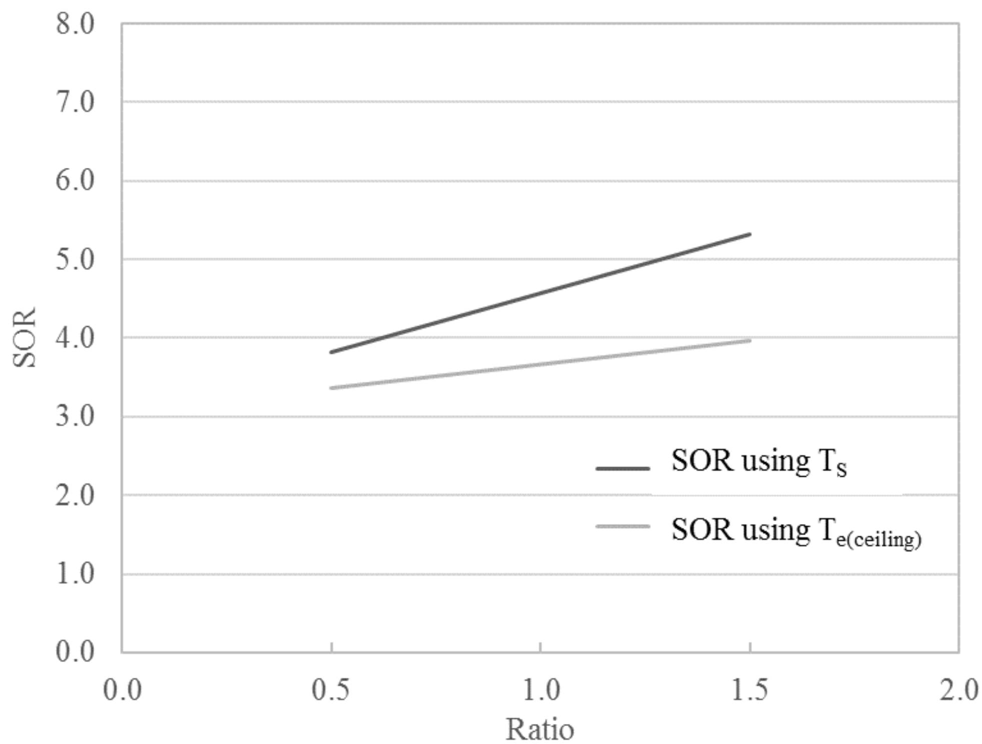

Figure 4.14 Sensitivity analysis of heat capacity of overburden on SOR in the Hilda Lake project

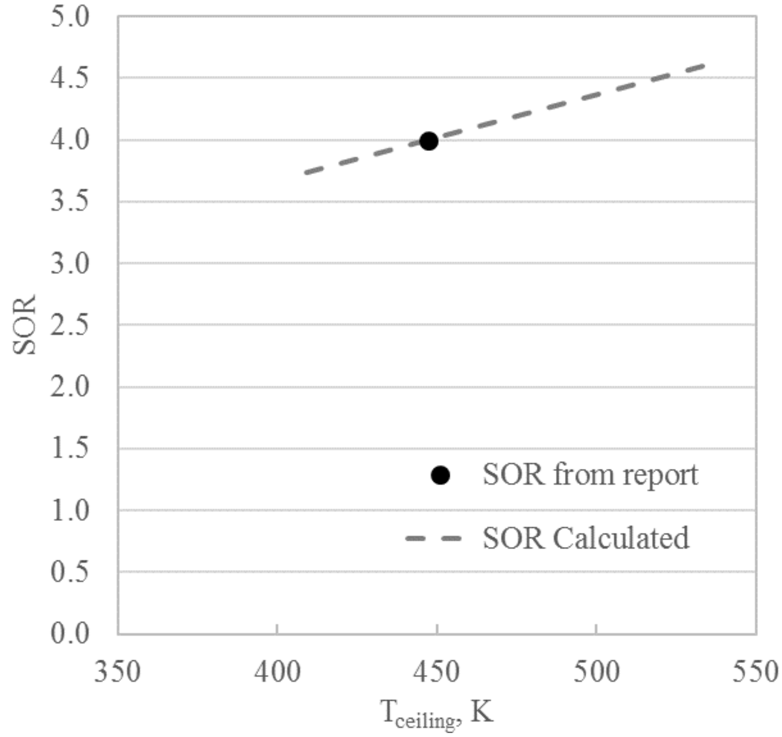

Figure 4.15 Sensitivity analysis of $T_{ceiling}$ on SOR calculation in the Hangingstone project

CHAPTER 5 CONCLUSIONS

This thesis presented an analytical model for non-isothermal compositional flow along the edge of a steam chamber in SAGD. The research was motivated by the question as to how temperature is supposed to vary along the edge of a steam chamber for a given bitumen production rate. To address the question, global/local material balance equations were solved for oleic-phase flow rate along the steam-chamber edge that is linear. The oleic-phase composition also changes along the chamber edge since chamber edge temperature and equivalent phase composition are interdependent on each other. Analytical equations were presented for bitumen-production rate and SOR for a representative temperature at the midpoint of the edge of a steam chamber. Comparison of the analytical equations with fine-scale reservoir simulations showed that they are in good agreement when the assumptions made in the derivation are reasonably close to the simulation conditions. Conclusions are as follows:

1. Prior models tend to overestimate oil production rate substantially, because they use the injected-steam temperature as the chamber-edge temperature. Results in this research indicate that temperature at the midpoint of the edge of a steam chamber represents well the chamber-edge temperature to be used for bitumen-production and SOR for a linear chamber edge. The temperature that gives accurate results was observed to be 60%-90% of the injected-steam temperature in the simulation cases in this research. Unlike previous SAGD models, calculation of bitumen-production rate and SOR with the developed method requires information regarding a temperature that represents the energy balance for the steam chamber of interest.
2. The analytical solutions for oleic-phase flow rate and temperature along the edge of a steam chamber indicate that they vary with elevation. The linear edge of a steam chamber requires heat losses to occur to the over and underlying formation rocks. A constant temperature along the chamber edge results in the chamber shape described in Butler's models (Butler et al, 1981; Butler and Stephens, 1981), instead of a linear edge of Reis (1992).
3. Temperature profile ahead of a steam chamber from 1-D heat conduction is widely used in the analytical models of SAGD. However, this assumption is inaccurate near the top and bottom of a reservoir. For the top section, there is 2-D heat conduction due to the heat loss to the overburden in addition to the reservoir ahead of the chamber edge. For the bottom section, heat convection due to high-temperature fluid flow is ignored in the assumed profile of temperature. Results show that the temperature profile based on 1-D conduction is likely closer to the

temperature profile for the middle of the reservoir than to those near the top and bottom of the reservoir.

4. T_e calculation is not accurate near the top and bottom of a reservoir. Sensitivity analysis shows that there are some other reasons for the deviation except for the inaccurate temperature profile near the top and bottom of a reservoir. For the bottom part, the effect of two-phase flow on oil flow is significant. Also, oleic phase flow is not parallel to the edge of a steam chamber in the thick heated zone near the bottom. These factors deviate from assumptions used in the analytical model. Therefore, temperature at the midpoint gives the best calculation results for the proposed analytical model.
5. Application of the model to SAGD field data showed that the presented model gives most-accurate results in terms of bitumen-production rate in comparison with prior models, such as Butler's models (Butler et al., 1981; Butler and Stephens, 1981; Butler, 1994), Reis' model (1992). It can also be used to calculate T_e in field cases, and show that T_e varies with time in field operations. Deviation between calculation results and field measurements in terms of oil production rate can be an indicator of potential problems in operation; for example, non-uniform chamber development along the well pair.
6. SOR calculations in field operations are largely affected by the accuracy of heat capacity values. SOR results will change proportionally to heat capacity values. In addition, reservoir heterogeneity makes temperature not equal to steam temperature everywhere inside the chamber, which will affect SOR calculation.

There are limitations of the developed model. Because the model is based on an ideal homogeneous reservoir, it can be inferred that deviation will be larger when applied to heterogeneous reservoirs. Many factors were not considered for the analytical model, such as two-phase flow, heat convection, and emulsion flow. Moreover, this model is limited to SAGD during the second stage of its operation, i.e., the side-way expansion stage. More research can be done to address these limitations.

Due to the co-injection of solvent in reservoir, variation in chamber edge temperature will be more significant in ES-SAGD process. Different solvents are expected to exhibit different chamber edge temperature distributions and different concentrations in oleic phase because of their different properties. Due to the coupling effect of high temperature and solvent dilution in oleic phase on reduction of oil phase viscosity, different solvent will optimize SAGD to different extent.

Further application of the developed model to ES-SAGD will help find the optimized choice of solvent.

REFERENCES

Akin, S. 2005. Mathematical Modeling of Steam-Assisted Gravity Drainage. *SPE Reservoir Evaluation & Engineering* **8**(5): 372-376.

Ardali, M., Mamora, D.D. and Barrufet, M. 2010. A Comparative Simulation Study of Addition of Solvents to Steam in SAGD Process. Presented at Canadian Unconventional Resources and International Petroleum Conference, Calgary, Alberta, Canada, 19-21, October.

Azad, A. and Chalaturnyk, R.J. 2010. A Mathematical Improvement to SAGD Using Geomechanical Modelling. *Journal of Canadian Petroleum Technology* **49**(10): 53-64.

Bharatha. S., Yee C.T. and Chan M.Y. 2005. Dissolved Gas Effects in SAGD. Presented at the Canadian International Petroleum Conference, Calgary, Alberta, Canada, 7-9 June.

Butler, R.M., McNab, G.S. and Lo, H.Y. 1981. Theoretical Studies on the Gravity Drainage of Heavy Oil During In-Situ Steam Heating. *The Canadian Journal of Chemical Engineering* **59**: 455-460.

Butler, R.M. and Stephens, D.J. 1981. The Gravity Drainage of Steam-heated Heavy Oil to Parallel Horizontal Wells. *Journal of Canadian Petroleum Technology* **20**(02): 90-96.

Butler, R.M. 1985. A New Approach to Modelling Steam Assisted Gravity Drainage. *Journal of Canadian Petroleum Technology* **24**(3): 42-51.

Butler, R.M. 1987. Rise Od Interfering Steam Chambers. *Journal of Canadian Petroleum Technology* **26**(03): 70-75.

Butler, R.M. 1994. Steam-Assisted Gravity Drainage: Concept, Development, Performance and Future. *Journal of Canadian Petroleum Technology* **33**(2): 44-50.

Butler, R.M. 1994. Horizontal Wells for the Recovery of Oil, Gas and Bitumen, Petroleum Society Monograph Number 2. *Canadian Institute of Mining, Metallurgy & Petroleum*.

Butler, R.M. 1997. *Thermal Recovery of Oil and Bitumen.* Calgary, Alberta: Black book series, GravDrain Inc.

Carslaw, H.S. and Jaeger, J.C. 1959. *Conduction of Heat in Solids Second Edition*. Oxford Science Publications.

Chung, K.H. and Butler, R.M. 1988. Geometric Effect of Steam Injection on the Formation of Emulsions in the Steam-Assisted Gravity Drainage Process. *Journal of Canadian Petroleum Technology* **27**(1): 36-42.

Cokar, M., Kallos, M.S. and Gates, I.D. 2013. A New Thermogeomechanical Theory for Gravity Drainage in Steam-Assisted Gravity Drainage. *SPE Journal* **18**(04): 736-741.

Computer Modelling Group (CMG) Ltd. User Manual. Version 2014. Calgary, Alberta, Canada, 2014.

ConocoPhillips 2007. Innovative Energy Technologies Program Project Annual Report 2007.

ConocoPhillips Surmont SAGD 9426 & 9460. ERCB Annual Update: Surmont Project. June 2008.

Edmunds, N.R., Kovalsky, S.D., Gittins, S.D. and Pennacchoili, E.D. 1994. Review of Phase A Steam-Assisted Gravity Drainage Test. *SPE Reservoir Engineering* **9**(02): 119-124.

Edmunds, N. and Peterson, J. 2007. A Unified Model for Prediction of CSOR in Steam-Based Bitumen Recovery. Presented at the Canadian International Petroleum Conference, Calgary, Alberta, Canada, 12-14, June.

ERCB Staff Review and Analysis. 2010. Total E&P Canada Ltd. Surface Steam Release of May 18, 2006 Joslyn Creek SAGD Thermal Operation.

Farouq Ali, S.M. 2003. Heavy Oil – Evermore mobile. *Journal of Petroleum Science and Engineering* **37**(1): 5-9.

Gates, I. D. and Chakrabarty, N. 2006. Optimization of Steam Assisted Gravity Drainage in McMurray Reservoir. *Journal of Canadian Petroleum Technology* **45**(09): 54-62.

Gates, I.D. and Gutek, A.M.H. 2008. Process for In Situ Recovery of Bitumen and Heavy Oil. US Patent No. 7,464,756.

Gotawala, D.R. and Gates, I.D. 2009. Correlation between SAGD Steam Chamber Growth and Geological Heterogeneity. 15th European Symposium on Improved Oil Recovery, Paris, France.

Gotawala, D.R. & Gates, I.D. 2010. On the Impact of Permeability Heterogeneity on SAGD Steam Chamber Growth. *Natural Resource Research* **19**(2): 151-164.

Gupta, S., Gittins, S. and Picherack, P. 2005. Field Implementation of Solvent Aided Process. *Journal of Canadian Petroleum Technology* **44**(11): 8-13.

Gupta, S. and Gittins, S.D. 2006. Christina Lake Solvent Aided Process Pilot. *Journal of Canadian Petroleum Technology* **45**(9): 15-18.

Gupta, S. and Gittins, S.D. 2012. An Investigation Into Optimal Solvent Use and the Nature of Vapor/Liquid Interface in Solvent-Aided SAGD Process With a Semianalytical Approach. *SPE Journal* **17**(4): 1255-1264.

Irani, M. and Cokar, Marya. 2016. Discussion on the Effects of Temperature on Thermal Properties in the Steam-Assisted Gravity Drainage (SAGD) Process. Part 1: Thermal Conductivity. *SPE Journal* **21**(02):334-352.

Ito, Y., M. Ichikawa and T. Hirata, "The Growth of the Steam Chamber During the Early Period of the UTF Phase B and Phase I Projects," *Journal of Canadian Petroleum Technology* **40**(9): 29–36 (2001a).

Ito, Y., T. Hirata and M. Ichikawa, "The Effect of Operating Pressure on the Growth of the Steam Chamber Detected at the Hangingstone SAGD Project," *Journal of Canadian Petroleum Technology* **4**(1): 47–53(2001b).

JACOS Hangingstone SAGD 8788. Thermal In-Situ Scheme Progress Report to ERCB. Feb 2012.

Keshavarz, M., Okuno, R. and Babadagli, T. 2015a. A Semi-Analytical Solution to Optimize Single-Component Solvent Coinjection with Steam during SAGD. *Fuel* **144**: 400-414.

Keshavarz, M., Okuno, R. and Babadagli, T. 2015b. Optimal Application Conditions for Steam/Solvent Coinjection. *SPE Reservoir Evaluation & Engineering* **18**(1): 20-38.

Keshavarz, M., Harding, T. and Chen, Z. 2016. Modification of Butler's Unsteady-State SAGD Theory to Include the Vertical Growth of Steam Chamber. Presented at the SPE Heavy Oil Technical Conference, Calgary, Alberta, Canada, 7-9, June.

Kumar, A. and Okuno, R. 2015. Direct Perturbation of the Peng-Robinson Attraction and Covolume Parameters for Reservoir Fluid Characterization. *Chemical Engineering Science* **127**: 293-309.

Li, Q. and Chen, Z. 2015. A New Analysis on the Convective Heat Transfer at the Edge of the SAGD Chamber. SPE Annual Technical Conference and Exhibition, 28-30 September, Houston.

Mehrotra, A.K. and Svrcek, W.Y. 1986. Viscosity of Compressed Athabasca Bitumen. *Canadian Journal of Chemical Engineering* **64**(5): 844-847.

Miura, K. and Wang, J. 2012. An Analytical Model To Predict Cumulative Steam/Oil Ratio (CSOR) in Thermal-Recovery SAGD Process. *Journal of Canadian Petroleum Technology* **51**(04): 268-275.

Mojarad, M. and Dehghanpour, H. 2016. Analytical Modeling of Emulsion Flow at the Edge of a Steam Chamber During a Steam-Assisted-Gravity-Drainage Process. *SPE Journal* **21**(2): 353-363.

Nasr, T.N., Beaulieu, G., Golbeck, H. and Heck, G. 2003. Novel Expanding Solvent-SAGD Process "ES-SAGD". *Journal of Canadian Petroleum Technology* **42**(1): 13-16.

Okuno, R., 2015. Class notes for PET E 478 "Thermal Methods in Heavy Oil Recovery," University of Alberta, Canada.

Rabiei Faradonbeh, M., Harding, T. G. and Abedi, J. 2016a. Semi-analytical modeling of steam-solvent gravity drainage of heavy oil and bitumen: Steady state model with linear interface. *Fuel*. **183**: 568-582.

Rabiei Faradonbeh, M., Harding, T. G. and Abedi, J. 2016b. Semianalytical Modeling of Steam/Solvent Gravity Drainage of Heavy Oil and Bitumen: Unsteady-State Model With Curved Interface. *SPE Reservoir Evaluation & Engineering*.

Reis, J.C. 1992. A Steam-Assisted Gravity Drainage Model for Tar Sands: Linear Geometry. *The Journal of Canadian Petroleum Technology*. **31**(10): 14-20.

Sharma, J. and Gates, I.D. 2010. Multiphase Flow at the Edge of a Steam Chamber. *Canadian Journal of Chemical Engineering* **88**(3): 312-321.

Sharma, J. and Gates, I.D. 2011. Convection at the Edge of a Steam-Assisted-Gravity-Drainage Steam Chamber. *SPE Journal* **16**(3): 503-512.

Shell Canada Hilda Lake Pilot SAGD 8093. In Situ Oilsands Progress Presentation to ERCB. April 2008.

Sheng, J. 2013. Enhanced Oil Recovery Field Case Studies. 2013 Elsevier.

Venkatramani, A. and Okuno, R. 2016. Compositional Mechanisms in Steam-Assisted Gravity Drainage and Expanding-Solvent Steam-Assisted Gravity Drainage With Consideration of Water Solubility in Oil. *SPE Reservoir Evaluation & Engineering*. SPE-180737-PA.

Yazdani, A., Alvestad, J., Kjonsvik, D., et al. 2011. A Parametric Simulation Study for Solvent Co-injection Process in Bitumen Deposits. Presented at the Canadian Unconventional Resources Conference, Calgary, Alberta, Canada, 15-17 November.

Zargar, Z. and Farouq Ali, S.M. 2016. Analytical Treatment of SAGD - Old and New. Presented at the SPE Canada Heavy Oil Technical Conference, Calgary, Alberta, Canada, 7-9, June 2016.

Zhang, W., Youn, S. and Doan, Q. 2005. Understanding Reservoir Architectures and Steam Chamber Growth at Christina Lake, Alberta, by using 4D Seismic and Crosswell Seismic Imaging. SPE/PS-CIM/CHOA International Thermal Operations and Heavy Oil Symposium, Calgary, Alberta, Canada.

Zhou, W., Chen, S. and Dong M. 2016. Novel insights on initial water mobility: Its effects on steam-assisted gravity drainage performance. *Fuel* **174**: 274-286.

APPENDICES

APPENDIX I: Calculation of the constant "m" for simulation cases

Bitumen has high viscosity under reservoir temperature and its viscosity is sensitive to temperature. All thermal recovery methods for bitumen production are taking advantage of this property. As mentioned by Mehrotra and Svrcek (1986), how bitumen viscosity changes with temperature can be expressed as Equation (2.50) as follows:

$$\nu_s/\nu_o = [(T - T_R)/(T_S - T_R)]^m, \tag{2.50}$$

where the constant "m" is used for description of the relationship between kinematic viscosity and temperature.

The constant "m" is required to describe bitumen property and used in calculation of prior models. In the field, the constant "m" can be obtained by testing bitumen sample in the laboratory. In the calculation of simulation cases, this constant is obtained by the following method.

Simulation cases are run in the CMG (2014). Grid blocks lying outside steam chamber are those blocks where gas saturation equals to zero. With the help of CMG Results Report (2014), at a give time during production, temperature and kinematic viscosity of oleic phase in all grid blocks ahead of steam chamber edge are tabulated from simulation results. With generated table of temperature and kinematic viscosity, Matlab™ can give the value of "m" by regression.

APPENDIX II: Calculation of original oil in place

Original oil in place (OOIP) is the volume of all mobile oil in the porous reservoir. In Chapter 3, it is used to describe the cumulative production. For the sake of explicit comparison between cumulative production in various cases at different times, cumulative bitumen productions are expressed as the ratio of it to OOIP.

OOIP is calculated as the following:

$$OOIP = HW\Delta y\varphi\Delta S_o, \tag{AII-1}$$

where H is the reservoir thickness, W is the width of reservoir, Δy is the length of production well, φ is the reservoir porosity, ΔS_o is the reducible oil saturation which equals to the difference between initial oil saturation and residual oil saturation.